A STUDY OF PLASMA COLUMNS IN A LONGITUDINAL MAGNETIC FIELD

by

Ward Dean Halverson

S. B., Massachusetts Institute of Technology

(1956)

SUBMITTED IN PARTIAL FULFILLMENT

OF THE REQUIREMENTS FOR THE

DEGREE OF DOCTOR OF

SCIENCE

at the

MASSACHUSETTS INSTITUTE OF

TECHNOLOGY

January, 1965

Signature of Author .....
Department of Geology and Geophysics, January 11, 1965

Certified by .....
Thesis Supervisor

Accepted by .....
Chairman, Departmental Committee on Graduate Students

SUMMARY

A STUDY OF PLASMA COLUMNS IN A LONGITUDINAL MAGNETIC FIELD

by

Ward Dean Halverson

Submitted to the Department of Geology and Geophysics on January 11, 1965, in partial fulfillment of the requirements for the degree of Doctor of Science.

This is an experimental study of plasma diffusion in the positive column of helium, argon, and helium-mercury low pressure arc discharges in a homogeneous longitudinal magnetic field. Transverse diffusion is studied by observing the longitudinal electric field and radial potential drop as a function of magnetic field strength. Three types of plasma diffusion are studied: "classical", intermediate, and "turbulent" diffusion across the magnetic field lines. Results largely corroborate accepted theories of transverse diffusion, with a few notable exceptions. These include a "two mode" behavior of argon discharges and the apparent breakdown of turbulent diffusion theory in He and He-Hg discharges.

Thesis Supervisor: Francis Bitter

Title: Professor of Geophysics

TABLE OF CONTENTS

TABLE OF CHARTS AND ILLUSTRATIONS

ACKNOWLEDGMENTS

I would like to thank Professor Francis Bitter for his generous assistance in all aspects of this thesis. Discussions with Dr. John Waymouth were also very helpful. I thank the staffs of the Research Laboratory of Electronics and the National Magnet Laboratory for technical and other aid to this project.

This work was supported in part by the U. S. Army, the Air Force Office of Scientific Research, and the Office of Naval Research.

I. INTRODUCTION

The purpose of this thesis is to contribute to the growing knowledge of the behavior of ionized gases in magnetic fields. More specifically, it is an experimental investigation of the diffusion of low temperature plasma across magnetic field lines, against the Lorentz force which tends to inhibit diffusion. It is hoped that studies of this type will ultimately lead to better understanding of a wide range of plasma diffusion problems, whether they be of laboratory, planetary, or cosmic scale.

The experiment is conducted in low pressure arc discharges in pure helium, pure argon, and helium-mercury mixtures in a homogeneous longitudinal magnetic field. The behavior of the discharges is compared to theoretical predictions for three types of plasma diffusion: (1) "classical", in which collisions between particles provide the diffusion mechanism; (2) intermediate, where macroscopic plasma instabilities enhance the diffusion rate; and (3) "turbulent", in which the plasma is in chaotic motion somewhat resembling fluid-dynamic turbulence.

The experimental results largely corroborate accepted theories of transverse diffusion within their ranges of applicability, with a few notable exceptions. These include the existence of two modes of operation in argon discharges at relatively high magnetic fields and the apparent breakdown of turbulent diffusion theory for helium and helium-mercury discharges at high magnetic fields and large discharge radii.

II. BACKGROUND

2.1 "CLASSICAL" DIFFUSION

The "classical" theory of charged particle diffusion across magnetic fields has been presented many times (see, for example, Allis, 1956) and will be reviewed here only cursorily. We shall assume that the plasma is at low pressure (less then 10 mm Hg) and low temperature (electron temperature less than 10 electron volts) and that the principal mechanism causing charge diffusion is collisions with neutral particles. For this case the relations governing ion and electron flow in the plasma are the equations of charge and momentum conservation.

$$\frac{\partial n_\pm}{\partial t} + \nabla\cdot(n_\pm \vec{v}_\pm) = \nu_i n_- - \alpha n_+ n_- \tag{2.1}$$

$$m_\pm \frac{d\vec{v}_\pm}{dt} = \pm e(\vec{E} + \vec{v}_\pm \times \vec{B}) - \frac{\nabla p_\pm}{n_\pm} - m_\pm \vec{v}_\pm \nu_{c\pm} \tag{2.2}$$

In writing the "pressures" $p_\pm$, it is assumed that the ion and electron velocity distributions are nearly isotropic, but not necessarily Maxwellian. Other symbols are defined in Appendix IV. Note that Eqs. (2.1) and (2.2) are actually four equations with the (+) and (-) signs referring to ions and electrons, respectively.

In a d.c. discharge the inertia terms in Eqs. (2.2) are negligible if the ion and electron mean free paths are much smaller than the dimensions of the discharge. With this approximation, Eqs. (2.2) become

$$\vec{\Gamma}_\pm = n_\pm \vec{v}_\pm = -\nabla(D_\pm n_\pm) \pm \mu_\pm n_\pm (\vec{E} + \vec{v}_\pm \times \vec{B}) \tag{2.3}$$

where

$$\left.\begin{aligned} \mu_\pm &= \frac{e}{m_\pm \nu_{c\pm}} \\ D_\pm &= \frac{p_\pm}{n_\pm m_\pm \nu_{c\pm}} \end{aligned}\right\} \tag{2.4}$$

are the respective "mobilities" and "diffusion coefficients".

Eqs. (2.3) can be solved explicity for the ion and electron fluxes.

$$\vec{\Gamma}_\pm = \frac{1}{1+\mu_\pm^2 B^2}\Big[-\nabla(D_\pm n_\pm) \pm \mu_\pm n_\pm \vec{E} \pm \mu_\pm \vec{B}\times\nabla(D_\pm n_\pm) + \mu_\pm^2 n_\pm \vec{E}\times\vec{B} + \mu_\pm^2 \vec{B}\{\pm\mu_\pm \vec{B}\cdot(n_\pm \vec{E}) - \vec{B}\cdot\nabla(D_\pm n_\pm)\}\Big] \tag{2.5}$$

Longitudinal Magnetic Field

Given a constant, homogeneous magnetic field, $\vec{B} = \hat{u}_z B_z$, and small plasma currents ($\nabla\times\vec{B}\approx 0$), the radial and longitudinal components of Eqs. (2.5) are, in cylindrical coordinates,

$$\Gamma_{r\pm} = \frac{1}{1+\mu_\pm^2 B_z^2}\Big[-\frac{\partial}{\partial r}(D_\pm n_\pm) \pm \mu_\pm n_\pm E_r \mp \frac{B_z}{r}\frac{\partial}{\partial\theta}(D_\pm n_\pm) + \mu_\pm^2 n_\pm B_z E_\theta\Big] \tag{2.6a}$$

$$\Gamma_{z\pm} = -\frac{\partial}{\partial z}(D_\pm n_\pm) \pm \mu_\pm n_\pm E_z \tag{2.6b}$$

Magneto-Ambipolar Approximations

In order to simplify Eqs. (2.6) we make several more approximations which are usually valid for low pressure discharge columns in weak longitudinal magnetic fields

$$n_+ \approx n_- \approx n \tag{2.7}$$

$$\Gamma_{r+} \approx \Gamma_{r-} \tag{2.8}$$

$$E_\theta \approx 0\ ;\ \frac{\partial}{\partial\theta}(D_\pm n) \approx 0 \tag{2.9}$$

$$\nabla D_\pm \approx 0 \tag{2.10}$$

The quasi-neutrality approximation, Eq. (2.7) is accurate for plasmas whose Debye length is much smaller than the electron mean free path, which in turn is smaller than characteristic dimensions of the discharge column. In this case, significant charge separation will occur only in sheaths near electrodes and tube walls. The radial ion and

electron flux will be approximately equal, Eq. (2.8), in a plasma column that is long enough to have a negligible density gradient in the z direction. The radial flux equality is a direct consequence of the quasi-neutral approximation and the requirement of charge conservation. The assumption of azimuthal homogeneity, Eq. (2.9), postulates that there are no mechanisms causing azimuthal charge separation or density gradients. As we shall see, this assumption is good only for magnetic fields below a critical value at which instabilities arise. Eq. (2.10) states that the diffusion coefficients are independent of position in the discharge. This implies that the electron and ion temperatures are constant throughout the discharge. Eq. (2.10) allows us to remove $D_{\pm}$ from the gradient operators in Eq. (2.6), thereby simplifying the expressions which follow.

With assumptions Eqs. (2.7)-(2.10), the ion and electron fluxes of Eq. (2.6a) can be equated to solve for the radial electric field.

$$E_r = \frac{D_{\perp +} - D_{\perp -}}{\mu_{\perp +} + \mu_{\perp -}} \cdot \frac{1}{n} \cdot \frac{\partial n}{\partial r} \tag{2.11}$$

where

$$\begin{Bmatrix} D_{\perp \pm} \\ \mu_{\perp \pm} \end{Bmatrix} = \frac{1}{1 + \mu_{\pm}^2 B_z^2} \begin{Bmatrix} D_{\pm} \\ \mu_{\pm} \end{Bmatrix} \tag{2.12a, b}$$

By substituting Eq. (2.11) back into Eq. (2.6a) and rearranging, the radial plasma flux can be written

$$\Gamma_r = - \frac{\mu_+ D_+ + \mu_- D_-}{\mu_+ + \mu_-} \cdot \frac{1}{1 + \mu_+ \mu_- B_z^2} \cdot \frac{\partial n}{\partial r} \tag{2.13}$$

The coefficient of the density gradient in Eq. (2.13) is the usual ambipolar diffusion coefficient D_a multiplied by $(1 + \mu_+ \mu_- B_z^2)^{-1}$.

Substitution of Eq. (2.13) into Eq. (2.1) yields the ambipolar diffusion equation for a long plasma column in a homogeneous axial magnetic field,

$$\frac{\partial n}{\partial t} - D_{a\perp} \frac{1}{r} \frac{\partial}{\partial r} \left(r \frac{\partial n}{\partial r} \right) = \nu_i n - \alpha n^2 \tag{2.14}$$

where

$$D_{a\perp} = \frac{\mu_+ D_+ + \mu_- D_-}{\mu_+ + \mu_-} \cdot \frac{1}{1 + \mu_+ \mu_- B_z^2} \tag{2.15}$$

Eq. (2.14) can be solved analytically if volume recombination in the discharge is negligible compared to wall recombination. With this approximation plus the assumption of a steady-state plasma ($\frac{\partial n}{\partial t} = 0$), the solution of Eq. (2.14) is

$$n(r) = c_1 J_0\left(\sqrt{\frac{\nu_i}{D_{a\perp}}}\, r\right) + c_2 Y_0\left(\sqrt{\frac{\nu_i}{D_{a\perp}}}\, r\right)$$

c_1 and c_2 are constants to be determined by boundary conditions and J_0 and Y_0 represent zero-order Bessel functions of the first and second kind.

The boundary conditions require that the plasma density be finite at r = O and approach zero at the tube wall r = R. Thus c_2 = O and

$$\sqrt{\frac{\nu_i}{D_{a\perp}}} \approx \frac{2.405}{R} \tag{2.16}$$

The radial variation of the plasma density is given by the expression

$$n(r) = n(0) J_0\left(\frac{2.405}{R} r\right) \tag{2.17}$$

By substituting Eq. (2.17) into Eq. (2.11) and integrating, we find the radial potential drop,

$$V(r) - V(0) = \frac{D_{\perp -} - D_{\perp +}}{\mu_{\perp +} + \mu_{\perp -}} \ln\left[J_0\left(\frac{2.405}{R} r\right)\right] \tag{2.18}$$

Of course, Eqs. (2.17) and (2.18) will hold only away from wall sheaths where charge separation occurs. The sheath thickness, however, is of the order of a few Debye lengths and is usually much smaller than characteristic dimensions of the discharge.

2.2 "SIMON" DIFFUSION

Simon (1955) has criticized the application of "classical" magneto-ambipolar diffusion theory to arc chambers of length comparable to transverse dimensions. Because

the mobility of electrons in the magnetic field direction is so much greater than in the transverse direction, Simon postulated that the conducting end walls of a short arc chamber would effectively short-circuit the transverse electric field. The short-circuit mechanism would provide for the requirements of charge neutrality and allow the ions and electrons to diffuse at their intrinsic rates. Simon argued that the effect might also occur in chambers with non-conducting walls via charge migration in the wall sheath.

"Simon" diffusion has been the subject of several theoretical and experimental studies which indicate that the original theory must be considerably modified. Tonks (1960) and Zharinov (1960) analyzed the short-circuiting mechanism at the end walls and arrived at transverse diffusion coefficients somewhat different from Simon's, depending on the assumptions used. Probably the most thorough study was reported by Sato and Hatta (1963) who solved the density distribution problem rigorously and showed that Simon's assumptions were rather poor. Sato and Hatta's theory and their experiment in a short discharge with moveable conducting end walls indicate that the plasma diffuses according to "classical" magneto-ambipolar theory. Another experiment by Nedospasov (1958) in the positive column of an argon discharge in a magnetic field indicates that the radial charge diffusion is ambipolar, even within a few centimeters of the cathode spot.

2.3 THE POSITIVE COLUMN IN A MAGNETIC FIELD

The theory of the positive column of low pressure discharges was worked out by Schottky (1924) and von Engel and Steenbeck (1932) and has been reviewed quite well by Francis (1956). Mercury-rare gas discharge theory has been developed by Waymouth and Bitter (1956) and Cayless (1963). The theory will not be reviewed in detail here except for its more general aspects. Instead, we shall follow the method of Walsh et al. (1963) to develop invariant discharge scaling parameters.

Let us assume a cylindrical discharge column of radius R in a homogeneous axial magnetic field B. A two-component gas such as mercury vapor and rare gas is assumed,

one component providing most of the ionization and the other controlling the diffusion and mobility of the ions and electrons. The subscripts "m" (for "mercury") and "r" ("rare gas") will be used to distinguish the two gases. To apply the results to a single component discharge, it is only necessary to replace "m" subscripts by "r".

The basic relations governing the discharge are the equations of electron mobility, charge conservation, and energy balance. The discharge current I is given by the electron mobility expression, assuming that the ion current can be neglected.

$$I = C\, n_- \mu_-(p_r, p_m, T_-) E R^2 \tag{2.19}$$

where n_- is the average electron density in the column, C is an appropriate proportionality factor, and E is the axial electric field.

The equation of charge conservation has already been introduced in Section 2.1. Here we shall use an approximate form of Eq. (2.14),

$$\frac{n_- D_a(p_r, p_m, T_-)}{R^2(1 + \mu_+ \mu_- B^2)} \approx n_- \nu(p_r, p_m, T_-) + n_- n_* \epsilon(p_r, p_m, T_-) \tag{2.20}$$

The last term in Eq. (2.20) is introduced to account for non-linear effects in the ionization process, such as step-wise ionization or volume recombination. For these particular cases, the density n_* refers respectively to the density of excited atoms or the ion density. ν and ϵ are proportionality factors depending in general on electron temperature and gas densities.

The equation of energy balance equates the energy gained by electrons from the axial electric field with losses incurred in elastic and inelastic collisions with atoms of the neutral gases.

$$E I = n_- b(p_r, p_m, T_-) R^2 + n_- c(p_r, p_m, T_-) R^2 + n_- n_* d(p_r, p_m, T_-) R^2 \tag{2.21}$$

where b, c, and d are proportionality factors for energy losses to elastic collisions, inelastic collisions with atoms in the ground state, and non-linear inelastic losses (or gains).

Let us rewrite Eq. (2.20) and introduce the assumptions that D_a is inversely proportional to the rare gas pressure, ν is directly proportional to the mercury pressure, and ϵ is only a function of T_-.

$$\frac{D_{ao}(T_-)}{p_r R'} = p_m R' \nu_o(T_-) + n_* R' \epsilon(T_-) \tag{2.22a}$$

where

$$R' = R\sqrt{1 + \mu_+ \mu_- B^2} \tag{2.22b}$$

The zero subscripts indicate quantities at unit pressure.

Equations (2.19) and (2.21) can be rewritten under similar assumptions and combined to give

$$(ER')^2 C\mu_{-o} = (p_r R')^2 b_o(T_-) + p_r R' p_m R' c_o(T_-) + p_r R' p_m R' d(T_-) \tag{2.23}$$

Eq. (2.23) has been multiplied by $\sqrt{1 + \mu_+ \mu_- B^2}$ to provide factors similar to those in Eq. (2.22).

In principle, Eqs. (2.22) and (2.23) can be solved for T_- so that ER' can then be expressed as a function of $p_r R'$, $p_m R'$, and $n_* R'$. Since n_* may be difficult to measure in a discharge, it is desirable to relate it to directly measurable discharge parameters. Here we shall follow Walsh et al. and assume the relation

$$n_* = n_-^q p_r^r p_m^s R^t \Theta(T_-) \tag{2.24}$$

where $\Theta(T_-)$ is a function of electron temperature only. Substituting Eq. (2.19) for n_-, multiplying appropriate terms by $\sqrt{1 + \mu_+ \mu_- B^2}$, and rearranging, we find

$$n_* R' = \left[\frac{p_r R'}{ER'}\right]^q \left[\frac{I}{R^{(2q-t)/q} R'^{(r+s-1)/q}}\right]^q \cdot (p_r R')^r (p_m R')^s \Theta_1(T_-) \tag{2.25}$$

where Θ_1 has absorbed a few constants. Setting $n = (2q - t)/q$ and $m = (r + s - 1)/q$ it is then, in principle, possible to write

$$ER' = ER'\left(p_r R', p_m R', \frac{I}{R^n R'^m}\right) \tag{2.26}$$

Walsh, et al. find experimentally that ER is a relatively weak function of $p_m R$ for Hg-Ar discharges without a magnetic field. It may be, therefore, more convenient to take E/p_r as the basic scaling parameter to be related to the others. Dividing Eq. (2.26) by $p_r R'$

$$\frac{E}{p_r} = \frac{E}{p_r}\left(p_r R', p_m R', \frac{I}{R^n R'^m}\right) \tag{2.27}$$

E/p_r is perhaps the more conventional scaling parameter for single component gas discharges.

In mercury-rare gas discharges the principal non-linear effect is two-stage ionization by way of the 6^3P_1 resonance level. According to Kenty (1950), the density of mercury atoms in the metastable 6^3P_2 level (which contributes very significantly to the ionization) is approximately linear with electron density. Hence n_* represents the density of resonance atoms and is given approximately by

$$n_* \approx \tau n_- p_m \Theta(T_-) \tag{2.28}$$

where τ is the imprisonment time of resonance radiation (Walsh, 1957). When $p_r p_m R$ is low, Doppler broadening dominates the resonance lineshape and τ is approximately proportional to $p_m R$. At higher values of $p_r p_m R$, broadening due to collisions with the rare gas dominates, and τ is roughly proportional to $1/p_r$ (Walsh, 1957). In summary, when the main non-linear effect is two-stage ionization through the resonance level, we can say

$$\begin{aligned} &\text{low } p_r p_m R: && \frac{I}{R^n R'^m} \to \frac{I}{R R'} \\ &\text{high } p_r p_m R: && \frac{I}{R^n R'^m} \to \frac{I R'}{R^2} \end{aligned} \tag{2.29}$$

For Hg-Ar discharges at zero magnetic field Walsh et al. (1963) find both theoretically and experimentally that the transition from low to high regimes occurs at $p_r p_m R \approx 8 \times 10^{-2}$ mm^2-cm. Since collision broadening depends primarily on collision frequency,

one would expect the transition at lower values of $p_r p_m R$ for Hg-He discharges.

2.4 ANOMALOUS DIFFUSION IN THE POSITIVE COLUMN

For all gas discharge experiments performed to date in longitudinal magnetic fields, "classical" diffusion theory appears to account for the observed transverse plasma diffusion so long as the axial magnetic field B_z is lower than a critical value B_c. Above the critical field strength, anomalously large transverse diffusion has been observed in several types of experiments. (See recent reviews by Hoh, 1962; Golant, 1963; and Boeschoeten, 1964).

Perhaps the clearest departure from "classical" to "anomalous" diffusion occurs in the positive column of low pressure arc discharges, a fact discovered by Lehnert (1958). The theory of the positive column in an longitudinal magnetic field predicts that the axial electric field E_z in a constant current discharge should decrease monatonically as the radial diffusion losses are reduced by the magnetic field. As seen from the scaling parameters Eq. (2.27), the magnetic field increases the effective radius R' of the discharge; the diffusion time of ions and electrons is thus increased and less energy is needed to provide the ionization level required for the conduction current. As a result of the reduced energy requirement, the electric field decreases.

Lehnert (1958) and others (Hoh, 1962) have found that the axial electric field E_z behaves as expected only at magnetic field strengths lower than a critical value B_c. At the critical field strength the electric field begins to increase with B_z and the discharge electrical noise increases sharply. Allen et al. (1960) found by photographing the plasma column that a rotating helical instability is formed in the plasma at $B_z = B_c$. At low pressures the critical field is found to be relatively independent of discharge current, the quantity B_c/p scaling with Rp (Vdovin and Nedospasov, 1963). At $B_z \gg B_c$, the discharge plasma takes on a turbulent character, with irregular density fluctuations and electrical noise (Allen et al., 1960).

Theory of Kadomtsev and Nedospasov

A number of theories have been put forth to explain anomalous plasma diffusion, and many experiments have been, and are still being, performed to clarify the problem (for comment and references, see Hoh, 1962, or Boeschoten, 1964). Instability of the positive column has been most successfully described by Kadomtsev and Nedospasov (1960) (hereafter abbreviated KN).

Preceding from Eqs. (2.1) and (2.2) KN assumes that the plasma density and radial potential variation can be written

$$n = n_0 + n_1 \tag{2.30a}$$

$$V = V_0 + V_1 \tag{2.30b}$$

where n_1 and V_1 are small perturbations of the steady state quantities n_0 and V_0 given by Eqs. (2.17) and (2.18).

The density and potential perturbations are taken to be rotating helixes of the form

$$n_1 = f(r)\exp(im\theta + ikz - i\omega t) \tag{2.31a}$$

$$V_1 = g(r)\exp(im\theta + ikz - i\omega t) \tag{2.31b}$$

where m is an integer, and k is the wave number of the perturbation in the z direction.

Eqs. (2.31) are substituted into Eqs. (2.6) and (2.1), the resulting equations linearized, and simplified by assuming $\mu_- R_z \gg 1 \gg \mu_+ R_z$, $D_+ \approx 0$, and $\nu_{c+} \ll \omega$. The equations are then integrated over the discharge column to find a dispersion relation $\omega = \omega(k)$. For the m = 1 helix the stability condition Im $(\omega) \leq 0$ gives

$$KX^4 + FX^2 + G \geq 0.163 \frac{RE_z \mu_- X}{2.405 T_- \mu_+} \tag{2.32}$$

where T_- is in volts and

$$\left.\begin{aligned} K &= \frac{1.28+y}{y(1+y)} \\ F &= \frac{0.8(2+y)}{y} \\ G &= \frac{0.48(1+y)}{y} + 0.1\frac{\mu_-}{\mu_+(1+y)} \\ X &= \frac{\mu_- B_z R k}{3.83} \\ y &= \mu_+ \mu_- B_z^2 \end{aligned}\right\} \qquad (2.33)$$

The axial wave number of the least stable helix is determined by setting

$$\frac{\partial}{\partial k}[\,\mathrm{Im}(\omega)] = 0$$

KN find that the stability boundary is given by

$$\frac{RE_z}{2.405\,T_-} \leq 12.27\frac{\mu_+}{\mu_-}X(2KX^2+F) \qquad (2.34)$$

with

$$X^2 = \frac{-F+\sqrt{F^2+12KG}}{6K} \qquad (2.35)$$

Eq. (2.34) has been plotted by von Gierke and Wöhler (1962) and is reproduced in Fig. 2.1.

The rotation frequency of the helix is found from Re (ω) and is given by the approximate expression

$$f \approx \frac{10\mu_+ D_-}{\mu_-^2 B_z R^2} \qquad (2.36)$$

The physical mechanism of the KN instability has been described by Hoh and Lehnert (1961) and Kadomtsev (1962b). Instability of a helical density perturbation depends on the presence of a radial gradient of electrical conductivity perpendicular to the imposed electric and magnetic fields. The conductivity in the positive column is proportional to

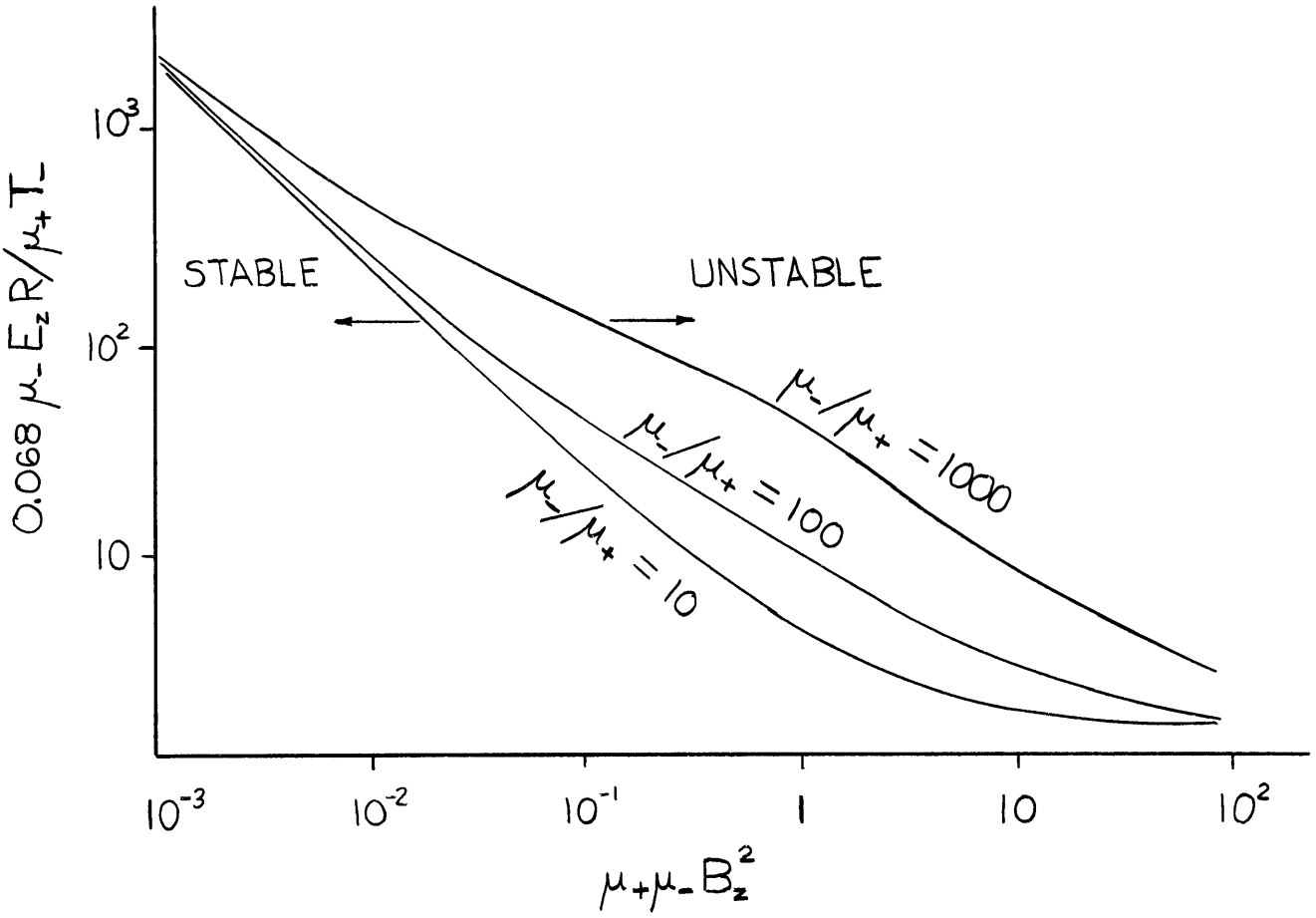

Fig. 2.1 Stability boundaries from KN theory. From von Gierke and Wöhler (1962).

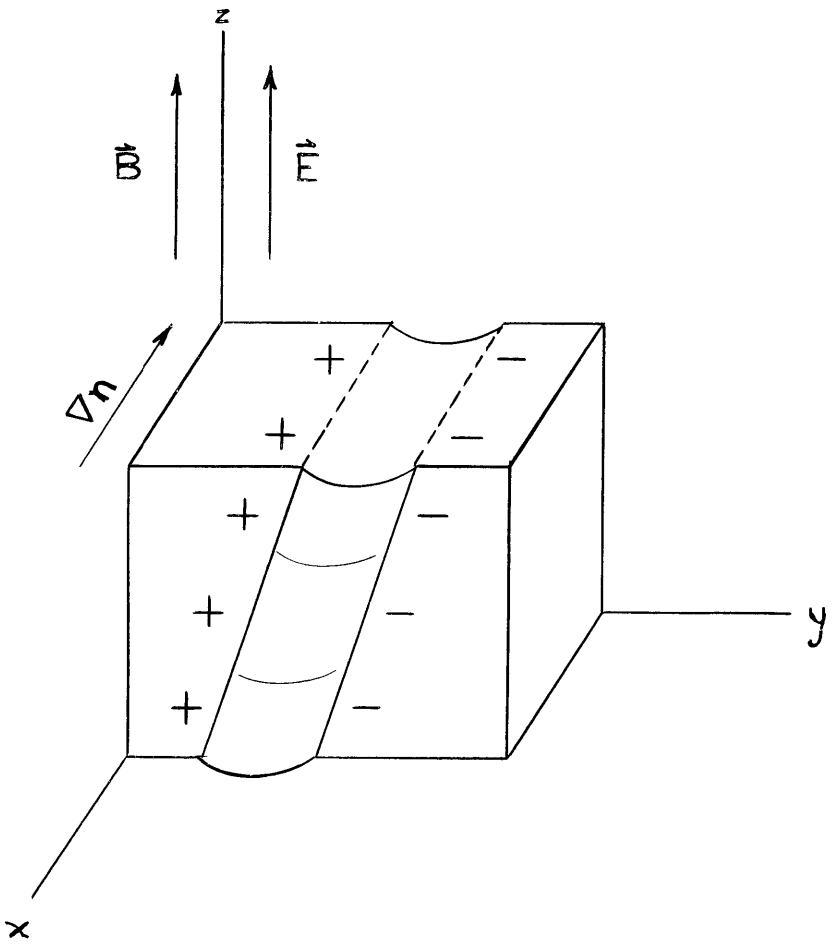

Fig. 2.2 Density perturbation in KN instability. For a cylindrical tube, x represents the radial direction.

the electron density and decreases with radius. A helical perturbation supplies a local region of higher density which becomes polarized by the axial electric field, Fig. 2.2. If the pitch of the helix is of the proper sense, the polarization electric field will have an azimuthal component which, when crossed with B_z, will increase the purturbation displacement. Charge diffusion, conduction, and the Hall current will tend to destroy the perturbation; the critical magnetic field occurs when the perturbation growth rate exceeds the rate of dissipation.

The theory was somewhat clarified by Johnson and Jerde (1962) who solved the problem without making KN's simplifying physical and mathematical assumptions. The more refined theory gives somewhat better comparison with experiment (Rugge and Pyle, 1964), but the KN theory remains a good approximation.

The KN theory has been tested experimentally for discharges in the rare gases, hydrogen, deuterium, and nitrogen (Golant, 1963; Boeschoten, 1964) at pressures from about 0.1 mm Hg to 10 mm Hg and discharge radii from 0.2 cm to 2.75 cm; the discharge positive columns have ordinarily been operated in a d.c. axial electric field, but Rugge and Pyle (1964) also tested the effect of an a.c. field. Johnson and Jerde (1964) have studied the effect of a time varying magnetic field. In all cases in this pressure range, the KN theory has accurately predicted the value of B_c and, when observable, the rotation frequency of the helical perturbation. The KN theory has also been applied with success to semiconductor rods in an axial magnetic field (Glicksman, 1961).

Akhmedov and Zaitsev (1963, 1964) have pointed out two effects not predicted by KN. First, the frequency of electrical noise associated with the plasma helices is found to increase with B_z above the critical magnetic field. Eq. (2.36) would predict the opposite effect, assuming that D_- is independent of B_z and that the linearized theory is still reasonably valid after the onset of instability. Second, they find that the critical magnetic field is lower than predicted for discharges at pressures from approximately 10 to 40 mm Hg in helium and in neon.

No theoretical explanation has been advanced to explain Akhmedov and Zaitsev's first observation, but it is likely that the KN theory, modified to include volume recombination and a radial temperature gradient, would explain the second.

Besides predicting the onset of instability, KN attempted to describe the radial plasma diffusion at $B_z > B_c$. They assume that the growth of the perturbation is soon balanced by plasma losses to the walls, so that the helix settles into a rotating stationary state. The increased plasma losses require a higher frequency of ionization and, in turn, increased E_z. KN compare the theory with E_z measurements in a helium discharge (Hoh and Lehnert, 1960) and find fairly good agreement for B_z up to 25% greater than B_c. At higher B_z, the theory predicts consistently low E_z; the observed plasma density is chaotic and can be qualitatively described as "turbulent".

2.5 TURBULENT DIFFUSION

Turbulence in ordinary fluids is far from being completely understood theoretically, and the added difficulties involved in effects of electric and magnetic fields in a turbulent plasma are formidable. The major problem in developing a theory of plasma turbulence is that the dynamics of the motion is described by strongly non-linear differential equations for which no general solutions have been found. A few qualitative and semi-quantitative theories have been proposed, however, which are reviewed here.

"Bohm Diffusion"

The first attempt to predict transverse diffusion in a turbulent plasma was by Bohm (1949) who suggested that the turbulent diffusion coefficient should be

$$D_B \approx \frac{1}{16} \frac{T_-}{B_z} \tag{2.37}$$

where T_- is in volts and B_z in w/m^2. Bohm postulated that the electric field of irregular plasma fluctuations, crossed with the magnetic field, provides the driving force of the

diffusion flow.

A simple argument can be made to support Bohm's postulate. Consider a small volume of plasma with a homogeneous magnetic field in the z direction and a density gradient in the-x direction. The flux of particles in the x direction will be given by

$$\Gamma_x = -D_x \frac{\partial n}{\partial x}$$

The diffusion coefficient D_x can be written by analogy to kinetic theory,

$$D_x \propto \langle v_x \lambda_x \rangle$$

λ_x is the distance that a blob of plasma travels with coherent motion in the $\pm$ x direction and v_x is its speed,

$$v_x = \frac{E_y}{B_z}$$

If the plasma potential fluctuation is of the order φ over a distance λ_y, then

$$E_y \approx \frac{\varphi}{\lambda_y}$$

and

$$D_x \propto \left\langle \frac{\varphi \lambda_x}{B_z \lambda_y} \right\rangle \tag{2.38}$$

As we see, Bohm estimated that

$$\left\langle \frac{\lambda_x \varphi}{\lambda_y} \right\rangle \approx \frac{1}{16} T_-$$

Spitzer (1960) and Yoshikawa and Rose (1962) have rederived Eq. (2.37) in greater detail, but they still start from the assumption of given turbulent plasma density fluctuations. The proportionality factor between D_x and T_-/B_z varies somewhat, depending on the assumptions used.

Kadomtsev's Turbulence Theory

Kadomtsev has attempted to account for the physical processes which drive the density fluctuations of turbulent plasmas in strong magnetic fields. For the positive column (Kadomtsev, 1962b) and for fully ionized plasmas with a transverse temperature gradient (Kadomtsev, 1962a), the KN instability with many excited azimuthal and longitudinal modes

is proposed to provide the turbulence. For inhomogeneous "collisionless" plasmas, Kadomtsev (1963) invokes a similar instability, Rudakov and Sagdeev's (1961) "drift-waves".

For the positive column in a strong longitudinal magnetic field, Kadomtsev (1962b) considers a small volume of plasma with electric and magnetic fields in the z direction and a density gradient in the - x direction, Fig. 2.2. Ion diffusion is neglected as well as, for $B \gg B_c$, the transverse electron mobility and diffusion coefficients $\mu_{\perp -}$ and $D_{\perp -}$ (Eqs. (2.12)). With these, plus the approximation $\mu_-^2 B^2 \gg 1$, the electron and ion velocities become, from Eqs. (2.5)

$$\vec{v}_{\perp -} \approx \frac{\vec{B}}{B^2} \times \left(\nabla \varphi - T_- \frac{\nabla n}{e n} \right) \tag{2.39a}$$

$$v_{z-} = \mu_- \frac{\partial \varphi}{\partial z} - D_- \frac{1}{n} \frac{\partial n}{\partial z} - \mu_- E_z \tag{2.39b}$$

$$\vec{v}_{\perp +} \approx \mu_+ \mu_{\perp +} \vec{B} \times \nabla \varphi - \mu_{\perp +} \nabla_\perp \varphi \tag{2.40a}$$

$$v_{z+} \approx -\mu_+ \frac{\partial \varphi}{\partial z} \tag{2.40b}$$

Note that the potential φ does not include the steady longitudinal field E_z. We have also made the substitution $D_- = \mu_- T_-$ in Eq. (2.39a), which is valid for a Maxwellian distribution of electron velocities.

Kadomtsev then assumes linear density and potential perturbations of the form $\exp [i k \cdot r - i \omega t]$, where $k^2 = k_x^2 + k_y^2 + k_z^2$. By substituting Eqs. (2.39) and (2.40) into the equations of charge conservation Eqs. (2.1) and linearizing, it is possible to obtain the dispersion relation for small oscillations.

$$\omega = (-k_z E_z \mu_- - i D_- k_z^2) \cdot \frac{\mu_+ k_z^2 + \mu_{\perp +} k_\perp^2 - i k_y \mu_{\perp +} \mu_+ B \frac{d}{dx} \ln n_o}{(\mu_+ + \mu_-) k_z^2 + \mu_{\perp +} k_\perp^2 + \frac{i k_y}{B(1 + \mu_+^2 B^2)} \frac{d}{dx} \ln n_o} \tag{2.41}$$

where $$k_\perp^2 = k_x^2 + k_y^2$$

To find the growth rate of small perturbations, we solve for the "increment," Im(ω). For the case of a highly magnetized plasma, i.e. $\mu_+^2 B^2 \gg 1$,

$$\mathrm{Im}(\omega) \approx E_z \sqrt{\mu_+ \mu_-} \frac{d \ln n_0}{dx} \frac{\gamma}{1+\gamma^2} \frac{k_y}{k_\perp} - D_- \frac{k_\perp^2}{\mu_+ \mu_- B^2} \cdot \frac{\gamma^2}{1+\gamma^2} \tag{2.42}$$

where

$$\gamma^2 = \mu_+ \mu_- B^2 \frac{k_z^2}{k_\perp^2}$$

From Eq. (2.42) we see explicitly that the growth of perturbations depends on the presence of an electric field and a density gradient.

For a prescribed k_y, the largest growth rate occurs for a perturbation with $k_y/k_\perp \to 1$; that is, $k_x \to 0$. The x wavelength of this perturbation is very long, so that a thick slab moves in the x direction. Further, the largest increment occurs for perturbations with a minimum value of $k_\perp$. Under these conditions, the second term of Eq. (2.42) can be dropped and the first has a maximum at $\gamma = 1$. Thus, the perturbation with the maximum growth rate has an increment given by

$$\omega_{i\,max} \approx \frac{1}{2} E_z \sqrt{\mu_+ \mu_-} \frac{d \ln n_0}{dx} \tag{2.43}$$

Under conditions wnere $\mu_+^2 B^2 \ll 1$, and the original assumptions still hold, Kadomtsev finds that the increment of the fastest growing perturbations is approximately

$$\omega_{i\,max} \approx \frac{0.32}{\mu_+ B} E_z \sqrt{\mu_+ \mu_-} \frac{d \ln n_0}{dx} \tag{2.44}$$

The similarity between Eqs. (2.43) and (2.44) suggests that Eqs. (2.43) can still be used when $\mu_+ B \approx 1$.

Kadomtsev points out that Eq. (2.43) is similar in form to the increment of convective instability of an inhomogeneous heavy fluid in a porous medium. Employing

the concepts of fluid dynamic turbulence, Kadomtsev relates the density fluctuation n_1 to the unperturbed density gradient by way of a "mixing length" ℓ (Prandtl, 1952).

$$n_1 \approx \ell \frac{dn_0}{dx} \tag{2.45}$$

Kadomtsev estimates the velocity fluctuation v_1 by

$$v_1 \approx \ell \omega_{imax}$$

The turbulent flux of particles across the magnetic field is then given approximately by $|n_1 v_1|$ or

$$\Gamma_x \approx - D_T \frac{dn}{dx} \tag{2.46}$$

where

$$D_T = \frac{\ell^2}{2} E_z \sqrt{\mu_+ \mu_-} \left| \frac{dn}{dx} \right| \tag{2.47}$$

for $(\mu_+ B)^2 > 1$, and

$$D_T = \frac{0.32 \ell^2}{\mu_+ B} E_z \sqrt{\mu_+ \mu_-} \left| \frac{dn}{dx} \right| \tag{2.48}$$

for $(\mu_+ B)^2 \ll 1$.

Note that Eq. (2.48) varies as 1/B like the Bohm diffusion coefficient, Eq. (2.37).

Kadomtsev argues by analogy with fluid dynamic trubulence that the mixing length ℓ should be proportional to the discharge tube radius R. By comparing with experimental data in He, H, and N, he concludes that the ratio ℓ/R is of the order of 0.1.

Kadomtsev has calculated the radial density distribution in a turbulent discharge (Kadomtsev, 1962b, Fig. 3). Further, he shows that the available data for the discharges at $B \gg B_c$ support the theory. Finally, he suggests that the greater electron mobility in a

turbulent plasma will cause the tube walls to charge up to a negative potential with respect to the center of the discharge,

$$V_r \approx - \frac{E_s}{E_o} T_- \tag{2.49}$$

where E_o and E_s are respectively the axial electric fields at zero magnetic field and in the turbulent state.

Very little experimentation has been performed to test Kadomtsev's theory. An experiment by Artsimovich and Nedospasov (1963) in a turbulent helium discharge at $B \approx 8 B_c$ and $\mu_+ B \approx 5$ indicates that the radial plasma density variation is very close to prediction when $Rp \leq 5 \times 10^{-2}$ cm-mm Hg. For $Rp \approx 5 \times 10^{-1}$ cm-mm Hg and $B \approx 3 B_c$, the radial density does not follow the theoretical curve, but for this case $\mu_+ B \approx 0.5$. The radial potential variation is completely different from Kadomtsev's estimate; the discharge tube walls were found to be positive with respect to the center. In another experiment in He at 0.15 mm Hg (Woehler, 1964) and magnetic field of 6,000 gauss, it is reported that the mixing length and radial density profile is not as predicted by Kadomtsev. Obviously, more experimentation is necessary to clarify the problem.

III. EXPERIMENTAL PROGRAM

3.1 PURPOSE

The general purpose of the experimental program is to test the validity of the theory of transverse plasma diffusion under conditions which have not yet been fully studied or never before encountered. To do this we have chosen to investigate diffusion in the positive columns of low pressure arc discharges in pure helium (He) and pure argon (Ar) at generally lower pressures, larger tube radii and higher magnetic fields than reported to date. In order to test the theory of transverse diffusion in simple two-component gas discharges, we have also studied the behavior of helium-mercury (He-Hg) positive columns in a longitudinal magnetic field.

Rare-gas discharges in longitudinal magnetic fields have been fairly extensively investigated in the past. In particular, experimental parameters in He discharges have been varied over a considerable range; and it has been found that "classical" diffusion theory, KN instability theory, and Kadomtsev's turbulence theory describe the transverse plasma diffusion with varying degrees of success (see Sections 2.4 and 2.5). Hoh and Lehnert (1960) and Paulikas (1961) have studied Ar discharges in longitudinal magnetic fields, but no data have been published at field strengths considerably greater than the critical magnetic field B_c. The He and Ar background data will serve as standards of comparison for the results of this experiment.

The mercury-rare gas discharge is rather well understood theoretically (Waymouth and Bitter, 1956; Cayless, 1963), and the effect of a longitudinal magnetic field is readily included in the theory (assuming "classical" diffusion, Section 2.3). Apparently no experimental investigations of mercury-rare gas discharges in magnetic fields have been published. Although there are probably no a priori reasons that diffusion theories developed for single component gas discharges might fail in more complex plasmas, experimental test is obviously necessary to complement the theory.

3.2 APPROACH

Two methods were adopted to study transverse plasma diffusion in the discharges in a longitudinal magnetic field. First, the axial electric field E_z was determined as a function of magnetic field B_z by measuring the potential drop between plasma probes mounted along the length of the discharge tube. (See Section 3.3 for details.) This measurement, although indirectly related to the transverse diffusion rate, has the advantage of being simple and well proved by other experimenters. The axial electric field reflects the average properties of the discharge plasma and is less sensitive to local perturbations than other parameters related to transverse diffusion. Second, the potential difference between probes at the center and wall of the discharges was used for a more direct measurement of the diffusion.

For "classical" magneto-ambipolar diffusion, the radial potential drop is given by Eq. (2.18). Ecker (1961) has shown theoretically that departures from classical diffusion should be strongly reflected in the radial potential drop. A difficulty for quantitative comparison of experiment with theory is estimation of the wall sheath thickness to include in Eq. (2.18). The effect of the magnetic field on the sheath is also not well known. Fortunately, the Bessel function in Eq. (2.18) varies slowly with small changes of the sheath thickness.

Another possible difficulty arises if the electron temperature varies radially in the discharge. Besides requiring modification of the effective diffusion coefficients in the plasma, a radial temperature gradient would change the relationship between the plasma potential and the measured "floating" probe potential. According to simple Langmuir probe theory (Loeb, 1955), the difference between floating and plasma potential is directly proportional to the electron temperature,

$$V_f - V \approx -\frac{T_-}{2} \ln\left(0.65 \frac{m_+}{m_-}\right) \qquad (3.1)$$

If the electron temperature varies with radius, the radial potential drop, defined as

$$V_r = V(R) - V(0) \tag{3.2}$$

will not be correctly given by measurements of the floating potential drop. In active rare gas and Hg-rare gas discharges it is probably valid to assume the electron temperature to vary no more than 20% radially, as long as the product $p_r R$ does not exceed approximately 10 mm Hg-cm (Francis, 1956; Verweij, 1960).

Past experimental work has shown that the electrical noise in plasmas in magnetic fields increases considerably at the onset of instabilities. A high-speed oscilloscope was used in the experiment to monitor noise on the plasma probes and at the anode of the discharge. The discharges were also observed visually for gross structure and with a hand spectroscope to detect impurity gases.

3.3. DESCRIPTION OF EXPERIMENT

3.3.1 Apparatus

The experimental system was designed for making measurements as a function of magnetic field at a number of different gas pressures, discharge radii, and currents. Fig. 3.1 shows a schematic diagram of the system.

The lamp current was provided by either a 0-2500 volt, 0.3 amp, regulated d.c. power supply or a bank of automobile storage batteries supplying approximately 384 volts. The current was limited by a ballast resistance variable between 0 and 1500 ohms. The cathode heating current was provided by a 12 volt storage battery.

The vacuum system consisted of a three stage oil diffusion pump followed by a mechanical forepump. A liquid nitrogen cold trap isolated the vacuum pumps from the discharge tube. An ionization gauge was used to measure pressures below 10^{-3} mm Hg and a Continental Vacuum Corporation Autovac gauge (Pirani type) was used to measure pressures above 10^{-2} mm Hg. The Autovac gauge was calibrated against a CVC Type GM-100A McLeod gauge also connected to the system.

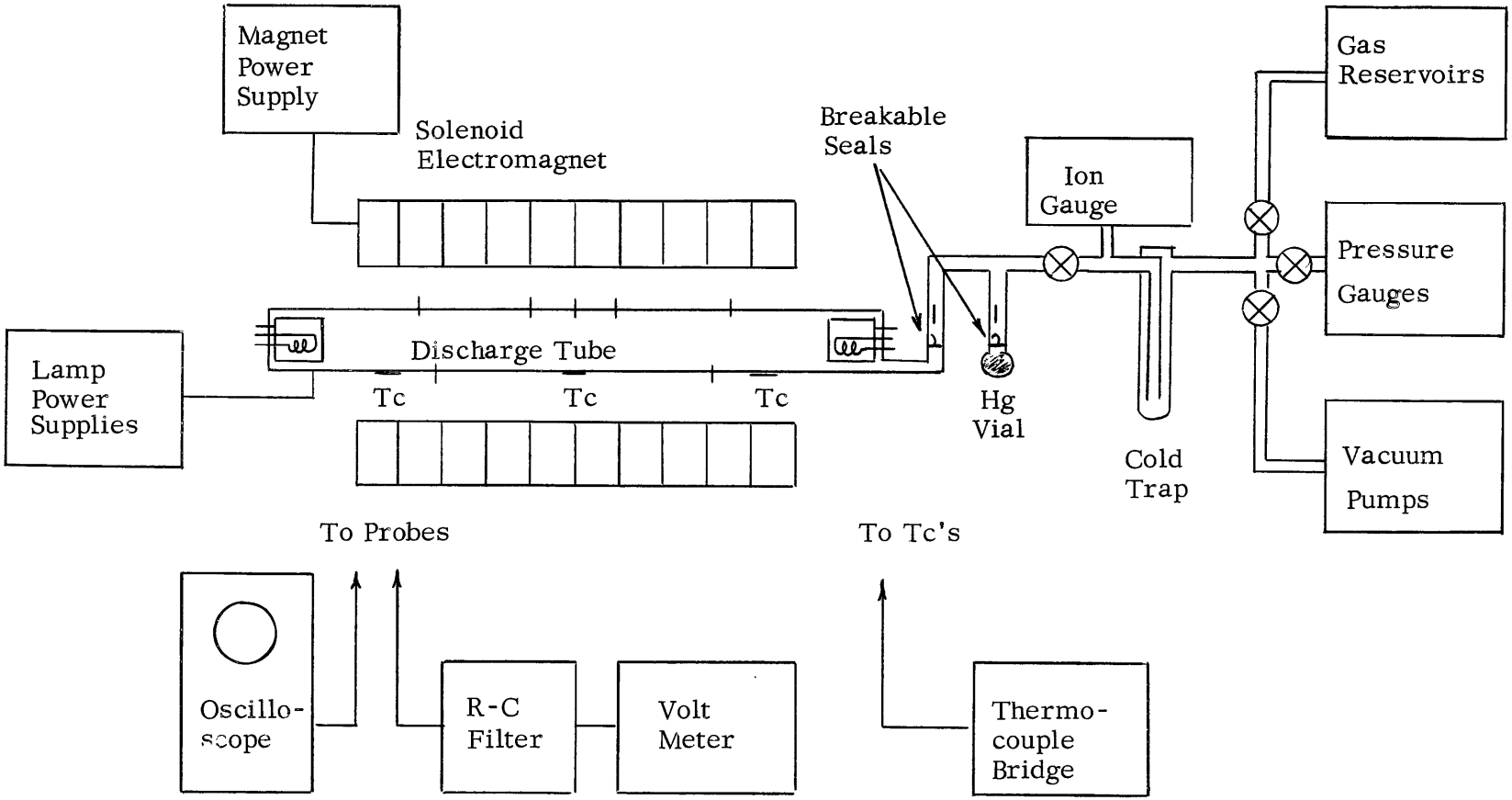

Fig. 3.1 Experimental arrangement.

The probe potentials were measured with a Keithley Model 610A vacuum tube electrometer with an R-C filter to suppress the noise generated in the plasma in a magnetic field. The time constant of the filter was 1 sec.

The lamp wall temperature was measured in three places with iron-constantin thermocouples fastened to the outside of the tubes by a layer of Teflon tape.

3.3.2 Discharge Tubes

Fig. 3.2 shows typical dimensions of the discharge tubes. The two Pyrex glass tubes had inside radii of 1.1 and 2.76 cm. The anode-cathode structures were identical at both ends of the lamps to permit reversing the direction of the discharge current. The anodes were stainless sheet steel cylinders, and the cathodes were flourescent lamp type double coiled tungsten wire with a tri-oxide coating. The cathodes were heated to red heat (approximately 900^{o}C) during operation.

The plasma probes were made of 40 mil tungsten wire. The plane center and wall probes were glass covered and cut flush to expose only the 40 mil diameter cross section. When the center probes face the discharge cathode, the plane wall probes are nearest the cathode end of the lamps. The plane wall probe of the 2.76 cm lamp was mounted radially opposite the center probe and flush with the tube wall; the plane wall probe in the 1.1 cm lamp was longitudinally offset 0.9 cm from the center probe because of the tube construction difficulties. The cylindrical wall probes protrude 3 mm into the tube and were arranged such that each wall probe was offset azimuthally by an angle of about 30^{o} from its immediate neighbors; the probes thus could not cast plasma "density shadows" on one another at high magnetic fields.

Before being installed in the experimental system, the lamps were processed in a bake-out vacuum system. The tubes were evacuated and baked at 350^{o}C until the background pressure was approximately 10^{-7} mm Hg. The cathodes were then activated, and the tubes filled with spectroscopically pure He to about 1 mm Hg pressure. The lamps were operated for at least an hour at 0.3 amp discharge current on

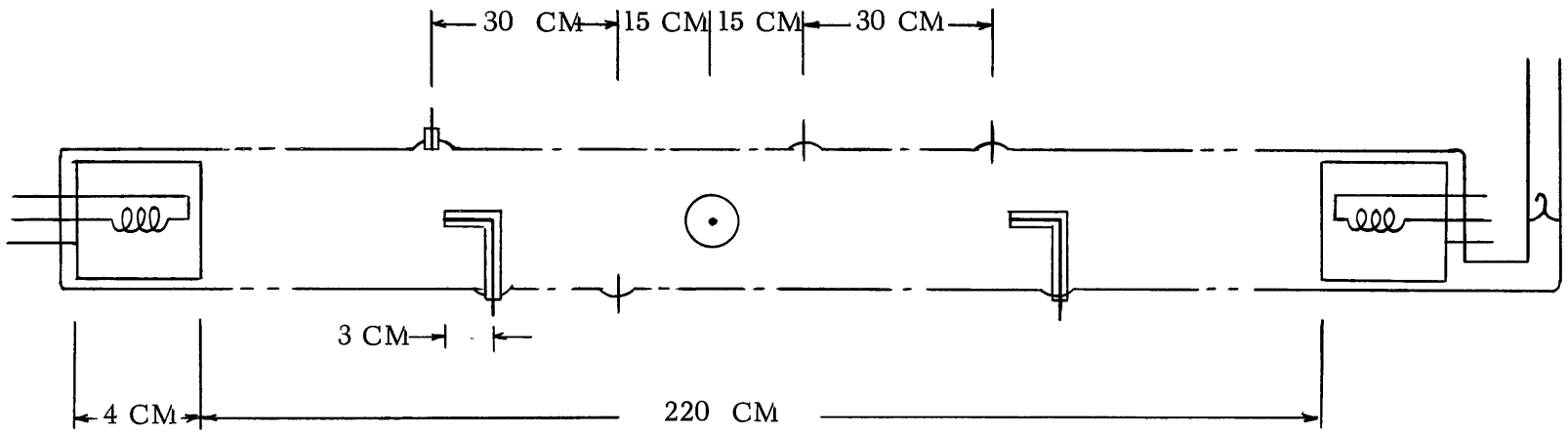

Fig. 3.2 Typical dimensions of discharge tubes. See text.

each cathode and periodically checked for purity with a hand spectroscope. The tubes were then re-evacuated and rebaked before being sealed off at a pressure of about 10^{-7} mm Hg.

After processing, the lamps were mounted in the solenoid and connected to the vacuum system by way of a breakable glass seal. The seal was not broken until the system pressure was below 5×10^{-7} mm Hg. The pressure was monitored as the lamps were opened to the vacuum system to be sure that no leaks or degassing had taken place in the tubes after being sealed. For the lamps used, no pressure increase was observed when the glass seal was broken.

3.3.3 Magnetic Field

The longitudinal magnetic field was produced by a water-cooled solenoid electromagnet provided by the M. I. T. National Magnet Laboratory. The longitudinal homogeneity of the field is within 3% over a 1.3 meter length. The radial variation of the field is less than 0.2% over the cross section of the discharge tubes. Fig. 3.3 shows the axial field over the length of the magnet, as measured by a Newport Instruments Type J integrating magnetometer. The magnetic field as a function of magnet current is taken to be 6.3×10^{-4} weber/meter^2 (w/m^2) per ampere.

For measurements at magnetic fields lower than 0.35 w/m^2, a current stabilized d.c. power supply provided the magnet power. The a.c. ripple is less than 0.05% at maximum power, and current stability better than 0.1%. One of the M. I. T. National Magnet Laboratory d.c. motor generators was used during measurements at higher fields. Here the current stability and ripple are as good, or better than above.

Fig. 3.4 is a photograph of the solenoid with the 2.76 cm radius tube mounted in it. A He-Hg discharge is visible in the tube.

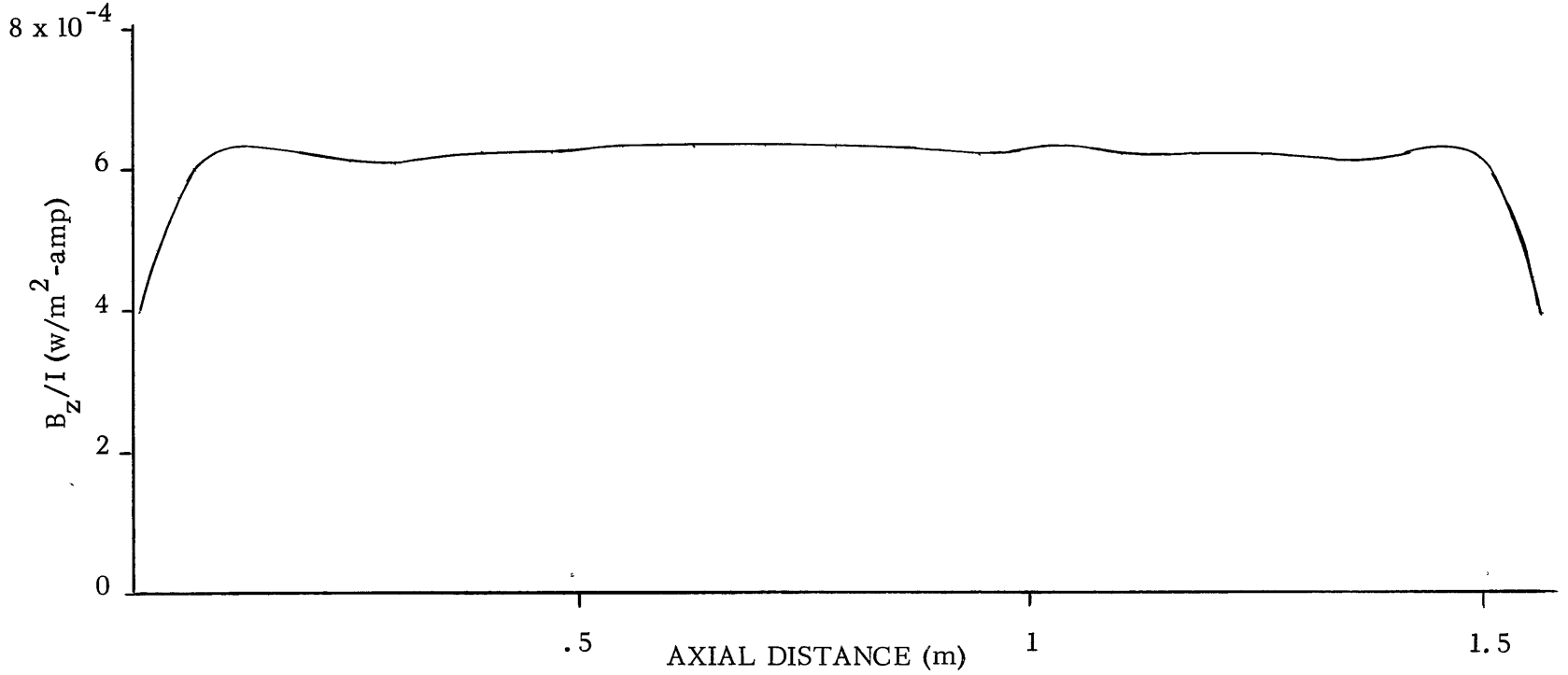

Fig. 3.3 Magnetic field of solenoid electromagnet.

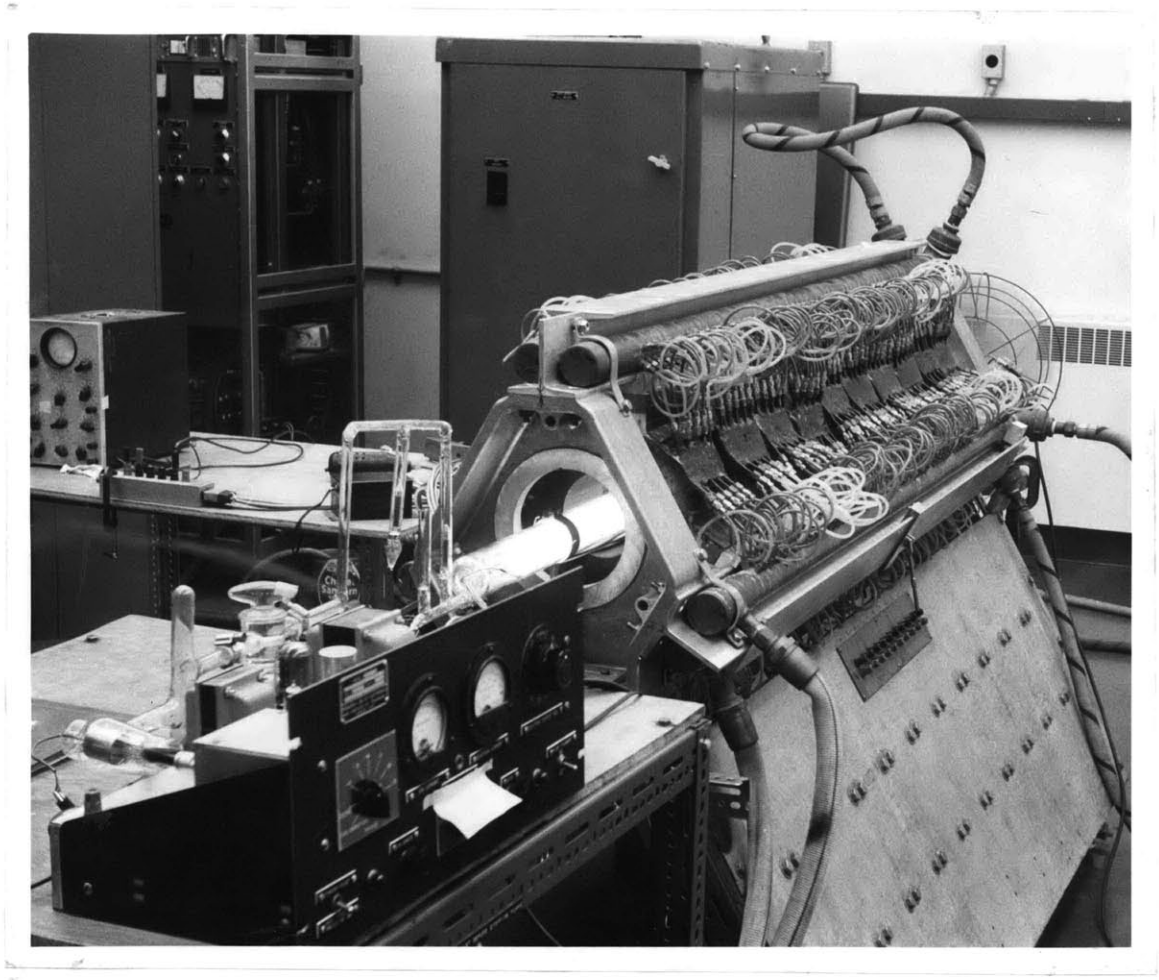

Fig. 3.4 Solenoid electromagnet and 2.76 cm radius lamp. Ionization gauge control in foreground. A He-Hg discharge is visible in lamp.

3.3.4 Measurement Procedure, He and Ar

As soon as the background pressure in the lamp and vacuum system had dropped well below 5×10^{-7} mm Hg, measurements could begin. The diffusion pump inlet valve was closed and spectroscopically pure gas admitted to the lamp and cold-trap assembly. The gas pressure was measured with the calibrated Autovac gauge. Fine pressure adjustments were made by slightly opening the diffusion pump inlet until the desired pressure was reached. The discharge was struck and operated for a few minutes at a current at least equal to the experimental value. The lamp was then re-evacuated and the above procedure repeated several times.

For the actual measurements the lamp inlet stopcock was closed before striking the discharge so that the gas density remained constant. The stopcock was opened and closed several times during each gas flush to accelerate any degassing of the valve. Measurements began only after the purity of the discharge was assured. The discharge purity was checked periodically with the hand spectroscope during each series of measurements.

The axial electric field was determined from the voltage drop between the two center plane probes. These values were checked by measurements between the several wall probes. The radial potential drop was measured between the center and wall plane probes and corrected, using the E_z data, for the wall probe offset in the 1.1 cm lamp. Measurements were taken with the discharge current in both directions in the lamp and were made as a function of decreasing as well as increasing magnetic field strength when possible. In all cases the zero magnetic field data were repeated after each experiment.

All discharges in He and Ar at 0.3 amp lamp current were powered by the electronic supply with about 700 ohms ballast resistance. Discharges with 0.5 amp

current in Ar were supplied by the 384 volt battery bank with ballast resistances of 150 to 550 ohms.

3.3.5 Measurement Procedure, He-Hg

After sufficient data had been gathered on the pure gases in a lamp, the tube was evacuated, the lamp inlet valve closed, and the mercury vial seal broken. The mercury was distilled into the lamp by differential heating until large drops appeared on the tube walls. Helium was admitted to the lamp after first freezing the mercury at the inlet end with a liquid nitrogen cooled blanket. This technique was also used when the helium was being pumped out of the tube between experiments. The lamp was evacuated before and after each set of measurements to ensure maximum gas purity.

The mercury vapor pressure in the discharge was estimated from the inside lamp wall temperature. The outside lamp wall temperature was measured with thermocouples and corrected for the temperature rise across the glass wall. The lamp wall temperature was monitored as a function of magnetic field during the measurements, but it was found to vary very little with magnetic field.

The axial electric field and radial potential drop in the He-Hg discharges were measured in the same manner as with the pure gases.

All Hg-Hg discharges were powered with the electronic supply with about 700 ohms ballast resistance.

3.4 RESULTS

3.4.1 Pure Helium

Figs. 3.5 and 3.6 summarize the experimental results for He discharges in the 1.1 cm and 2.76 cm radius lamps. The broken lines in Fig. 3.5 represent regions of rapid variation of axial electric field E_z and radial potential drop V_r, but where no actual measurements were performed. No E_z data are given for p = 0.05 mm Hg in

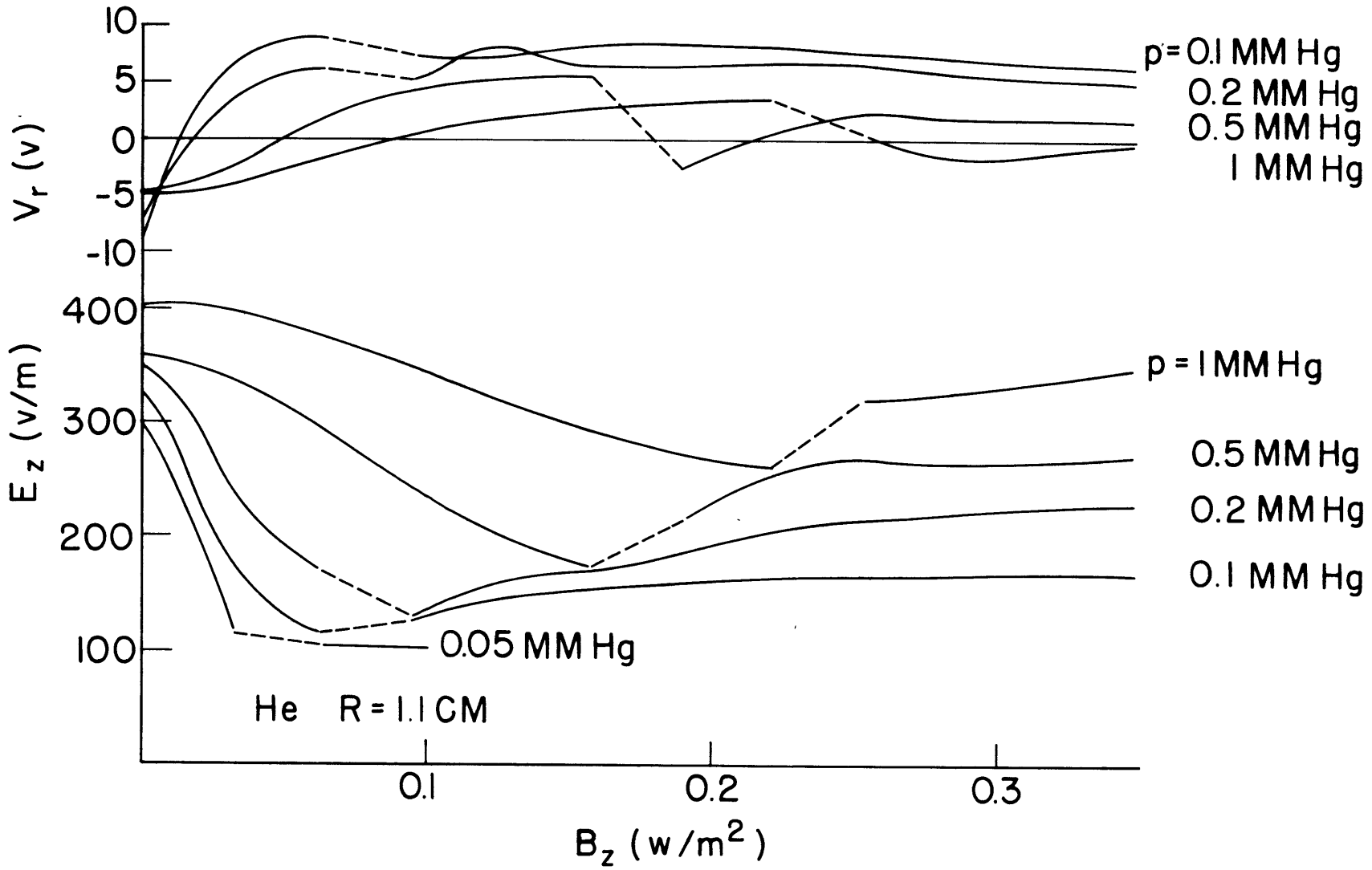

Fig. 3.5 Pure He results. Lamp current I_z = 0.3 amp. Broken lines indicate regions where no measurements were made. V_r data for probes nearest anode.

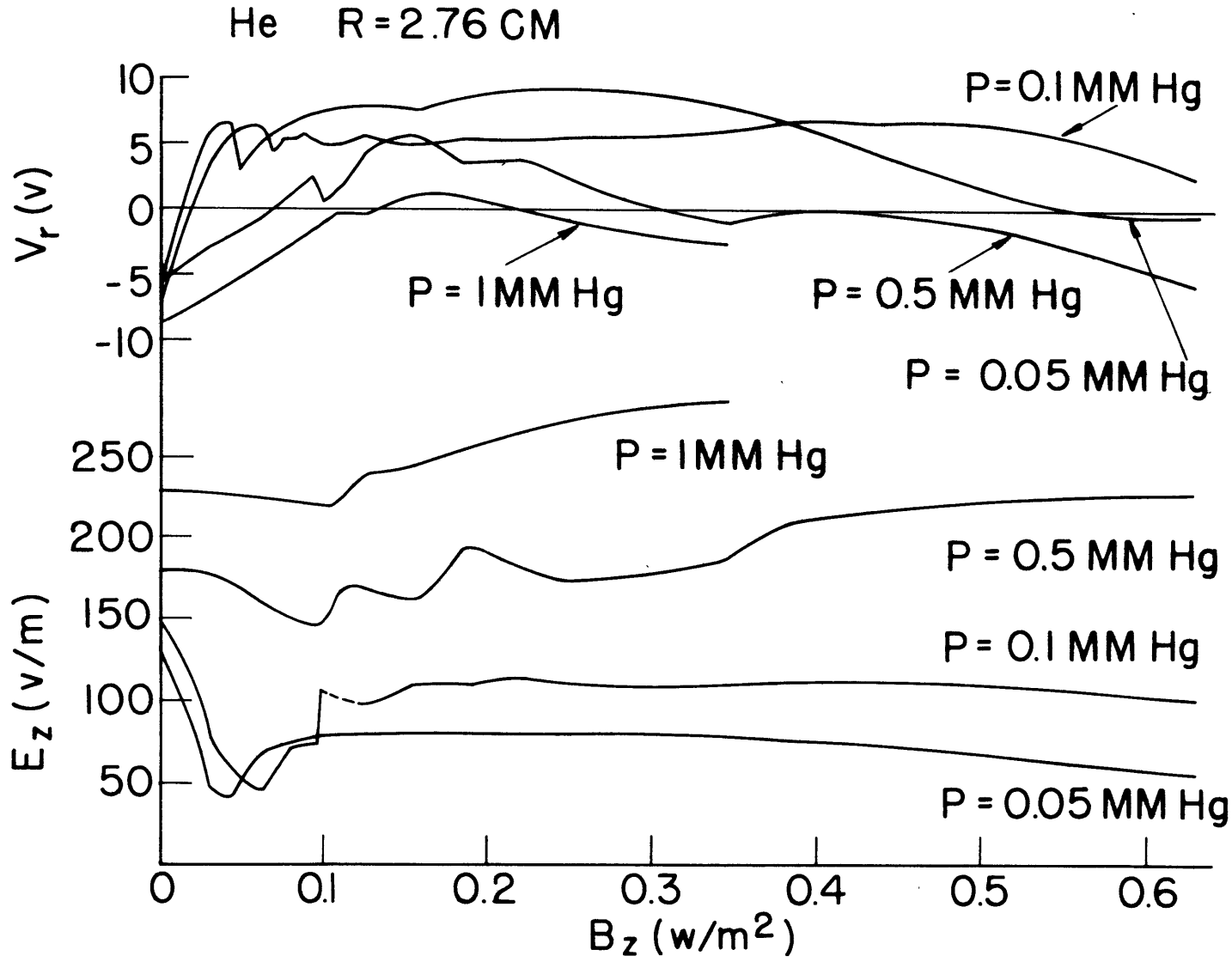

Fig. 3.6 Pure He results. I_z = 0.3 amp. V_r data for probes nearest anode.

Fig. 3.5 above magnetic fields of 0.1 w/m^2 because the discharge extinguishes itself at this point.

The magnetic field B_z was varied in 3.15×10^{-2} w/m^2 steps for measurements in the 1.1 cm lamp, except at p = 0.05 mm Hg where the interval was 6.3×10^{-3} w/m^2 for B_z greater than 0.06 w/m^2. The magnetic field interval for the 2.76 cm radius lamp was 3.15×10^{-2} w/m^2, except near the E_z minimum ($B_z \approx B_c$), where it was 6.3×10^{-3} w/m^2, and at fields higher than 0.35 w/m^2, where it was 6.3×10^{-2} w/m^2.

The He pressures indicated in Figs. 3.5 and 3.6 are measured values at $24^{o}C$. Reduced pressures to $0^{o}C$ are 0.92 times the measured values. Trials with the lamp inlet stopcock open showed that the helium density did not change sensibly over the course of an experiment for pressures greater than 0.1 mm Hg. At 0.1 mm Hg and below, however, there was a "pumpout" effect which gradually lowered the pressure with time. This phenomenon was very pronounced at 0.05 mm Hg where the pressure in the 1.1 cm lamp was halved in 10 to 15 minutes of discharge operation. Similar "pumpout" has also been observed in earlier experiments (Francis, 1956; Hoh and Lehnert, 1960).

The lamp current I_z was 0.3 amp for all He data reported here. A series of measurements of 0.15 amp showed no unexpected differences from the 0.3 amp results.

The axial electric field data for the 2.76 cm radius lamp were repeatable within about 1% for magnetic fields below the critical magnetic field B_c. For fields much greater than B_c, the data were repeatable within 4%. The E_z data were unchanged by reversing the lamp current direction with respect to the center plane probes or the magnetic field. The reproducibility of E_z data in the 1.1 cm radius lamp was the same as above for He pressures greater than 0.1 mm Hg. At 0.1 and 0.05 mm Hg the E_z data were repeatable to only about 5% because of the rapid variation of the gas density due to "pumpout".

The radial potential drop V_r for B_z less than B_c was repeatable within 10% for the 1.1 cm radius lamp at pressures of 1 and 0.5 mm Hg. For lower pressures the measurements could be reproduced only within about 1 volt. The 2.76 cm lamp V_r data were repeatable within about 5% and 1 volt for the same conditions.

All V_r data reported in Figs. 3.5 and 3.6 were made with lamp current direction such that the measurement probes were nearest the discharge anode. Data with the probes near the cathode show anomalously large positive values of V_r at high magnetic fields. At the same time the luminous discharge plasma became visibly collimated in the center of the tube near the cathode end of the solenoid. Apparently the electrons were concentrated toward the center of the lamp by the converging magnetic field lines and a radial space charge electric field was set up. The effect is most pronounced at low pressures.

At low magnetic fields the wall probe E_z measurements were within 2% of the center probe data for both discharge lamps. In the 1.1 cm radius lamp at $B_z \approx B_c$ the wall probes indicated consistently higher values of E_z than the center probes. The discrepancy ranged from 2% at p = 1 mm Hg to 18% at p = 0.05 mm Hg. The wall probe E_z was within 5% of the center probe data for magnetic fields much greater than B_c and pressures greater than 0.1 mm Hg. At p = 0.1 and 0.05 mm Hg the wall probe data were respectively 8% higher and 25% lower than the center probes' at $B_z \approx 0.35$ w/m^2. The wall probe E_z data for the 2.76 cm radius lamp at $B_z \approx B_c$ were within 2% of the center probe results, with no particular direction of difference. At high fields, $B_z \gg B_c$, the wall probes indicated E_z values consistently lower than the center probes. The percentages of difference were 2% at p = 1 and 0.5 mm Hg, 5% at p = 0.1 mm Hg and 15% at p = 0.05 mm Hg at magnetic fields of 0.35 w/m^2.

The noise in the lamps at zero magnetic field was principally due to moving striations. The average noise voltage observed at the cylindrical wall probes of the 1.1 cm lamp was approximately 1% of the total lamp voltage for p = 1 mm Hg and 0.2% for p = 0.5 mm Hg. Below 0.3 mm Hg the zero magnetic field noise was less than

0.03% of the total lamp voltage, and no moving striations were observed. The noise level increased gradually with magnetic field, but showed a sudden sharp increase at $B \approx B_c$. For magnetic fields greater than B_c the probe noise voltage was approximately 5% of the total lamp voltage at p = 1 and 0.5 mm Hg, and 3% for p less than 0.2 mm Hg. The noise voltage observed on the plane probes was less than on the cylindrical probes by at least a factor of 10, probably because of the smaller surface area of the plane probes and the relatively low input impedence of the oscilloscope (10^6 ohms).

3.4.2 Pure Argon

Figs. 3.7-3.9 show experimental results for discharges in argon. The measurement procedure was the same as for He results, except that V_r measurements in the 1.1 cm lamp were made with the probes nearest the discharge cathode.

The most striking phenomenon in the Ar discharges was the existence of two modes of operation at p = 0.5, 0.1, and 0.05 mm Hg in the 2.76 mm lamp. The "low-voltage" mode was characterized by very low axial electric field E_z and very low light output from the plasma in the magnetic field. In the "turbulent" mode E_z was much higher and the discharge tube was completely filled with bright plasma. Mode changes are shown by broken arrows in Figs. 3.8 and 3.9. The transitions were always abrupt, and in some cases the discharge would not stabilize because of fluctuations between the two modes (i.e., p = 0.1 mm Hg, $B_z = 0.56$ w/m^2, Fig. 3.8; and p = 0.05 mm Hg, $B_z = 0.44$ w/m^2, Fig. 3.9). The transition from the turbulent to low voltage modes shows hysteresis at p = 0.05 mm Hg, Fig. 3.9. The upward and downward broken arrows show the mode transitions at increasing and decreasing B_z, respectively.

The magnetic field was varied in 3.15×10^{-2} w/m^2 steps for measurements up to 0.35 w/m^2; at this point the interval was increased to 6.3×10^{-2} w/m^2. More frequent measurements were made near the onset of the turbulent mode of operation

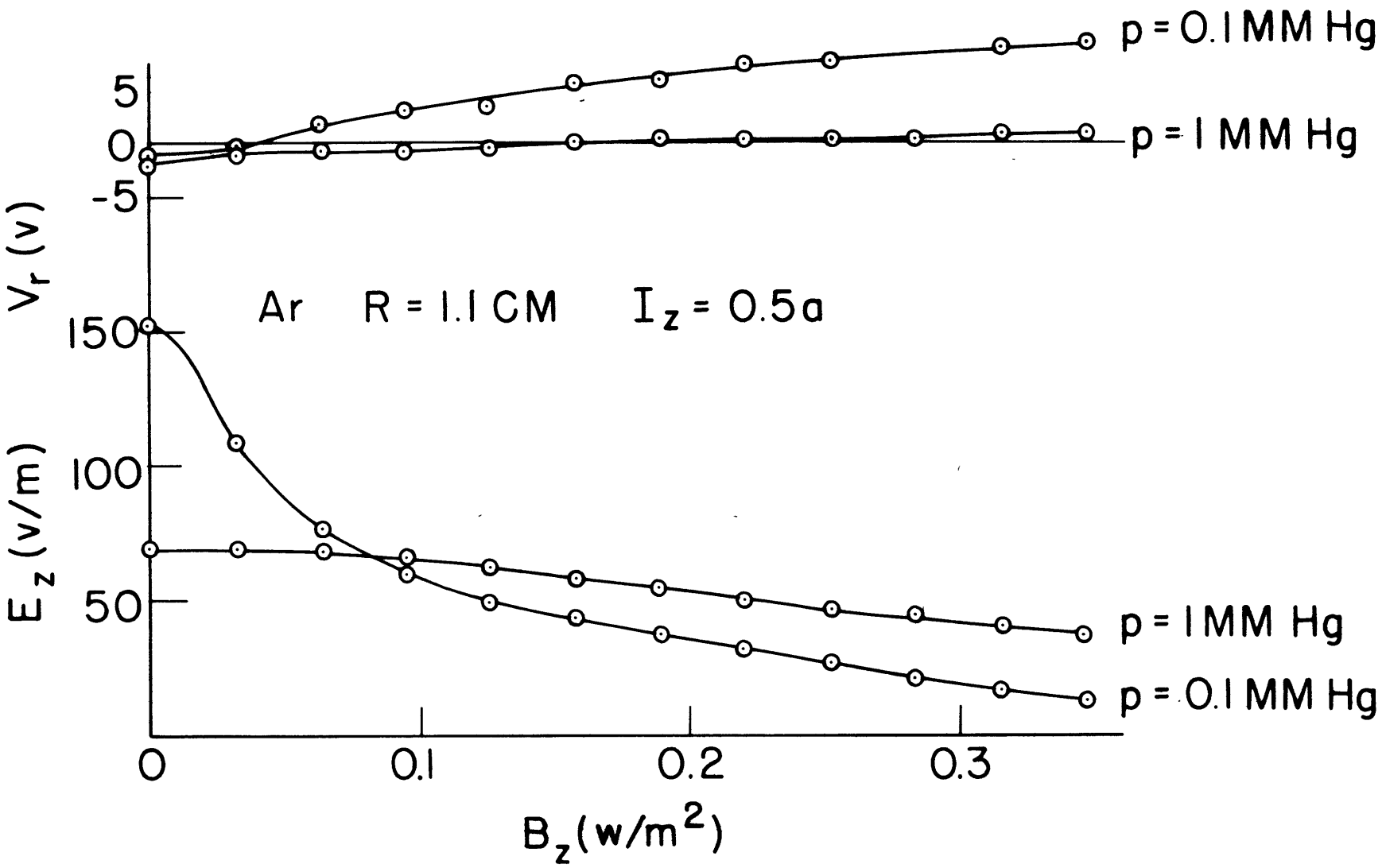

Fig. 3.7 Pure Ar results. V_r data for probes nearest cathode.

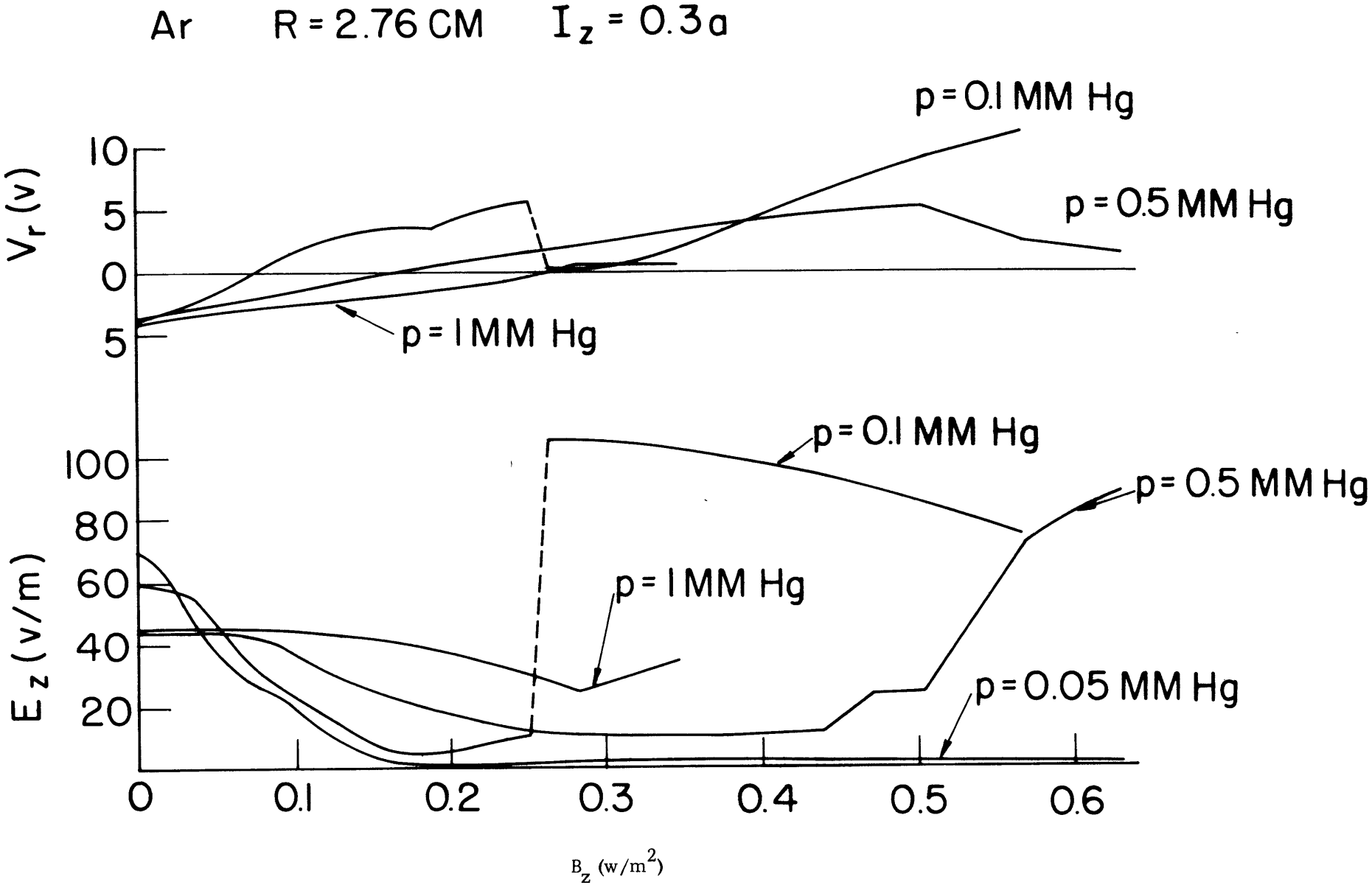

Fig. 3.8 Pure Ar results. V_r data for probes nearest anode.

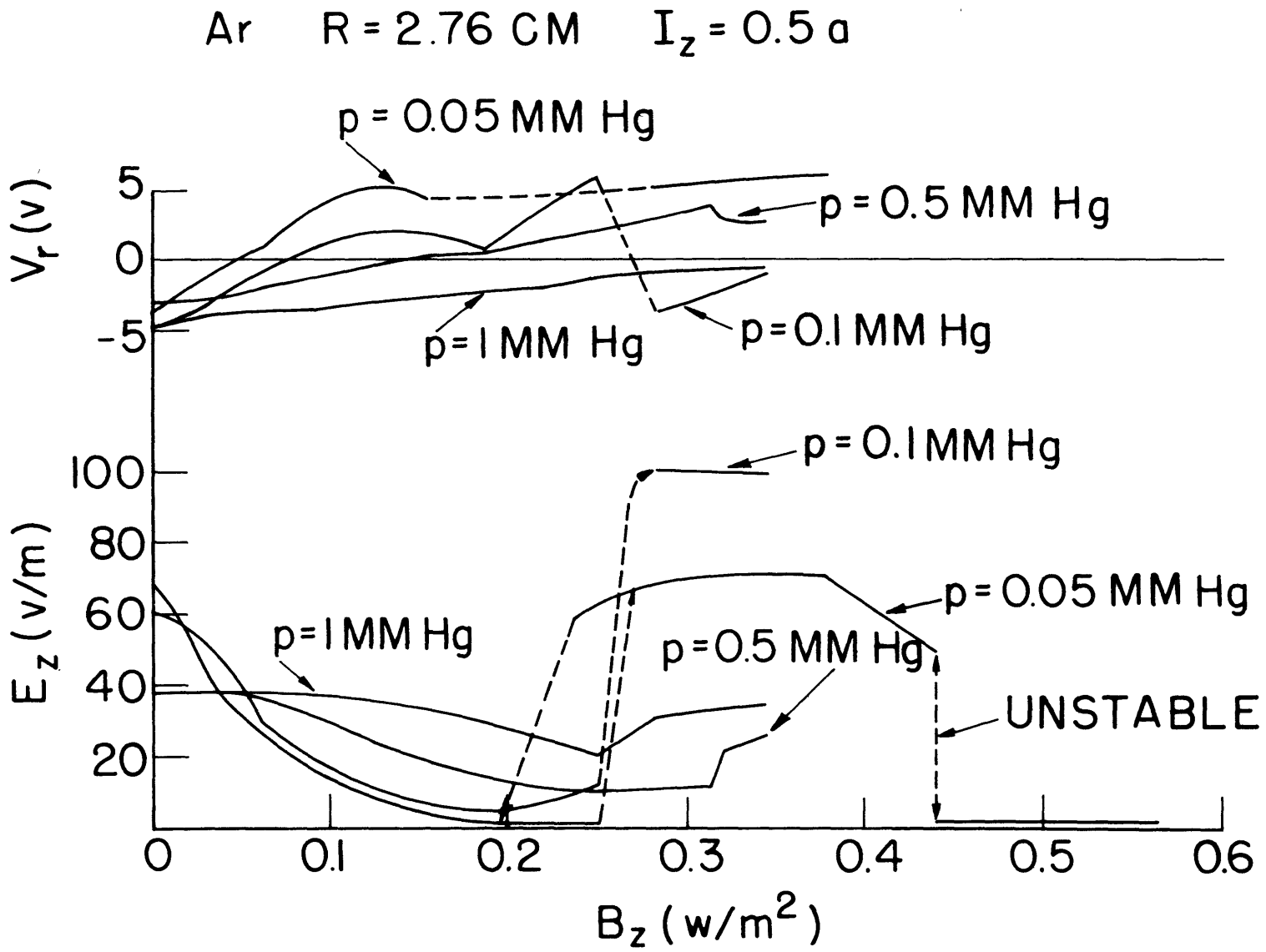

Fig. 3.9 Pure Ar results. Upward (downward) arrows indicate mode changes with B_z increasing (decreasing). V_r data for probes nearest anode.

at low pressures in the 2.76 cm radius lamp.

The indicated pressures were measured at 24°C. Tests with the lamp inlet valve open demonstrated that the Ar density did not change appreciably over the course of an experiment at pressures greater than 0.1 mm Hg. Argon "pumpout" was observed at 0.1 mm Hg in the 1.1 cm lamp and at 0.05 mm Hg in the 2.76 cm lamp.

The axial electric field data for the 1.1 cm radius tube were reproducible to 2% at all values of the magnetic field. Measurements at 0.1 mm Hg must be made rapidly to achieve this accuracy because "pumpout" reduces the gas pressure significantly.

E_z measurements in the 2.76 cm lamp were reproducible to 2% at magnetic fields less than about half of that corresponding to E_z minimum. At higher fields E_z was reproducible to about 5% for pressures of 1 and 0.5 mm Hg. At 0.1 mm Hg and B_z near the E_z minimum ("low-voltage" mode), the axial electric field was reproducible within about 1 volt/meter. In the "turbulent" mode the E_z data were reproducible to 15% between gas changes; with the same gas they were repeatable to 2%. For p = 0.05 mm Hg, the low-voltage mode electric field was reproducible within about 0.5 v/m; in the turbulent mode (Fig. 3.9) the data were reproducible within 5% for B_z less than 0.38 w/m^2. From 0.38 w/m^2 to 0.44 w/m^2 the turbulent mode became unstable, and measurements were unreliable because of rapid fluctuations between the low-voltage and turbulent modes of operation.

The V_r reproducibility was within about 1 volt at all magnetic fields and pressures except p = 0.05 mm Hg in the 2.76 cm tube. At this pressure the electrical noise in the tube was so severe for $B_z > 0$ that only limited V_r data were taken at I_z = 0.5 amp and none at I_z = 0.3 amp.

The axial electric field calculated from wall probe data agreed within 2% of center probe measurements for both lamps at zero magnetic field. The wall and

center probe data agreed to 5% for magnetic fields below about half of the E_z minimum field. In the 1.1 cm lamp at $B_z \approx 0.35$ w/m^2, the wall probes indicated 5% (p = 1 mm Hg) and 14% (p = 0.1 mm Hg) lower values of E_z than the center probes. In the 2.76 cm lamp near the E_z minimum the wall probes indicated 20% low E_z for p = 1 and 0.5 mm Hg. At p = 0.1 and 0.05 mm Hg in the 2.76 cm lamp the wall probe measurements showed negative E_z in the low-voltage mode of operation. The wall probe E_z values were approximately -2 v/m and -3 v/m respectively for these pressures. The low frequency electrical noise on the wall probes was of the same order of magnitude as the potential drop between them, and the negative E_z may be due to false readings. In the turbulent mode the wall probes indicated 20% higher E_z for p = 0.1 and 0.05 mm Hg than the center probe data.

The electrical noise in the 1.1 cm radius lamp was not noted for Ar discharges. In the 2.76 cm lamp the noise was regularly observed at the discharge anode and only occasionally on the probes. At $B_z = 0$ the noise was due to moving striations and, in some cases, to anode oscillations. The zero magnetic field noise voltage at the anode was about 4% of the total lamp voltage at p = 1 and 0.5 mm Hg and about 3% at p = 0.1 and 0.05 mm Hg. The noise increased near the E_z minimum to about 10% of the total lamp voltage. In the turbulent mode of operation, the magnitude of the noise voltage increased, but the percentage of the total lamp voltage decreased to about 6%.

3.4.3 Helium-Mercury

Figs. 3.10-3.18 show experimental results for discharges in He-Hg mixtures. In Fig. 3.18 the results are given for measurements with the center probes facing the anode and the V_r measuring probes nearest the anode of the discharge.

The data points represent consecutive measurements with increasing magnetic field. The He gas is changed before reversing the direction of the discharge current; and apparently the data spread is mainly a result of changing the He and not the

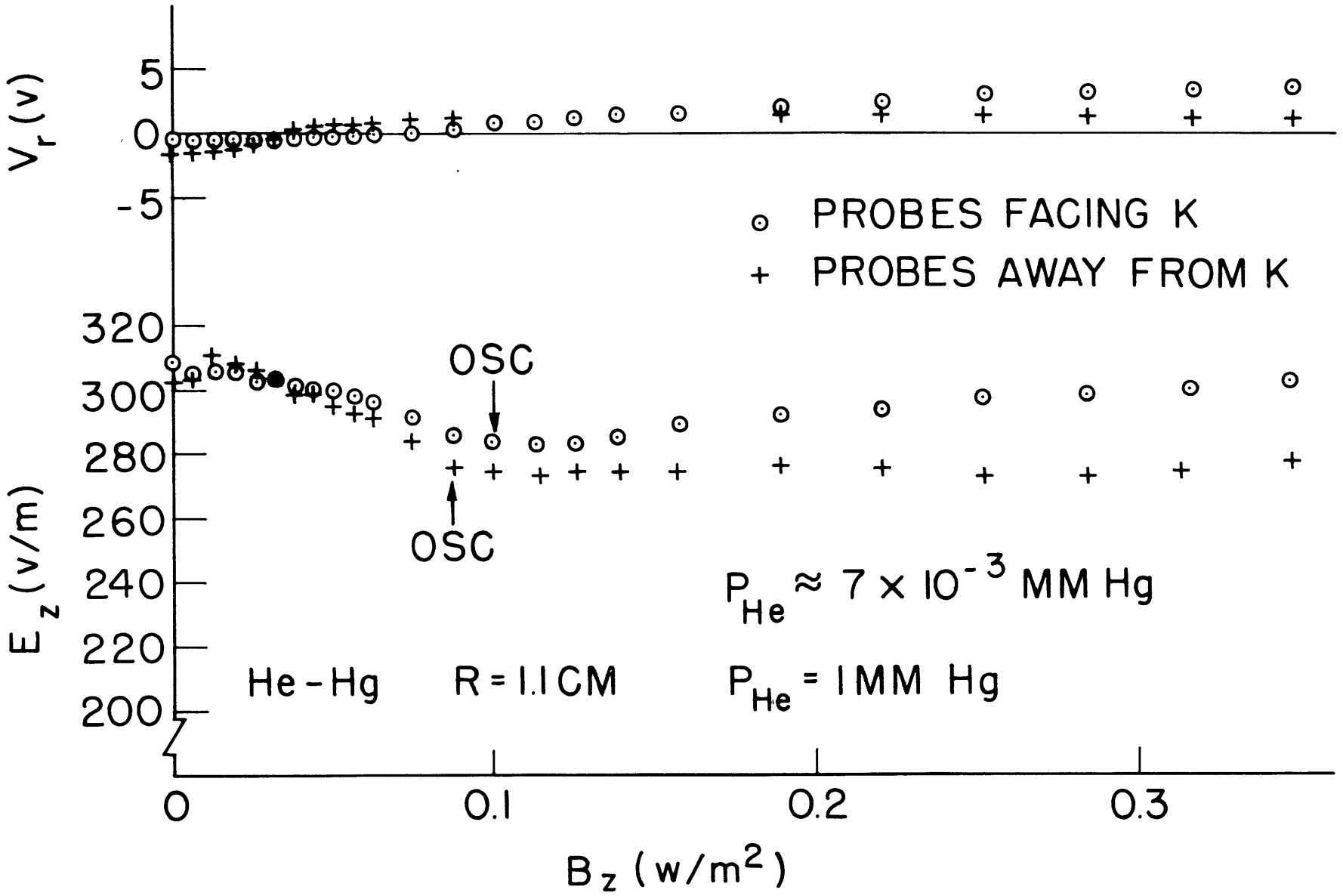

Fig. 3.10 He-Hg results. I_z = 0.3 amp. OSC indicates clear onset of noise

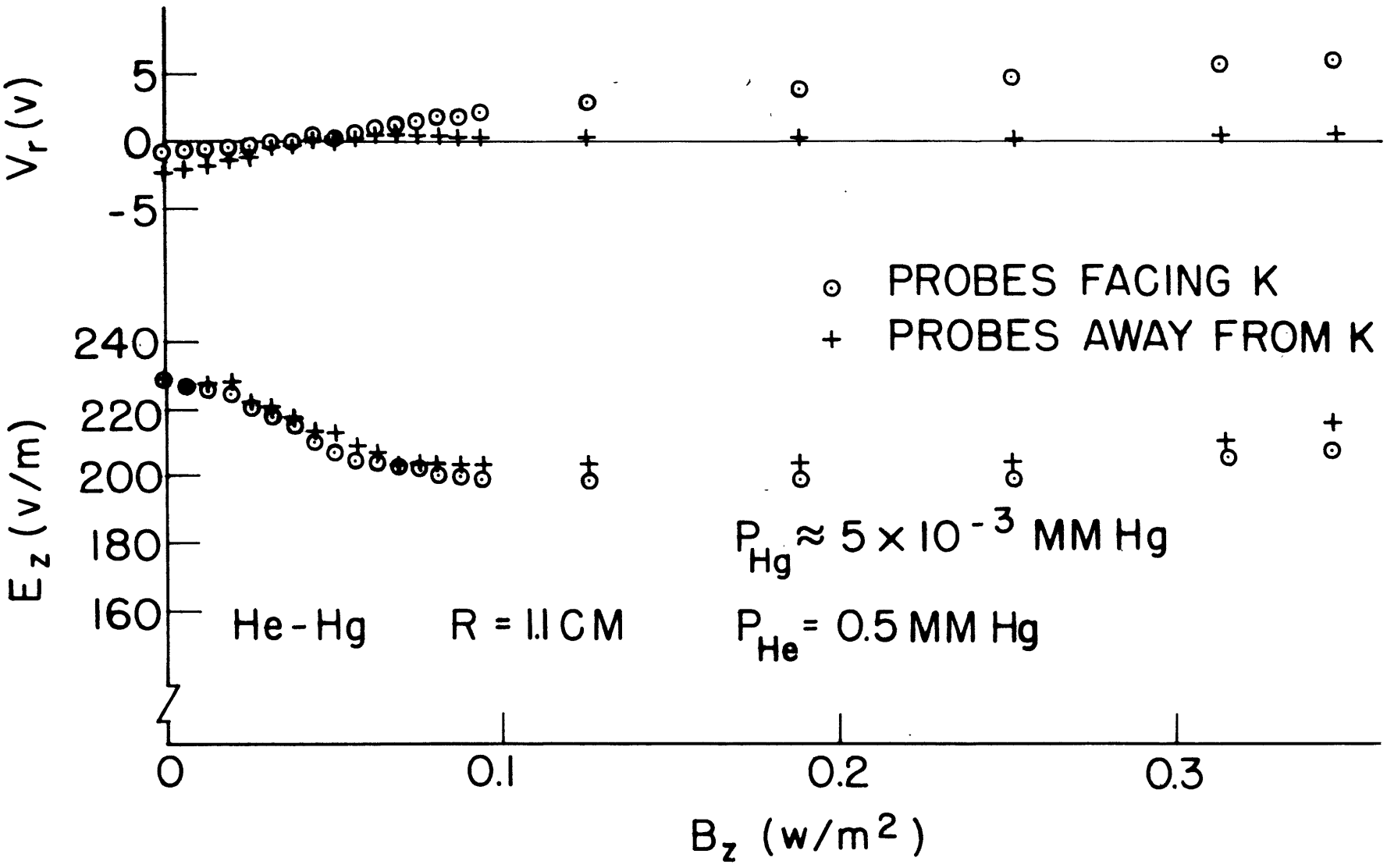

Fig. 3.11 He-Hg results. I_z = 0.3 amp.

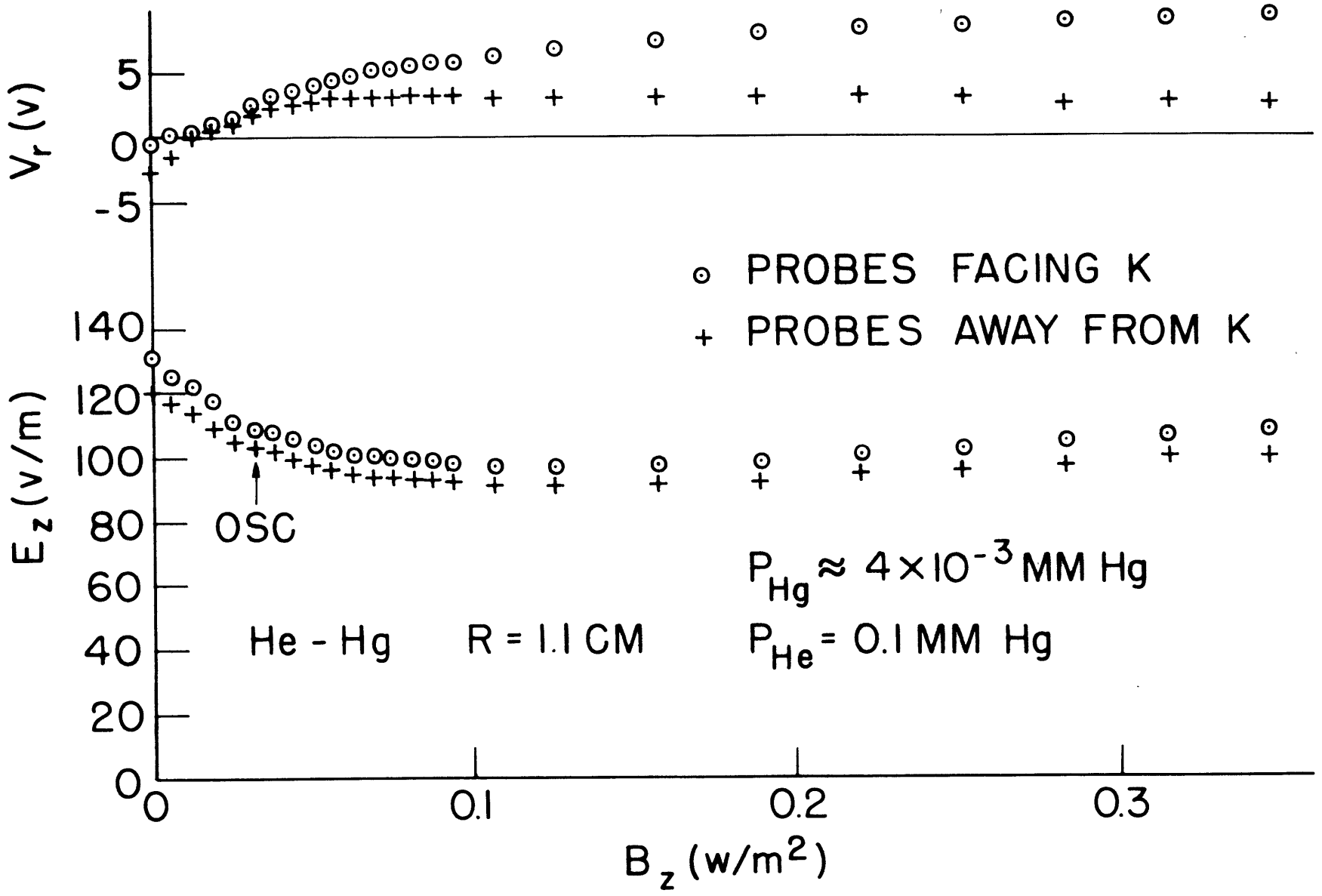

Fig. 3.12 He-Hg results. I_z = 0.3 amp. OSC indicates clear onset of noise.

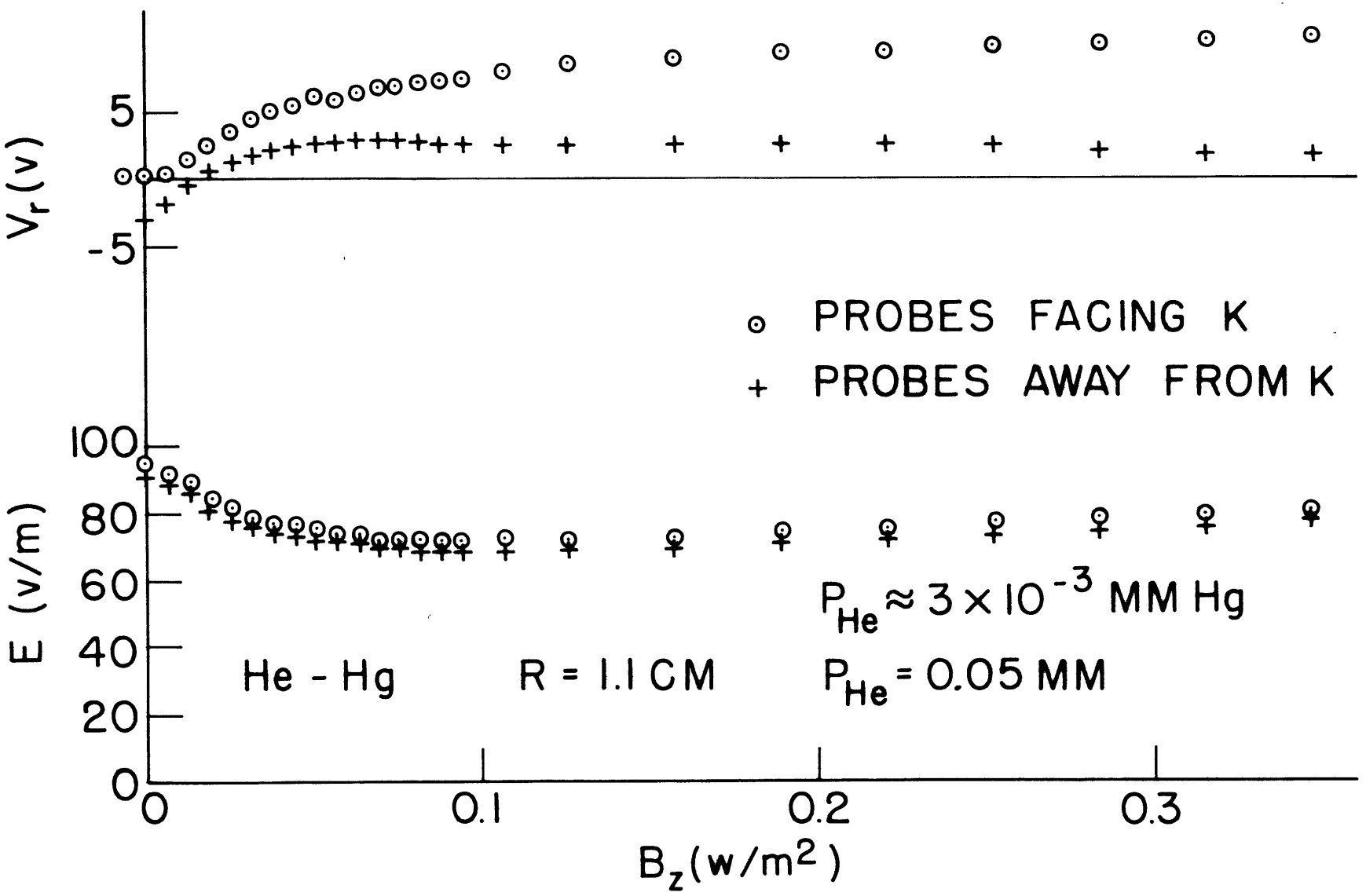

Fig. 3.13 He-Hg results. I_z = 0.3 amp.

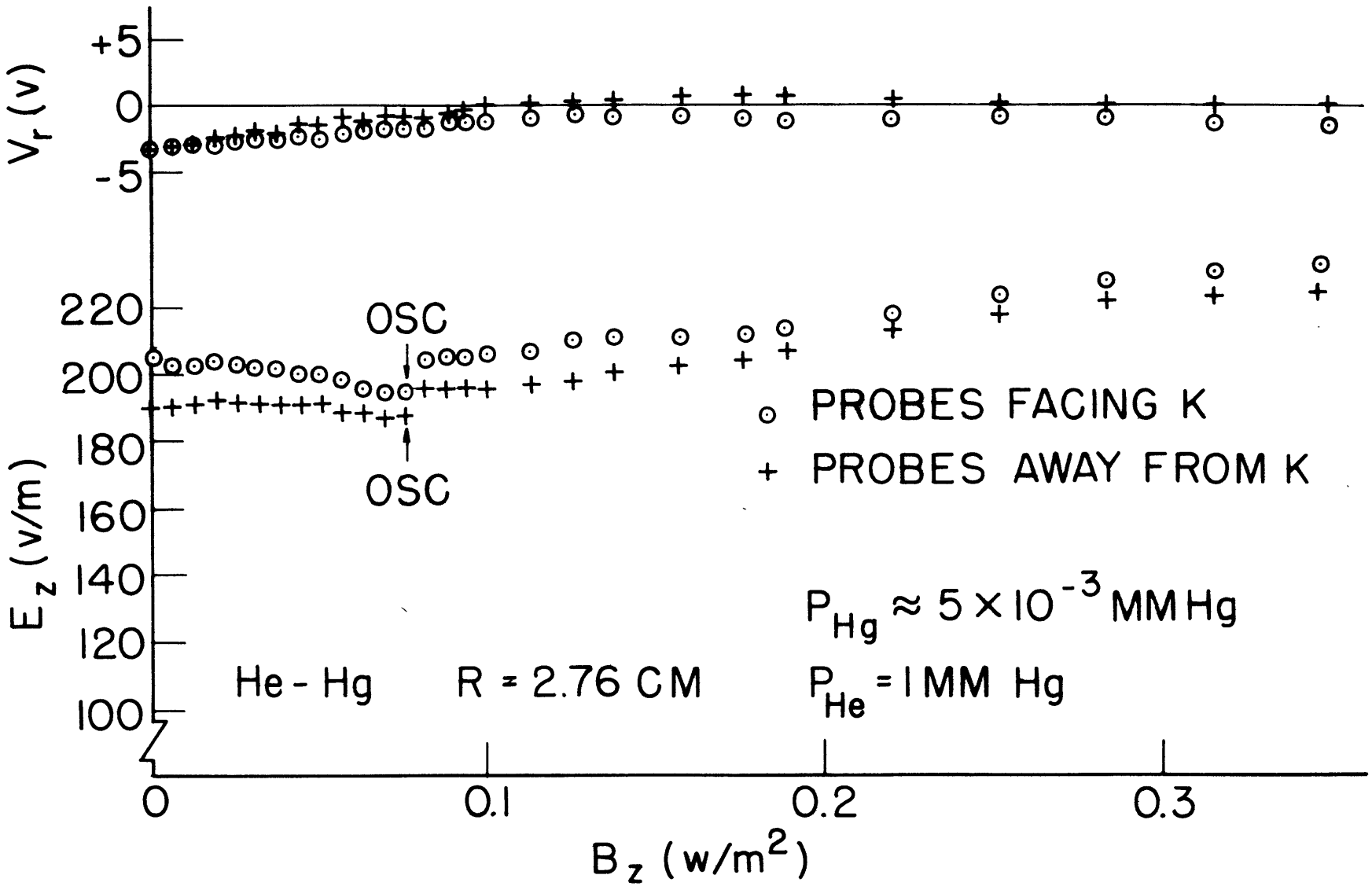

Fig. 3.14 He-Hg results. I_z = 0.3 amp. OSC indicates clear onset of noise.

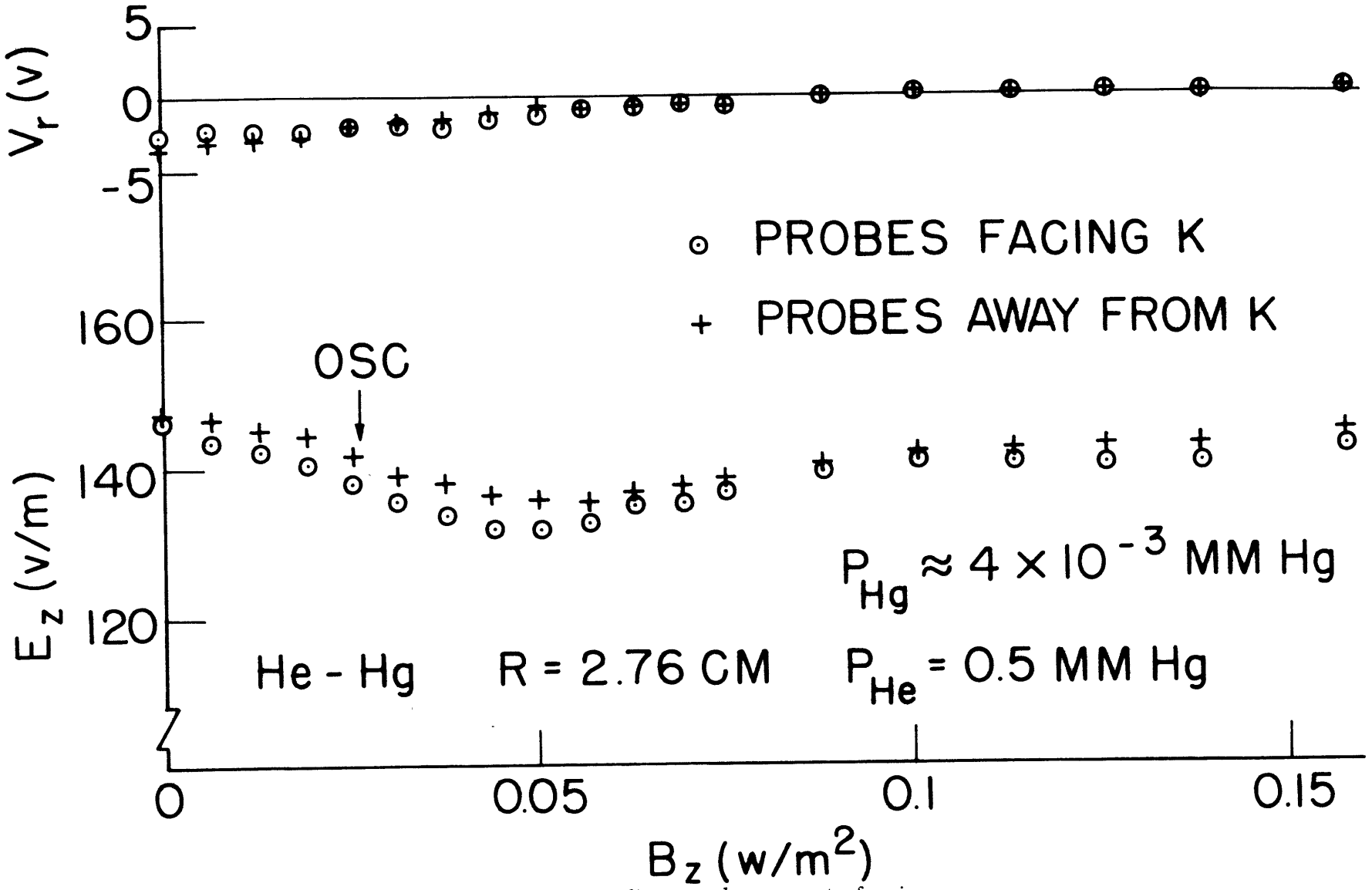

Fig. 3.15 He-Hg results. I_z = 0.3 amp. OSC indicates clear onset of noise

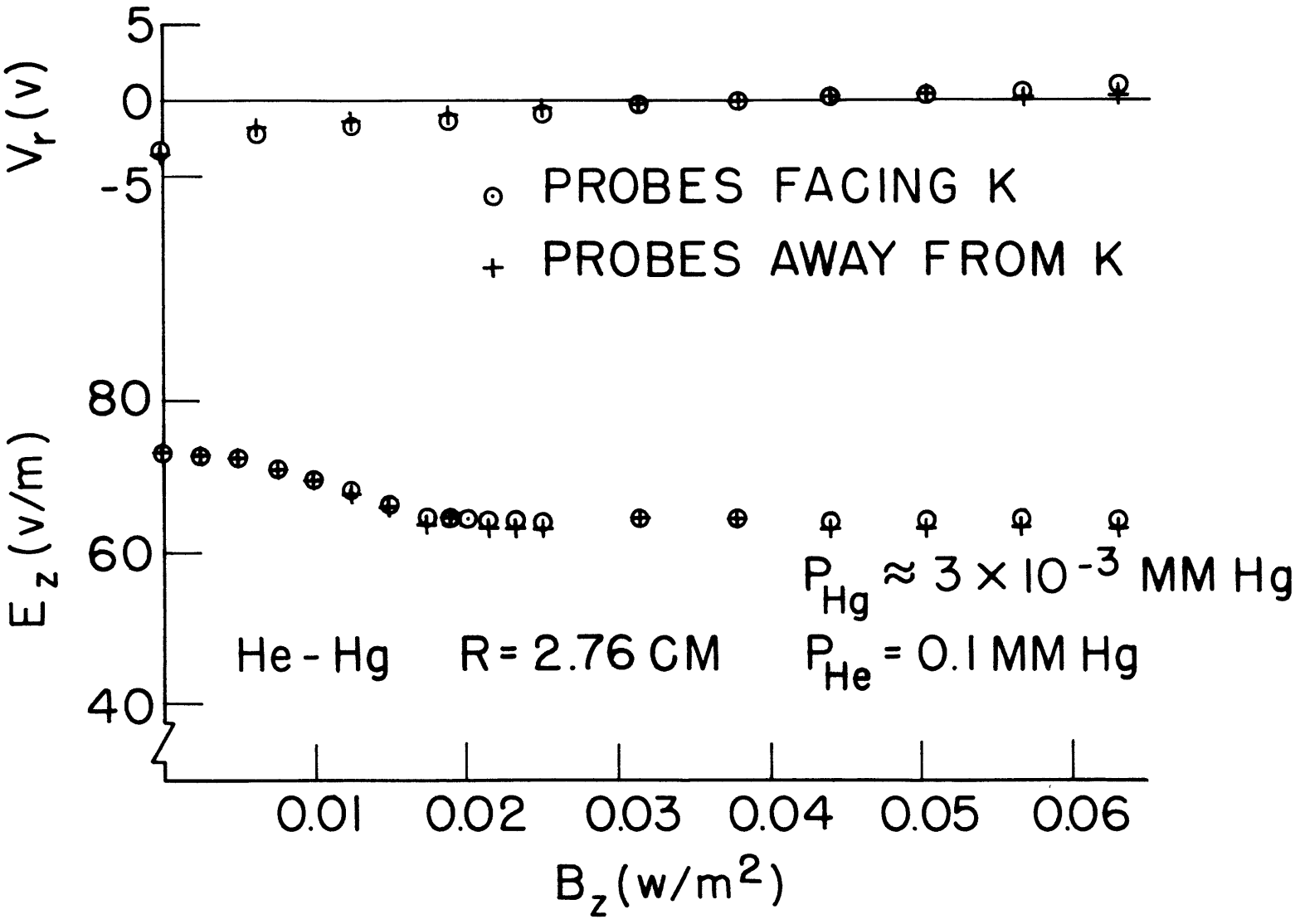

Fig. 3.16 He-Hg results. I_z = 0.3 amp.

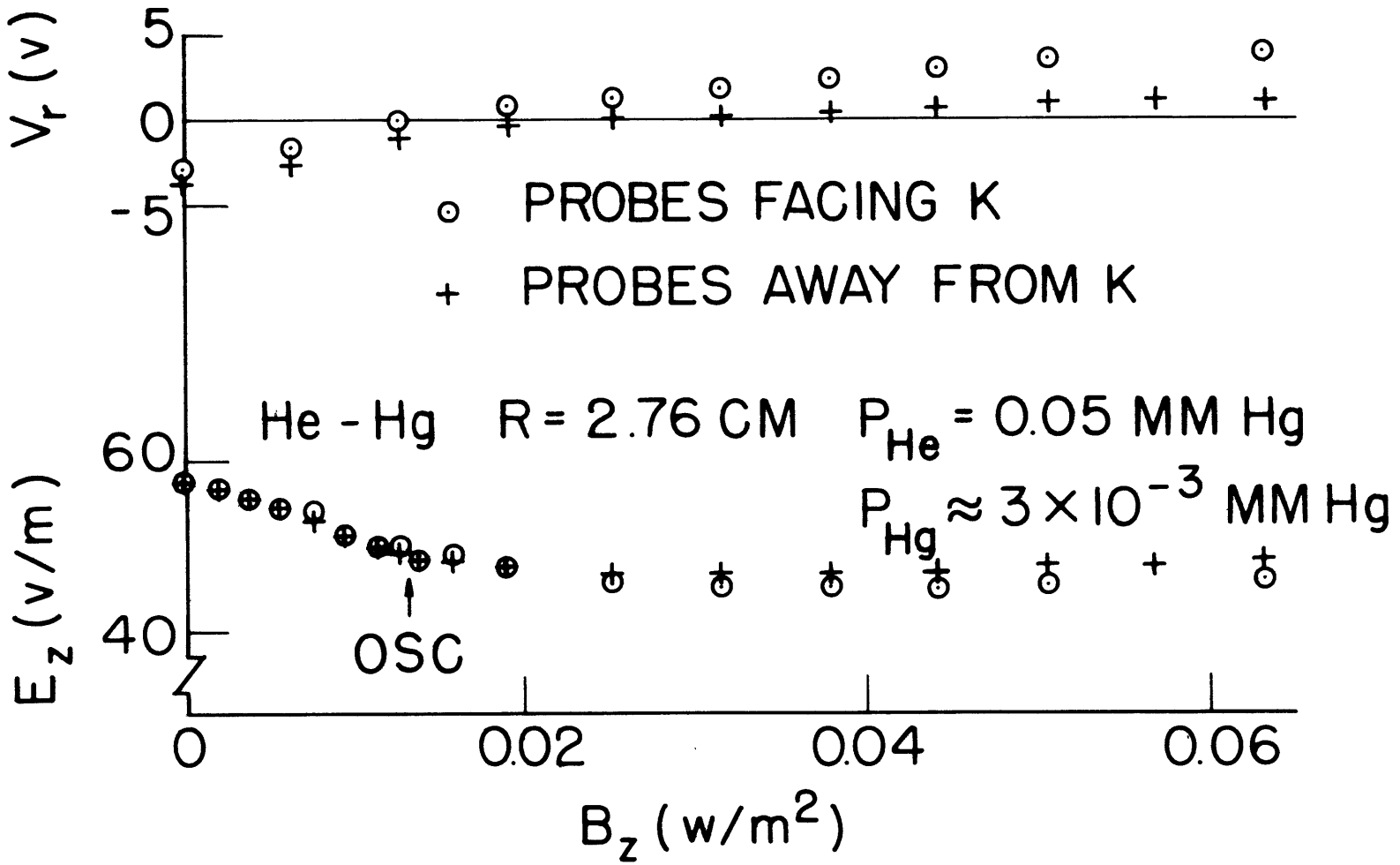

Fig. 3.17 He-Hg results. I_z = 0.3 amp. OSC indicates clear onset of noise.

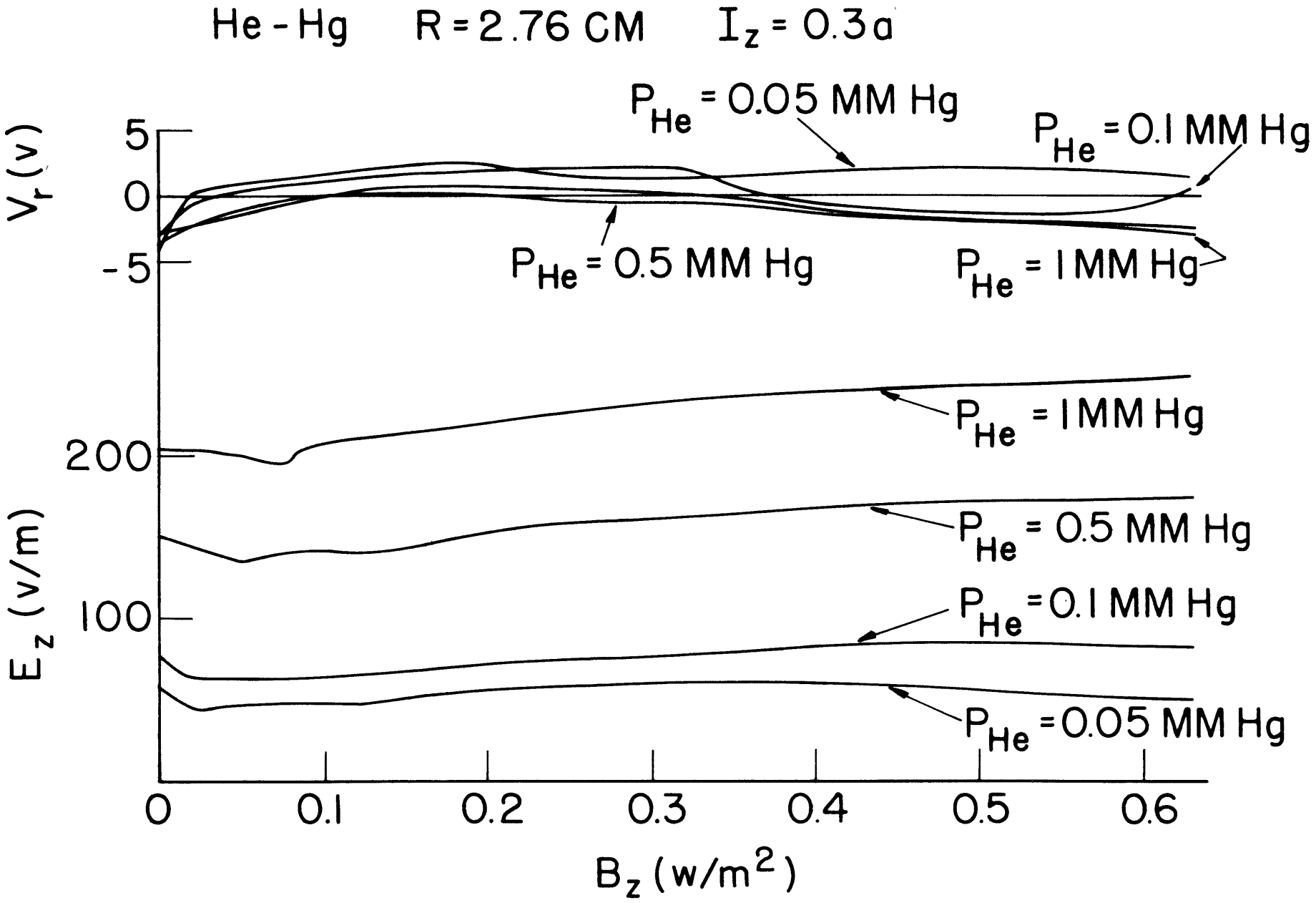

Fig. 3.18 He-Hg results at high B_z. $p_{Hg} \approx 5 \times 10^{-3}$, 4×10^{-3}, 3×10^{-3}, and 3×10^{-3} mm Hg for p_{He} = 1, 0.5, 0.1, and 0.05 mm Hg respectively. I_z = 0.3 amp. V_r data for probes nearest anode.

current direction. The V_r measurements, however, show both effects.

The magnetic field intervals for the data of Fig. 3.18 were the same as in Figs. 3.14-3.17 for low magnetic fields. For intermediate fields the interval was 3.15×10^{-2} w/m^2, and for fields above $B_z = 0.38$ w/m^2 it was 6.3×10^{-2} w/m^2.

The helium pressures are measured values at 24°C. The approximate mercury vapor pressures were found from the tube wall temperature during discharge operation. The indicated Hg pressures are probable minimum values; the actual pressures may be as much at 50% greater because of errors due to thermal gradients along the unequally cooled tube surface. Although the presence of Hg in the lamps prevented the monitoring of He "pumpout", the E_z and V_r reproducibility (see below) indicates that the He density remained constant over the approximately two hours' time required for a set of measurements. Only at $p_{He} = 0.05$ mm Hg was "pumpout" probably observed during long sets of measurements.

Typical reproducibility of the axial electric field data between He fills is indicated in Figs. 3.10-3.17. Measurements made with the same He fill are repeatable to less than 2% except at p = 0.05 mm Hg, where E_z slowly decreases with time. Rapid data taking at this pressure allows less than 2% reproducibility. The V_r data measured at a given end of the discharge can be reproduced within about 0.2 volts for the same He fill, and within about 1 volt after changing the He.

The axial electric fields calculated from wall probe data agree with center probe measurements within 1% for both lamps at $B_z = 0$. In the 1.1 cm lamp at $p_{He} = 1$ and 0.5 mm Hg the wall probe data were within 1% of the center probe E_z for all magnetic fields. For $p_{He} = 0.1$ mm Hg the wall probe E_z was 1% low at $B_z \approx 0.13$ w/m^2 and 2% low at $B_z \approx 0.35$ w/m^2 when the center probes faced the cathode. When the center probes faced the anode, the corresponding differences were 3% and 5% high. At $p_{He} = 0.05$ mm Hg the wall probe E_z was 3% low at

$B_z \approx 0.13$ w/m^2 and 6% low at $B_z \approx 0.35$ w/m^2 with the center probes facing the cathode. With the center probes facing the anode the corresponding differences were 4% and 10% high.

In the 2.76 cm radius lamp at p_{He} = 1 mm Hg the wall probes agreed with the center probes within 1% up to magnetic fields of 0.38 w/m^2. Above this field the wall probe E_z was lower than the center probe measurements when the center probes faced the cathode; at B_z = 0.63 w/m^2 the wall probe E_z was 8% low. With the center probes facing the anode the wall probes were 3% low at B_z = 0.63 w/m^2. At p_{He} = 0.5 mm Hg the wall probes indicated E_z about 2% low for magnetic fields less than 0.3 w/m^2 with the discharge current in either direction; and at $B_z \approx 0.63$ w/m^2 the wall probes indicated 4% low E_z with the center probes facing the cathode and 1% low when facing the anode. At p = 0.1 mm Hg the wall probe E_z was within 2% of the center probe data for all B_z when the center probes faced the anode. When the center probes faced the cathode, the wall probe E_z was 3% low for B_z less than 0.3 w/m^2 and 7% low at $B_z \approx 0.6$ w/m^2. At p = 0.05 mm Hg the wall probe E_z was 5% low for B_z less than 0.3 w/m^2 and 40% low at $B_z \approx 0.6$ w/m^2 with the center probes facing the cathode. With the center probes facing the anode the corresponding differences were 4% and 20% low.

The differences between wall and center probe measurements of E_z may tend to accentuate the divergences of the E_z data in Figs. 3.10-3.17. Measurements in the pure gases, however, suggest that the center probe E_z values are more reliable than wall probe data. The wall probes have considerably more noise on them than the center probes and are in a region of lower plasma density. Slight misalignments of the tube axis with respect to the magnetic field lines would probably be more apparent at the walls than at the center of the discharge. The variation of the total lamp

voltage as a function of B_z also follows the center probe E_z curves well.

The major source of electrical noise in the discharge tubes at $B_z = 0$ was anode oscillations. No clear evidence of moving striations was observed in either lamp. In the 1.1 cm lamp the average noise voltage on the wall probes at B_z below the E_z minimum was approximately 0.3% of the total lamp voltage. The "OSC" arrows in Figs. 3.10 and 3.12 indicate noise increases to about 0.6%. Above the E_z minimum the probe noise was about 1% of the total lamp voltage. In the 2.76 cm lamp the electrical noise was monitored at the discharge anode. At $p_{He} = 1$ mm Hg the zero magnetic field noise was about 0.4% of the total lamp voltage. At $B_z = 0.075$ w/m^2 the noise increased to 1% and above this field the noise was about 3% of the total lamp voltage. At $p_{He} = 0.5$ mm Hg the noise was approximately 0.1% for B_z less than 0.05 w/m^2; here it increased to 0.3%. Above this point the noise gradually increased to about 4% of the total lamp voltage. At $p_{He} = 0.1$ mm Hg very little noise was observed below magnetic fields of 0.018 w/m^2; here it increased to about 2% of the total lamp voltage, and at higher magnetic fields it was about 8% of the lamp voltage. At $p_{He} = 0.05$ mm Hg the noise was about 0.2% of the total lamp voltage for B_z below 0.013 w/m^2, where it increased to 1%. At higher fields the noise increased to about 6% of the total lamp voltage.

The anode oscillations in the 2.76 cm radius lamp could usually be stopped by carefully placing a permanent magnet near the discharge anode. This allowed a more careful study of the onset of instabilities. Table 3.1 shows the frequency of oscillations observed on the wall probes at the onset of noise. The discharges are quiet within the sensitivity of the oscilloscope at magnetic fields less than the lowest indicated in Table 3.1 for a given He fill. The higher frequency oscillations at $p_{He} = 1$ and 0.5 mm Hg are clean sinusoids. The lower frequency oscillations were more irregular and usually modulated by the higher frequency component. The lower frequency

TABLE 3.1

OSCILLATIONS NEAR ONSET OF NOISE

He-Hg DISCHARGE, R = 2.76 CM

P_{He} (mm Hg)	P_{Hg} (mm Hg)	B_z (w/m^2)	f (Kc/sec)	Remarks
1	5×10^{-3}	0.0630	3.6	Clean sinusoid
		0.0693	2.4	Fair sinusoid
0.5	4×10^{-3}	0.0453	21.3	Sinusoid
		0.0473	4.9	Modulated sinusoid
		0.0453	21	Sinusoid
		0.0460	5	Modulated sinusoid
		0.0479	4.7	Sawtooth
0.1	3×10^{-3}	0.0157	20	Fair sinusoid
		0.0202	11	Irregular but periodic
		0.0145	20	Fair sinusoid
		0.0189	6.3	Irregular but periodic
0.05	3×10^{-3}	0.0107	20	Irregular but periodic
		0.0126	7.3	Fair sinusoid
		0.0095	22	Irregular but periodic
		0.0132	7.2	Fair sinusoid
		0.0126	20	Irregular but periodic
		0.0138	6.7	Fair sinusoid

component always had greater amplitude than the higher frequency oscillations by a factor of 2 to 5. At magnetic fields stronger than indicated in Table 3.1 the noise waveforms were usually very irregular with no predominant frequency component. The results were independent of the direction of the discharge current except at p_{He} = 0.1 mm Hg where the lower frequency component was shifted by reversing the lamp current.

IV. DISCUSSION

4.1 "CLASSICAL" DIFFUSION

4.1.1 Helium and Argon

Other investigators have compared the theory of "classical" transverse diffusion to experiment for inert gases (see, for example, reviews by Hoh, 1962; Golant, 1963; and Boeschoten, 1964) and no attempt will be made here to repeat this work. Only a comparison to other experimental results will be made below.

The scaling parameter E_z/p has been plotted against pR in Fig. 4.10 for the helium discharges at zero magnetic field. These data for both the R = 1.1 cm and 2.76 cm tubes agree extremely well with zero magnetic field results by Hoh and Lehnert (1960), Zaitsev and Vasil'eva (1960), and Paulikas (1961) for He discharges under comparable experimental conditions. The curves of E_z as a function of B_z for the 1.1 cm lamp, Fig. 3.5, are parallel to $E_z(B_z)$ curves of Zaitsev and Vasil'eva (1960) and Paulikas (1961) for He discharges under only slightly different experimental conditions. Since the zero magnetic field E_z/p data and the critical magnetic fields (Section 4.2.1) also agree well, we can conclude that the results are consistent. The $E_z(B_z)$ data for the R = 2.76 cm lamp at He pressures of 1 and 0.5 mm Hg are similar to Paulikas' R = 2.75 cm "short tube" (L = 78 cm) results, where the axial electric field E_z drops somewhat more slowly with B_z than in the "long tube" (L = 200 cm). The data for p = 0.1 mm Hg in the 2.76 cm lamp are similar to an approximately comparable study by Artsimovich and Nedospasov (1963).

The quantity E_z/p is plotted against pR in Fig. 4.11 for the argon discharges at zero magnetic field. Experimental results by Klarfeld (Francis, 1956; p. 116) are plotted in the same way in Fig. 4.11 for an Ar discharge with R = 1.0 cm and

lamp current I_z = 0.3 amp. The axial electric field E_z is a fairly strong function of I_z/R^n (See Section 2.3) for argon discharges, and the agreement appears satisfactory in this light.

The E_z versus B_z curve for p = 1 mm Hg, R = 1.1 cm (Fig. 3.7), compares very well with results of Hoh and Lehnert (1960) for a p = 0.92 mm Hg argon discharge in a R = 1.0 cm tube and lamp current of 0.7 amp. The data of Fig. 3.7 for p = 0.1 mm Hg are quite similar to Paulikas' results for p = 0.12 mm Hg, R = 1.27 cm, and I_z = 0.2 amp; however, he shows an E_z upturn at B_z = 0.18 w/m^2 which is not found here.

Apparently, no data are available for comparison to the argon discharge results for the R = 2.76 cm tube.

4.1.2 Helium-Mercury

Figs. 4.1-4.4 show the measured axial electric field E_z and radial voltage drop V_r against B_z compared with theory for the He-Hg discharges. Predicted E_z values are calculated from the theory of Waymouth and Bitter (1956) (hereafter abbreviated WB) modified to include the effect of magneto-ambipolar diffusion. The zero magnetic field values of E_z are usually normalized to the observed values by multiplying the computed E_z by a factor of the order of 1. See Appendix I for details. The radial potential drop V_r is calculated from Eq. (2.18) using the Einstein relation

$$D_\pm = \mu_\pm T_\pm \tag{4.1}$$

which holds for Maxwellian distributions of velocity. (Temperatures are in units of electron volts.) The electron temperature T_- and mobility μ_- are taken from the WB calculations. The mercury ion temperature T_+ is calculated by equating ion energy gain from the observed E_z to losses from elastic collisions

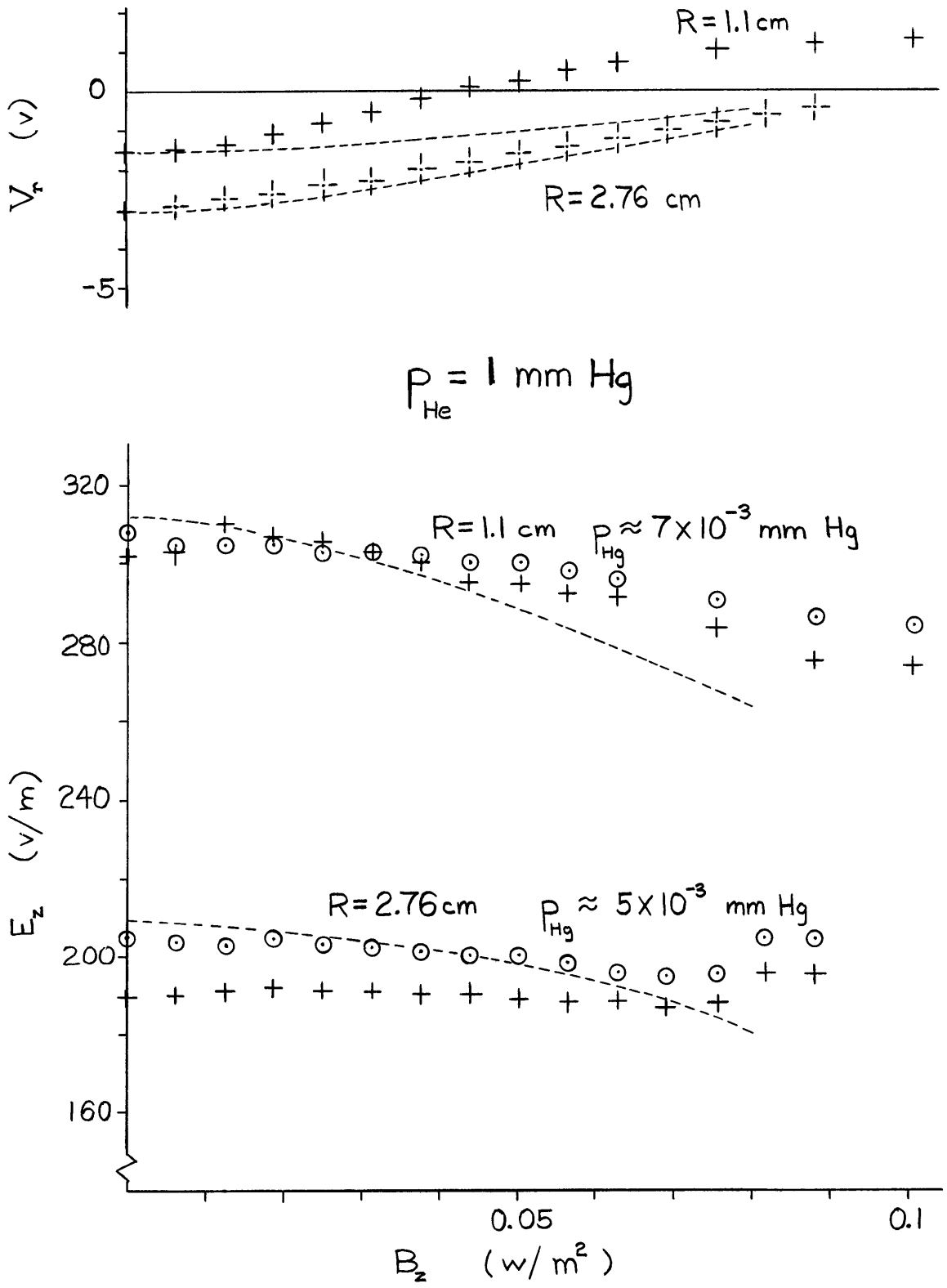

Fig. 4.1 Comparison of "classical" diffusion theory (broken curves) with He-Hg results. V_r data for probes nearest anode. I_z = 0.3 amp.

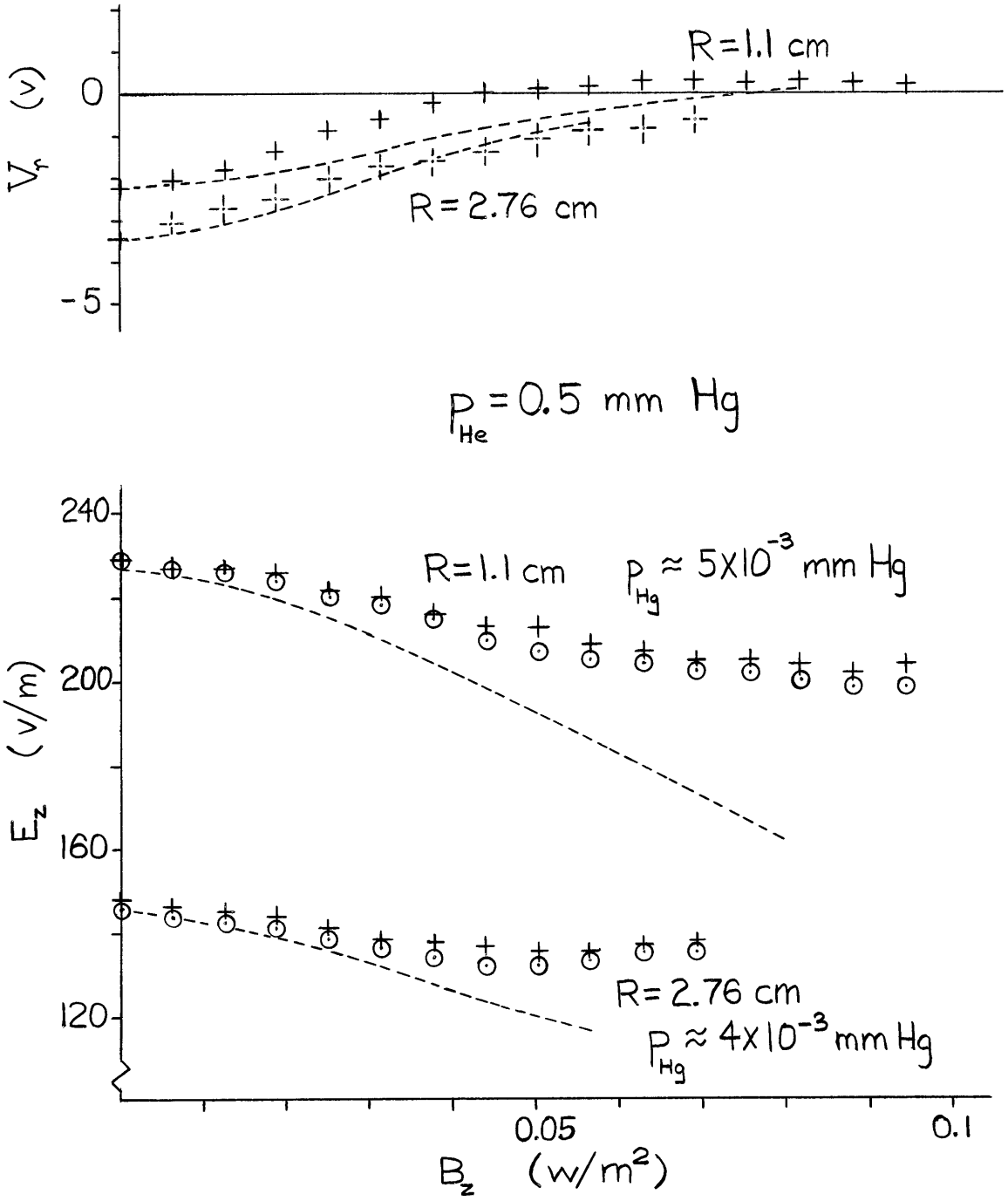

Fig. 4.2 Comparison of "classical" diffusion theory (broken curves) with He-Hg results. V_r data for probes nearest anode. I_z = 0.3 amp.

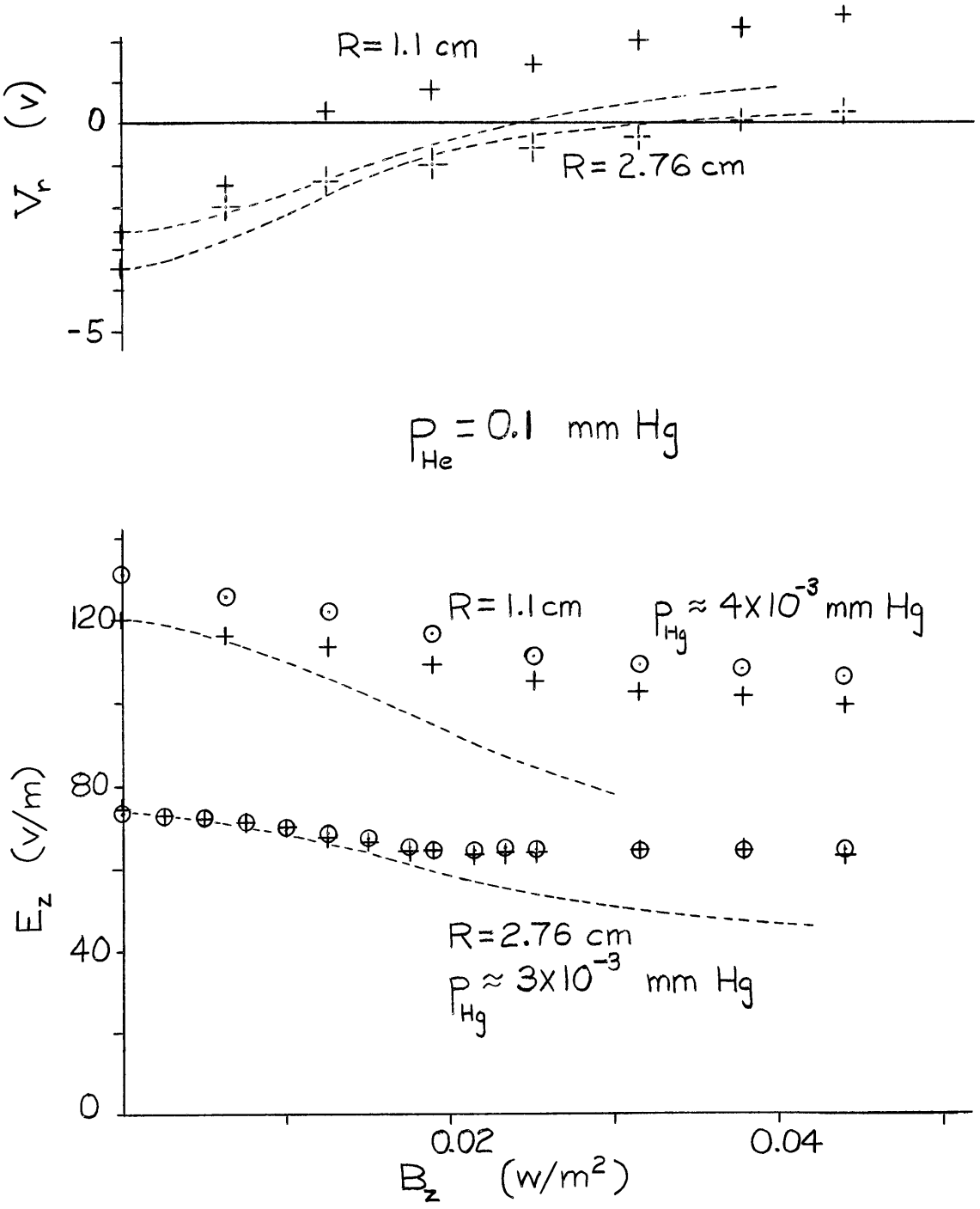

Fig. 4.3 Comparison of "classical" diffusion theory (broken curves) with He-Hg results. V_r data for probes nearest anode. I_z = 0.3 amp.

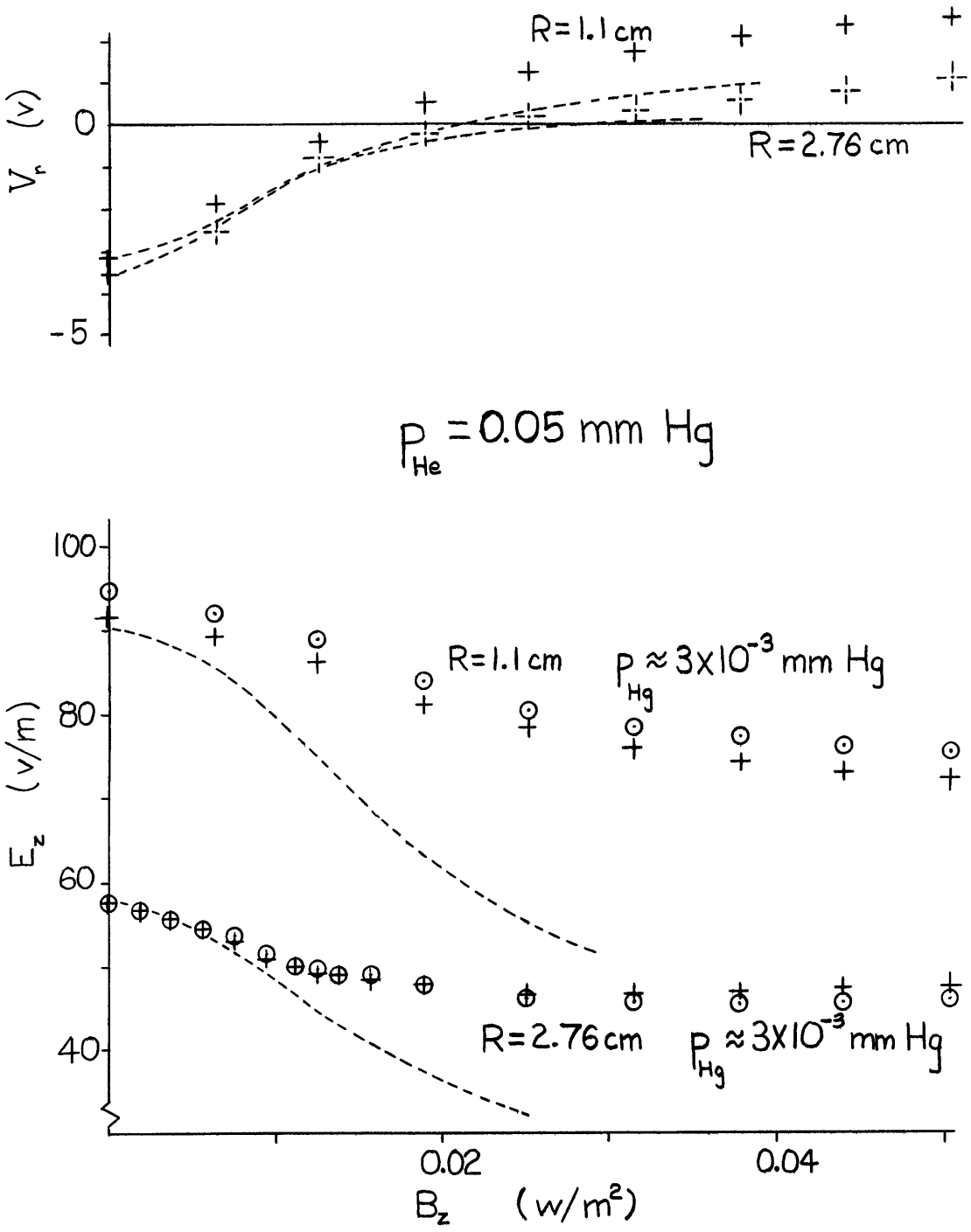

Fig. 4.4 Comparison of "classical" diffusion theory (broken curves) with He-Hg results. V_r data for probes nearest anode. I_z = 0.3 amp.

with He atoms and elastic and charge exchange collisions with Hg atoms. (See Appendices II and III.) The ion velocity distribution is assumed to be Maxwellian, for want of a better approximation. Since the ion mean free path is always less than the radius of the lamps (Appendix II), this approximation may be justifiable. The logarithmic factor in Eq. (2.18) is found by normalizing the V_r calculations to the experimental data at zero magnetic field (Appendix III). This factor is assumed to remain constant as B_z is applied.

Figs. 4.1-4.4 show that the WB theory agrees fairly well with E_z observations for the R = 2.76 cm tube, but rather poorly for the 1.1 cm tube. Agreement between theoretical V_r and experiment is surprisingly good for the 2.76 cm lamp, but poor in the 1.1 cm case.

The slope of the theoretical V_r curve is given approximately by

$$\frac{\partial V_r}{\partial B_z} \approx \frac{2\mu_{\perp+}(T_+ + T_-)}{B_z^3 \mu_- (\mu_{\perp+} + \mu_{\perp-})^2} |F| \qquad (4.2)$$

where $\mu_{\perp+}$ is assumed to be constant and $(\mu_- B_z)^2 \gg 1$. F represents the logarithmic term in Eq. (2.18).

In the experimental situation here, $\mu_\perp \approx \frac{1}{\mu_- B_z^2} > \mu_{\perp+}$ at low B_z, and Eq. (4.2) reduces further to

$$\frac{\partial V_r}{\partial B_z} \approx 2\mu_+ \mu_- B_z (T_+ + T_-)|F| \qquad (4.3)$$

Eq. (4.3) suggests several possibilities to explain the failure of the classical theory for V_r in the 1.1 cm lamp. First, the ions may have a velocity distribution which is far from Maxwellian at the higher electric fields and smaller tube radius of the 1.1 cm lamp. This would invalidate the classical theory and possibly lead to a greater $V_r(B_z)$ slope. Second, the term $\mu_+ \mu_-$ may be too small, although Fig. 4.5 below indicates the contrary. Third, the $E_z(B_z)$ curves indicate that the error in the theoretical T_- calculation is greater for the R = 1.1 cm lamp than for R = 2.76 cm; larger T_- would improve both the E_z and V_r theoretical curves. Finally, in my opinion, the most probable explanation is that the empirically found logarithmic factor F is incorrect. The experimental values of V_r are corrected for a 0.9 cm longitudinal offset between the probes in the 1.1 cm lamp (See Section 3.3.2), and it is likely that the magnitude of the correction factor was too small. One would expect the radial potential drop at $B_z = 0$ to be greater in the 1.1 cm lamp than in the 2.76 cm lamp under comparable conditions, because of the higher electron temperature and density gradient. Figs. 4.1-4.4, however, show exactly the opposite for every helium pressure, with the greater V_r discrepancies at the higher values of E_z. The difference in V_r found by reversing the direction of the axial electric field, Figs. 3.10-3.13, also supports the view that the V_r correction for the probe offset was wrong. Adding about -2 volts to the R = 1.1 cm V_r experimental data for p_{He} = 1 and 0.5 mm Hg, -1.5 volts for p_{He} = 0.1 mm, and -1 volt for p_{He} = 0.05 mm brings the theoretical and experimental V_r curves into almost exact agreement.

This error is very likely a result of a plasma disturbance caused by the center probe structure. Several investigators have reported increased axial electric field on the anode side of probes and other structures protruding into gas discharge columns. Barnes (1962), for example, finds a bright glow on

the anode side of a 0.17 mm rod protruding radially into rare gas discharges at pressures from 1 to 7 mm Hg. The disturbance produces increased wall current for about 4 cm on either side of the probe. Little (1964) and Verweij (1960) observe similar phenomena in Hg-rare gas discharges. In the former case, the visual perturbation extends approximately 12 cm away from the obstruction on the anode side and about 2 cm on the cathode side.

A locally increased E_z would increase the magnitude of V_r correction for the R = 1.1 cm experimental data of Figs. 4.1-4.4 and improve the agreement with theory. The plasma density disturbance in the probe region may also invalidate Eq. (2.18) at zero magnetic field, which is based on the assumption of undisturbed, classical ambipolar diffusion. The disturbance may add to the observed V_r disagreement when the direction of E_z is reversed.

Fig. 4.5 is a plot of E_z/p_{He} against $p_{He} R\sqrt{1 + \mu_+\mu_- B_z^2}$, quantities which were shown to be discharge scaling parameters in Section 2.3. The values of $E_z(0)/p_{He}$ at zero magnetic field fall on approximately the same line for both tubes. In principle, the curves of $E_z(B_z)/p_{He}$ should follow the $B_z = 0$ scaling line for classical diffusion. Fig. 4.5 shows that, although they are fairly straight lines for low B_z, the curves have a considerably smaller initial slope than expected, especially at the lower He pressures. Smaller μ_+ or μ_- would increase the slope of the curves in Fig. 4.5, but decreased ion mobility would accentuate the error of the E_z calculations by reducing the ambipolar diffusion losses. The electron mobility, however, may well be somewhat too large. Brown's data (1959; p. 51) shows average electron mobility in He to be 76 m^2--mm Hg/v-s, which is higher than the calculated mobility (Appendix I) for electron temperatures less than 20,000°K.

4.1.3 Volume Recombination

The discrepancy between WB theory and experiment for He-Hg discharges and the broad E_z versus B_z minima in He-Hg and

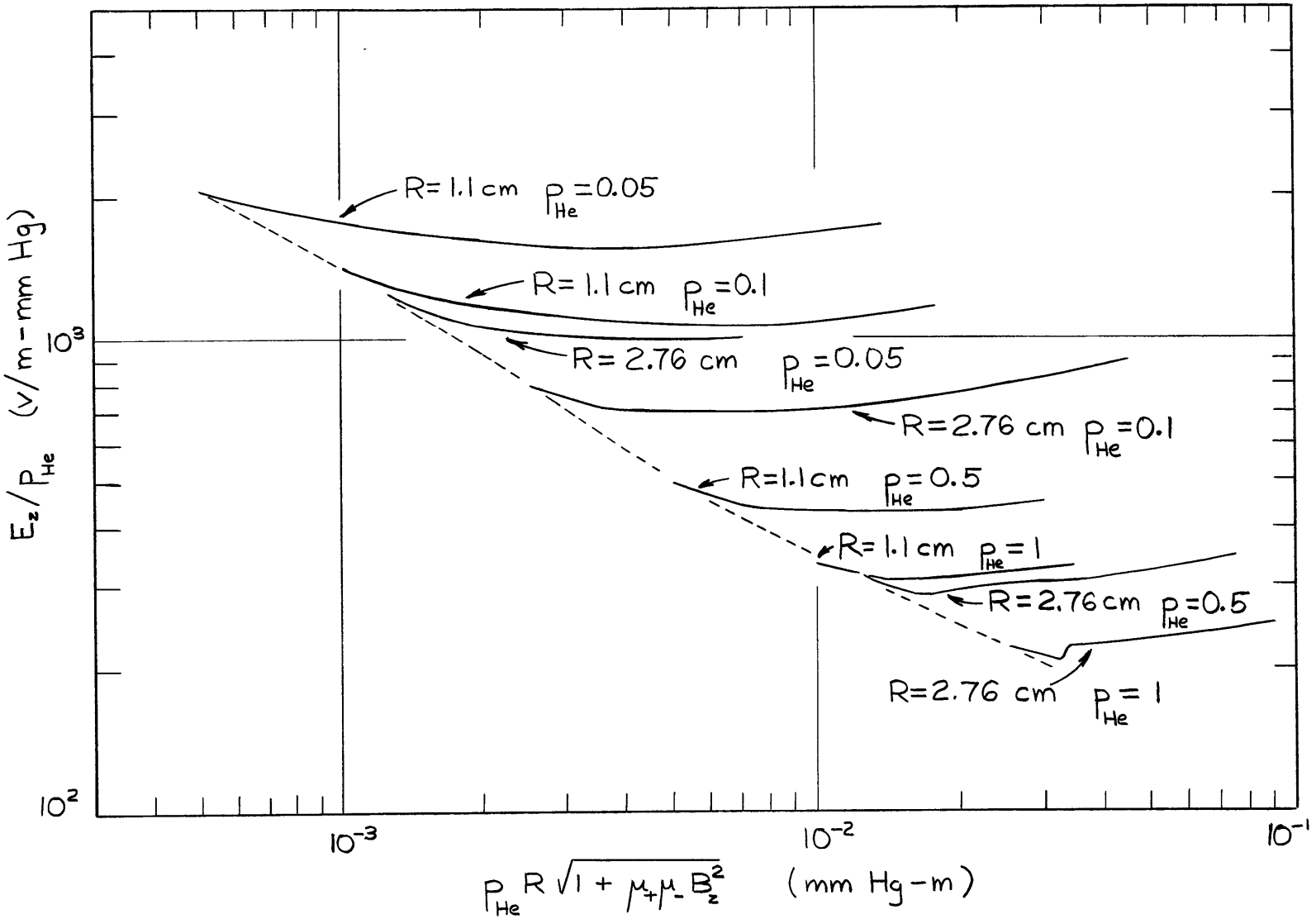

Fig. 4.5 He-Hg results plotted using discharge scaling parameters. Broken curve is E_z/p_{He} at $B_z = 0$.

Ar data suggests that the magnetic field may be reducing radial diffusion to the point where volume recombination plays an important role. Considerable volume recombination would keep E_z higher than expected by providing an energy loss mechanism which is not accounted for in the theory.

To test the importance of volume recombination, we write Eq. (2.14) in the approximate form

$$\frac{\partial n}{\partial t} \approx -D_{a\perp}\frac{n}{\Lambda^2} + \nu_i n - \alpha n^2 \qquad (4.4)$$

where Λ is the diffusion length, equal to R/2.405 for a cylindrical discharge column. From Eq. (4.4) we see that volume recombination will be the dominant charge loss mechanism when

$$\alpha n \gg \frac{D_{a\perp}}{\Lambda^2} \qquad (4.5)$$

The left and right hand expressions in Eq. (4.5) are respectively the inverse characteristic times for an ion to disappear by volume recombination and diffusion.

Recombination coefficients, α, are usually measured in "afterglow" experiments (Brown, 1959; ch. 8). The decay of the electron density is monitored as a function of time after a discharge is interrupted, and recombination coefficients calculated from this variation. The electron and ion temperature rapidly approach the gas temperature, and the dominant volume recombination mechanism is dissociative recombination of electrons with molecular ions (Brown, 1959; p. 195). Typical dissociative recombination

coefficients for Ar_2^+ ions are from 3.6×10^{-13} m^3/sec to 1.4×10^{-12} m^3/sec (Kretschmer and Petersen, 1963) for afterglows at pressures from 1 to 4 mm Hg. The same authors find the recombination coefficient of Hg_2^+ ions to be 3.5×10^{-12} m^3/sec for Hg vapor at pressures from 0.7 to 3 mm Hg. For Hg vapor in He at 1.8 mm Hg Biondi (1953) finds that α varies linearly from 5×10^{-13} to 1.5×10^{-12} m^3/sec for Hg pressures from 1.4 to 45 mm Hg. Biondi states that dissociative recombination is dominant at Hg pressures above approximately 1 mm Hg.

Atomic ions can recombine by three-body collisions with two electrons and by radiative recombination. Very little is known about three-body recombination, and its effect is probably small in low density plasmas. The coefficient of radiative recombination for Ar is $2 \times 10^{-16} m^3$/sec and for Hg is 2.3×10^{-16} m^3/sec for electron temperatures from 2,000 to 3,000°K (Brown, 1959; p. 195).

Table 4.1 shows $D_{a\perp}/\Lambda^2$ and αn for some Ar and He-Hg discharges of this experiment. In every case, diffusion losses are much greater than radiative recombination losses. Dissociative recombination losses, however, are potentially very large compared to diffusion, even at zero magnetic field.

The question whether or not dissociative recombination is important in active discharges, with pressures less than 1 mm Hg and electron temperatures of the order of a volt, has apparently not been resolved. Biondi's (1953) data for He-Hg afterglows indicate that dissociative recombination would not be important when Hg pressures are in the micron range. This conclusion is consistent with a Hg ion mobility experiment by Kovar (1964) who finds Hg_2^+ ions only for E/p less than 100 v/cm-mm Hg. For argon, however, the situation may be different. Measurements of argon ion mobilities find both Ar^+ and Ar_2^+ at all E/p tested (See references in Brown, 1959; ch. 3). An afterglow experimental determination of argon ion mobility by Oskam and Mittelstadt (1963) indicates the

TABLE 4.1

COMPARISON OF DIFFUSION AND RECOMBINATION LOSSES FOR Ar AND He-Hg DISCHARGES

Gas	R (cm)	p (mm Hg)	(Assumed) T_- (e.v.)	D_a/Λ^2 (sec^{-1})	B_z=0.1 w/m^2 $D_{a\perp}/\Lambda^2$ (sec^{-1})	B_z=1 w/m^2 $D_{a\perp}/\Lambda^2$ (sec^{-1})	Radiative Recombination* $\alpha_r n$ (sec^{-1})	Dissociative Recombination† $\alpha_d n$ (sec^{-1})
Ar	2.76	0.92	1.5	1.5×10^3	1.1×10^3	37	23	4.1×10^4
Ar	2.76	0.092	2.0	2.2×10^4	4.9×10^2	5.2	1.4	2.6×10^3
He-Hg	2.76	$p_{He} = 0.92$ $p_{Hg} = 5\times10^{-3}$	1.2	1.1×10^4	5.2×10^3	97	10	1.6×10^5
He-Hg	2.76	$p_{He} = 0.046$ $p_{Hg} = 3\times10^{-3}$	1.8	7.8×10^4	1.1×10^3	11	2.5	3.8×10^4

* $\alpha_r (Ar^+) = 2 \times 10^{-16}\ m^3/sec$; $\alpha_r (Hg^+) = 2.3 \times 10^{-16}\ m^3/sec$

† $\alpha_d (Ar_2^+) = 3.6 \times 10^{-13}\ m^3/sec$; $\alpha_d (Hg_2^+) = 3.5 \times 10^{-12}\ m^3/sec$

presence of Ar_2^+ ions at pressures down to at least 0.5 mm Hg. Even the dominant process of molecular ion formation is in dispute. Most authors feel that the molecular ions are formed by three-body collisions between an atomic ion and two neutral atoms. Myers (1963) believes, however, that He_2^+ ions are formed by collisions between pairs of metastable atoms. At low pressure the probability of collision between metastable atoms in active discharges is probably higher than for three-body collisions between ions and neutrals.

It is almost certain that the atomic ions will outnumber the molecular ions at low pressures. This fact was well demonstrated by Phelps and Brown (1951) with a mass spectrometer on a He afterglow experiment. The density of He^+ in He at 3 mm Hg was about 8 times that of He_2^+ at time t = 0. Assuming that the molecular ions are formed by three-body collisions, the He^+ density then should be about 800 times greater than He_2^+ at a pressure of 0.3 mm Hg. Reducing the argon $\alpha_d n$ in Table 4.1 by a factor of 10 for p = 0.92 mm and by a factor of 1,000 for p = 0.092 mm Hg does not significantly reduce the importance of dissociative recombination in the former case but does in the latter.

4.2 KN INSTABILITY

4.2.1 Helium and Argon

The experimental results will not be analyzed in great detail for the onset of the KN instability in helium discharges. Many other references are available (Boeschoten, 1964) for this; furthermore, the magnetic field increment in this experiment was not fine enough to make critical tests of the phenomenon in He. Fig. 4.6 shows the critical magnetic field B_c compared with a compendium of other workers' He results by Akhmedov and Zaitsev (1963). The agreement appears to be quite good.

Much less data on the KN instability in argon are available in the literature.

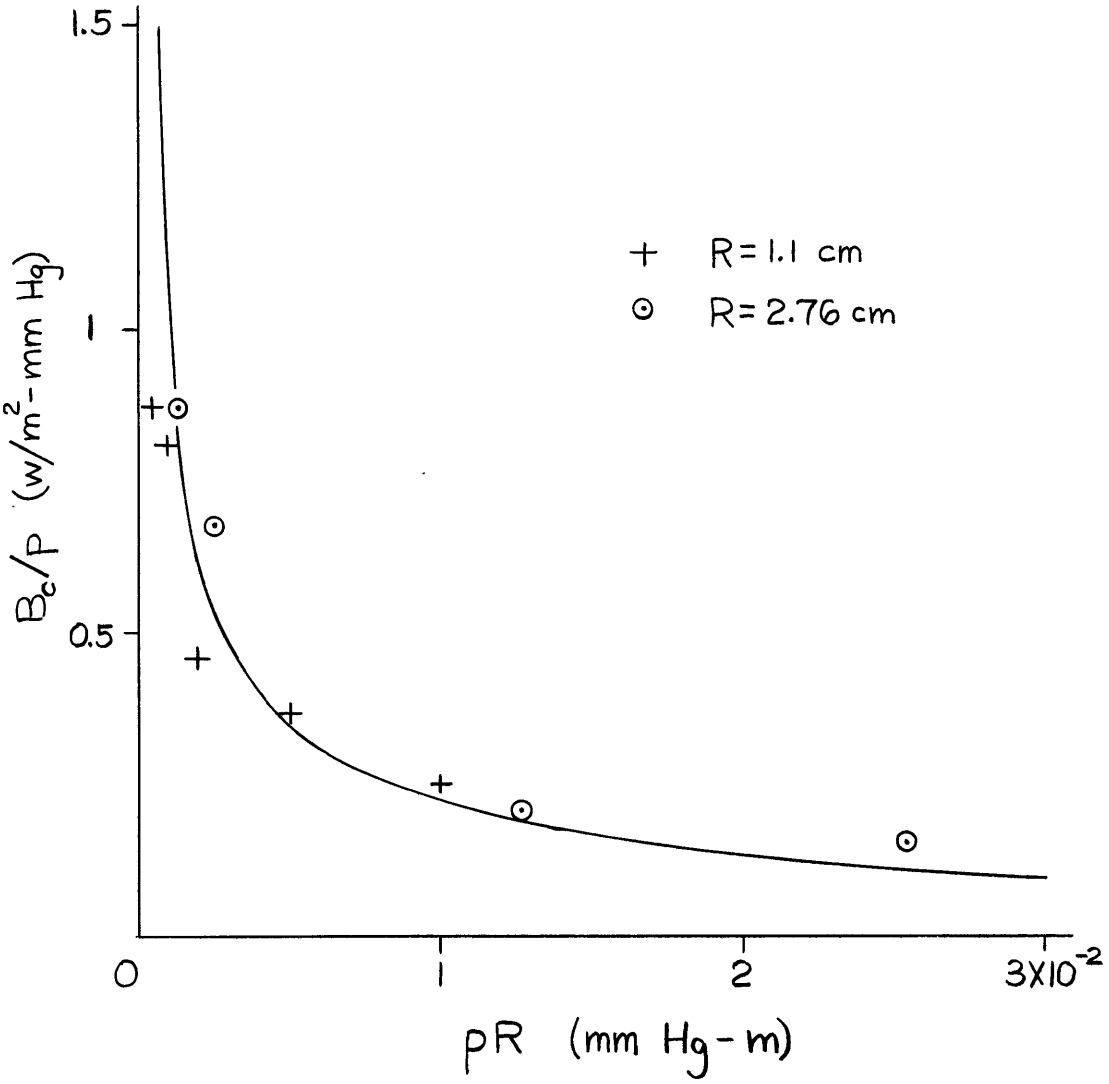

Fig. 4.6 Scaled critical magnetic fields for He. Curve is a compendium of other workers' results (Akhmedov and Zaitsev, 1963).

No evidence of a critical magnetic field for Ar in the 1.1 cm lamp is found in this experiment for B_z up to 0.35 w/m^2. This is as expected for p = 1 mm Hg, since Hoh and Lehnert (1960) do not find an instability until $B_z \approx 0.37$ w/m^2 under comparable conditions. Paulikas (1961), however, finds a critical magnetic field at $B_z = 0.18$ w/m^2 in a R = 1.27 cm lamp with p = 0.12 mm Hg and lamp current of 0.2 amp. The difference in lamp current and tube radius may account for the discrepancy, since the electron temperature, mobility, and E_z are fairly strong functions of current in Ar discharges. The possibility of a small amount of gas contamination in this experiment also exists; Paulikas (1961) states that admixtures of 1% foreign gas yield $E_z(B_z)$ curves from which B_c cannot be deduced. The contamination, however, must be less than is detectable with a hand spectroscope, and is certainly less than 1%.

There is no comparable data available for the onset of instability in the 2.76 cm lamp. In any case, except at p = 1 mm Hg, there is apparently no sharp onset of instability until the transition to the "turbulent mode". (See Section 3.4.2). Neither the magnetic field for minimum E_z nor the change to the turbulent mode can be scaled (Section 2.4) as predicted by KN. The onset of turbulence is rather sensitive to lamp current for all Ar pressures tested, coming in at generally lower B_z with increased I_z.

4.2.2 Helium-Mercury

The scaled critical magnetic fields B_c/p_{He} are plotted against $p_{He}R$ in Fig. 4.7 for the onset of oscillations, minimum E_z, and predicted values from the KN theory. The theoretical B_c is calculated using the observed axial electric field at the suspected value of B_c and the electron temperature and mobility from the WB computations.

The KN theoretical B_c agrees well with the onset of noise in the

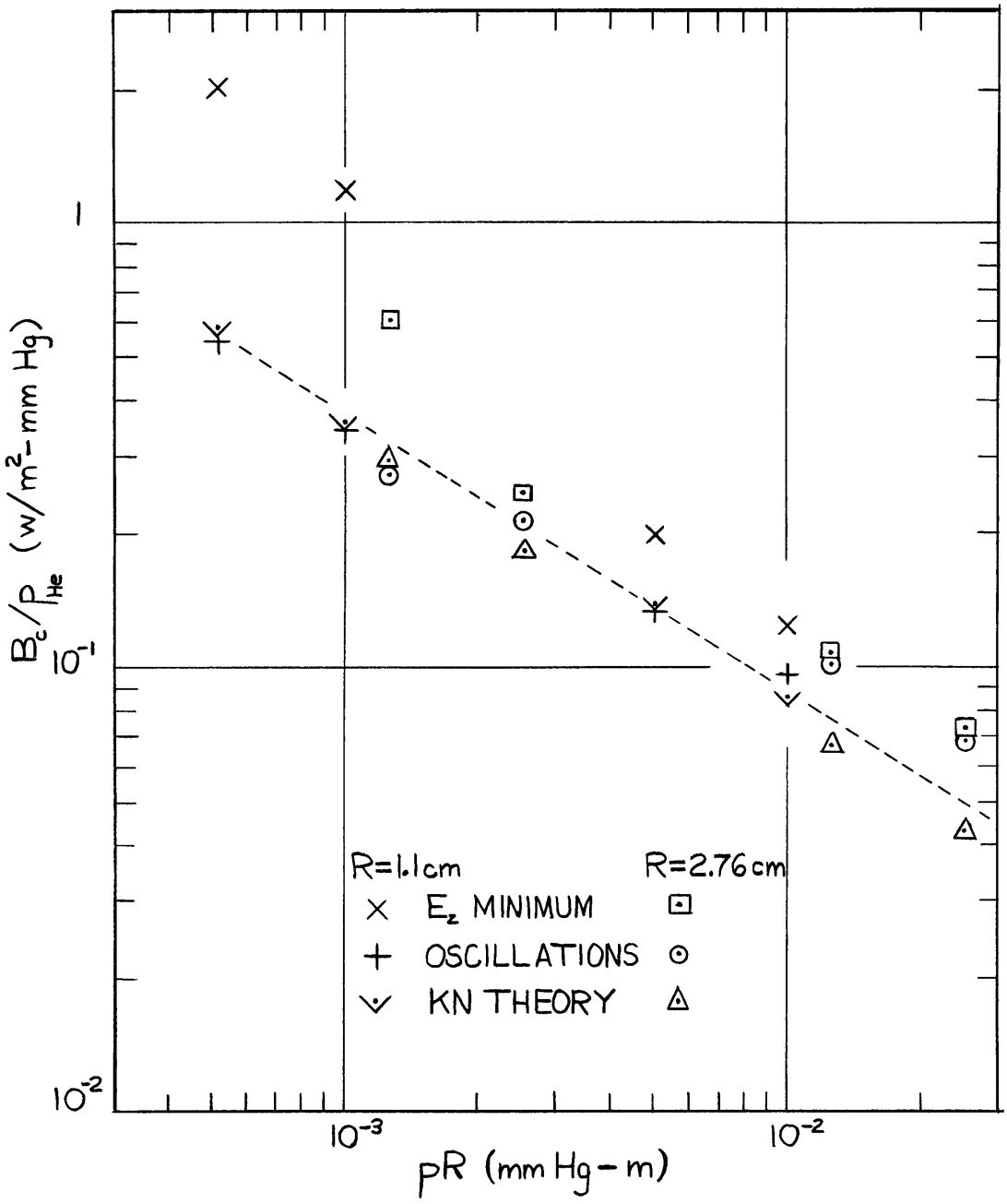

Fig. 4.7 Scaled critical magnetic fields for He-Hg.

R = 1.1 cm lamp, and fairly well with the onset of noise in the 2.76 cm lamp for He pressures of 0.1 and 0.05 mm Hg. At p_{He} = 0.5 and 1 mm Hg, however, the experimental B_c for the 2.76 cm lamp are considerably greater than predicted. Smaller electron mobility, discussed in Section 4.1.2, will not account for the difference. A decrease of electron mobility in He to 70 m^2-mm Hg/v-s and a corresponding increase of T_- will raise the theoretical points for p = 1 and 0.5 mm Hg approximately to the broken line in Fig. 4.7, but no higher. A calculation of the wavelength of the helical instability from the term X of Eq. (2.33) gives wavelengths of 12.5 cm for p_{He} = 1 mm Hg and 20 cm for p_{He} = 0.5 mm Hg, both of which are much shorter than the tube length. The KN theory, therefore, should be valid under these experimental conditions.

Fig. 4.8 shows the scaled oscillation frequency f/p_{He} versus $p_{He}R$ for noise in the 2.76 cm lamp (Table 3.1) and the rotational frequency of the KN instability, calculated from Eq. (2.36) at the observed B_c. Electron mobility and temperature are taken from WB calculations. Agreement between the theory and the lower frequency experimental points is very good, considering the approximate knowledge of T_- and μ_-.

The success of KN theory in predicting the oscillation frequencies for the 2.76 cm lamp is in direct contrast with the apparent failure to predict the critical magnetic field at p_{He} = 1 and 0.5 mm Hg. The oscillation frequency agreement supports the values of μ_- and T_- used in the B_c calculations as well as the contention that the instability is of the KN type. A possible explanation of the failure to predict B_c is that the effective radius of the discharge is less than 2.76 cm before the onset of instability. An effective discharge radius of 0.5R would make B_c calculations agree with the onset of oscillations for p_{He} = 1 mm Hg. At p_{He} = 0.5 and 0.1 mm Hg, effective discharge radii of

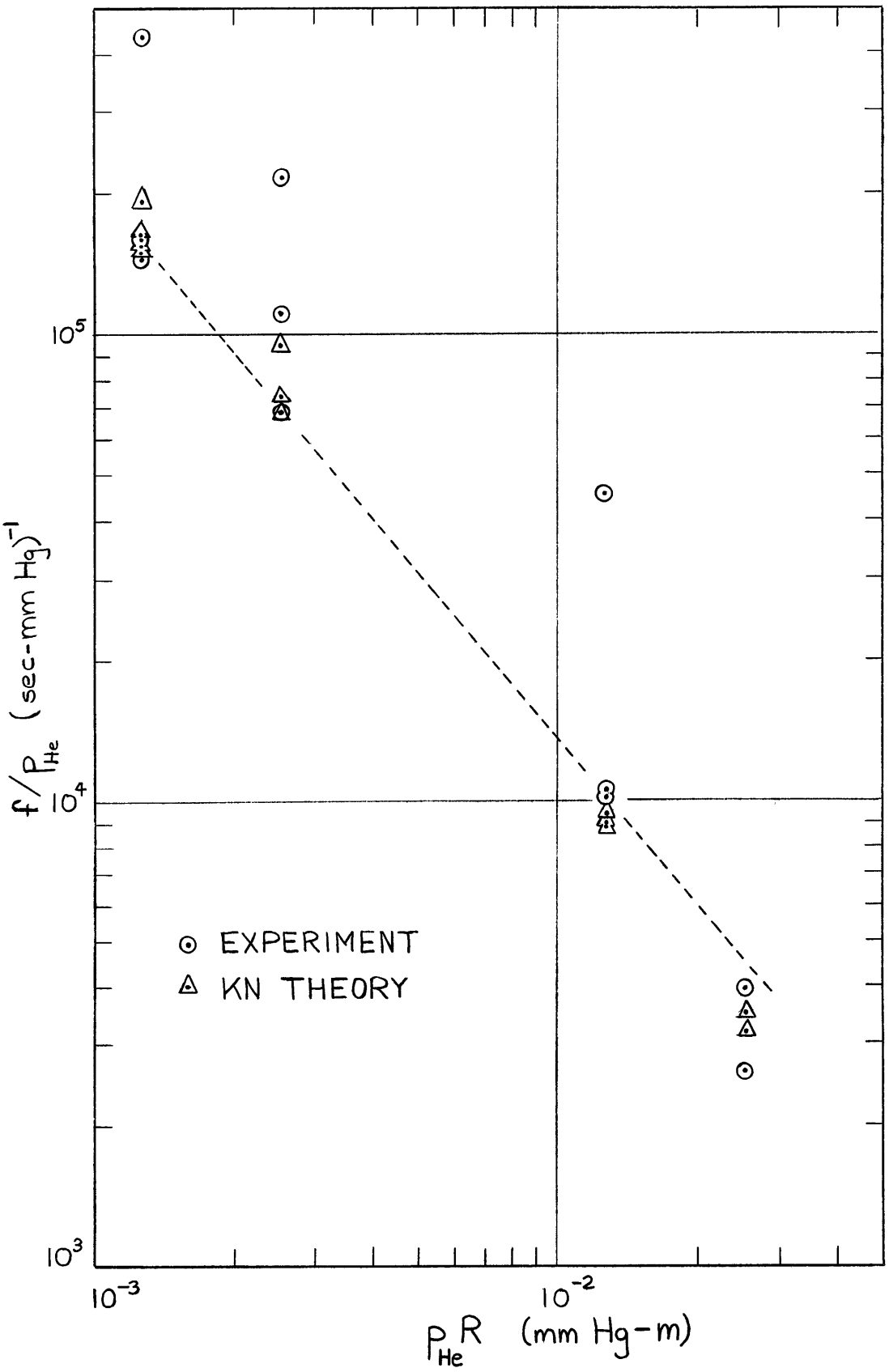

Fig. 4.8 Scaled oscillation frequencies for He-Hg in R = 2.76 cm tube.

0.6R and 0.8R would make theoretical B_c agree with experiment. The visual discharge is, in fact, somewhat channeled toward the center of the 2.76 cm tube at the higher He pressures. This explanation, however, would require that the rotating helix fill the entire tube radius as soon as B_c is reached, since the rotation frequency, Eq. (2.36), is proportional to R^{-2} and apparently correctly represented by R = 2.76 cm.

4.3 TURBULENT DIFFUSION

Table 4.2 shows the magnetic field at which the quantity $\mu_+ B_z = 1$. For a given discharge, we would expect Kadomtsev's (1962b) theory of turbulent diffusion to apply above this field. For this experiment, limited to magnetic fields less than 0.63 w/m^2, the theory should be applicable to the He discharges from p = 0.5 mm Hg to 0.05 mm Hg, Ar discharges at p = 0.05 mm Hg, and He-Hg discharges at p = 0.1 and 0.05 mm Hg.

4.3.1 Helium

Referring to Figs. 3.5 and 3.6 we see that, for B_z considerably greater than the point $\mu_+ B_z = 1$, E_z does tend to a "saturation" value, E_s, and stays constant over a considerable range of B_z. To test whether the saturation values agree with Kadomtsev's theory, the ratio of E_s to the zero magnetic field $E_z(0)$ is plotted in Fig. 4.9 along with the theoretical curve for He (Kadomtsev, 1962b) for a mixing length $\ell = 0.15R$. Theory and experiment agree well for the R = 1.1 cm lamp and for p = 0.1 and 0.05 mm Hg for the R = 2.76 cm lamp. At p = 0.5 mm Hg in the 2.76 cm lamp there is a clear departure from the theory, and at p = 1 mm Hg agreement is probably poor, although E_s has not yet been reached at $B_z = 0.63$ w/m^2.

It is likely that the mixing length ℓ is no longer proportional to the tube radius at $p \geqslant 0.5$ mm Hg. A longer mixing length in Eq. (2.47) would increase

TABLE 4.2

MAGNETIC FIELD B_z (w/m^2) AT WHICH $\mu_+ B_z = 1$

Ion	Gas Pressure (mm Hg) 1	0.92	0.46	0.184	0.092	0.046
He^+	1.23	1.13	0.566	0.227	0.113	0.0566
He_2^+	0.814	0.749	0.374	0.150	0.0749	0.0374
Ar^+	8.23	7.57	3.79	1.51	0.757	0.379
Ar_2^+	6.92	6.36	3.18	1.27	0.636	0.318
Hg^+-He	0.782	0.728	0.420	0.234	0.173	0.142 ($p_{Hg} = 2 \times 10^{-3}$)
Hg^+-He	1.22	1.17	0.859	0.673	0.612	0.581 ($p_{Hg} = 10^{-2}$)

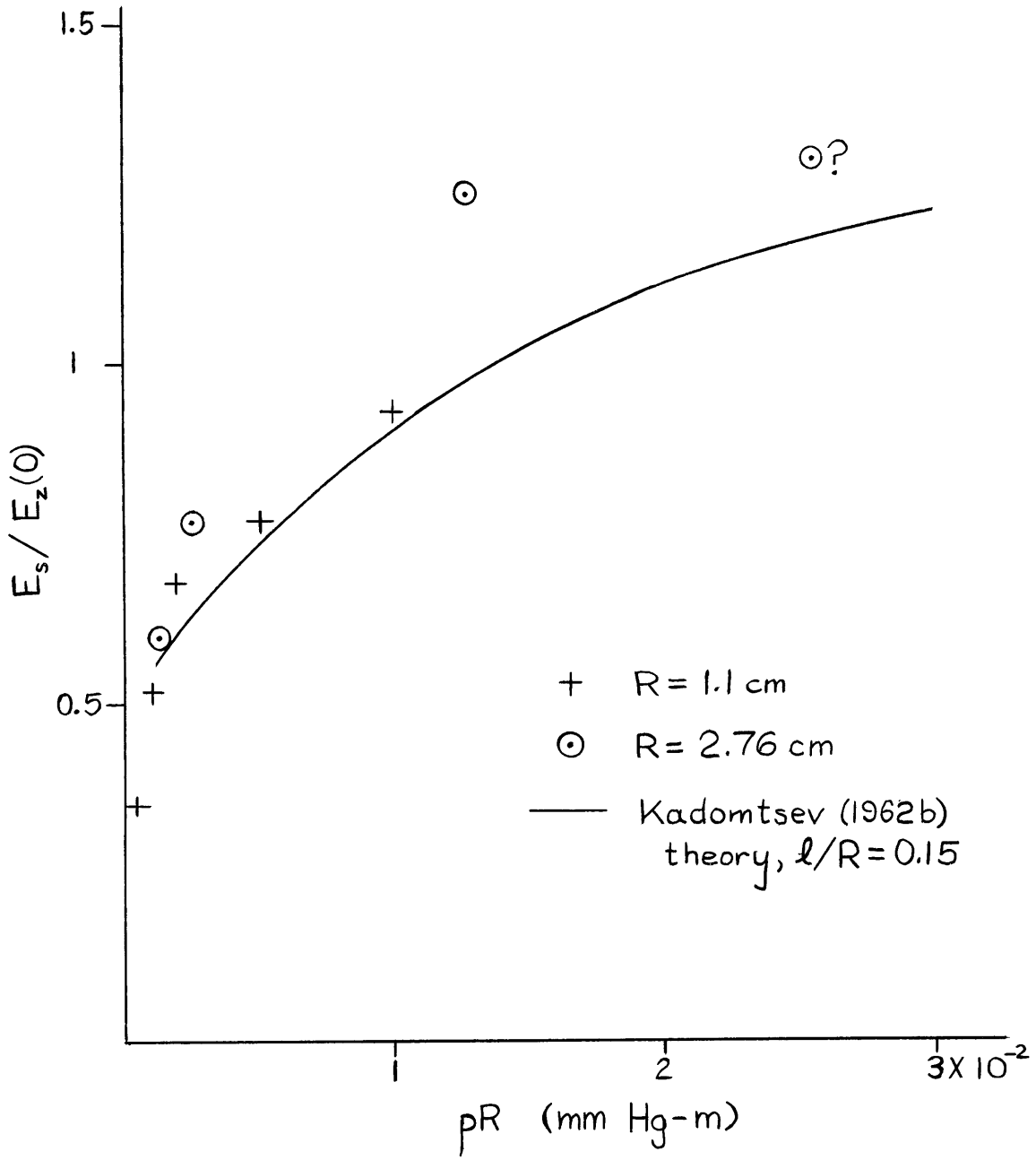

Fig. 4.9 "Saturation" electric field in turbulent He discharges compared with Kadomtsev (1962 b) theory.

turbulent losses and give a higher value of E_s. Further, the presence of radial temperature gradients in the plasma at these pressures may increase the turbulent diffusion by other than Kadomtsev's mechanism.

The axial electric field begins to decrease again with B_z after reaching the saturation value. This behavior contradicts Kadomtsev's turbulent diffusion theory and suggests that a new phenomenon is beginning to control the transverse charge diffusion. To test the B_z dependence of this diffusion, $E_z(B_z)/p$ is plotted in Fig. 4.10 against pRB_z and $pR\sqrt{B_z}$ for the 2.76 cm lamp at He pressures of 0.1 and 0.05 mm Hg and $B_z > B_z(E_s)$. The zero magnetic field $E_z(0)/p$ are plotted against pR on the same figure. If the transverse diffusion rate is proportional to B_z^{-2}, as in classical diffusion when $\mu_+ \mu_- B_z^2 \gg 1$, E_z/p vs. pRB_z should fall on a line parallel to $E_z(0)/p$ on a logarithmic plot. If the transverse diffusion rate is proportional to B_z^{-1}, as in "Bohm diffusion", E_z/p vs. $pR\sqrt{B_z}$ should be parallel to the $E_z(0)/p$ line.

These statements can be made only if the turbulence does not seriously change the scaling relations of the discharge. Kadomtsev (1962b) argues that the fluctuation of E_z is only about $\pm 10\%$, and, therefore, does not appreciably change the electron temperature dependence on E_z/p. In this case the turbulent discharges should scale as at zero magnetic field.

From Fig. 4.10 it appears that the transverse diffusion is closer to the B_z^{-2} type for p = 0.05 mm Hg. For p = 0.1 mm Hg there are not enough data to come to a definite conclusion, although the curve plotted against $pR\sqrt{B_z}$ may be approaching the slope of the zero field line.

4.3.2 Argon

The "turbulent mode" Ar discharges do not show "saturation" values of E_z;

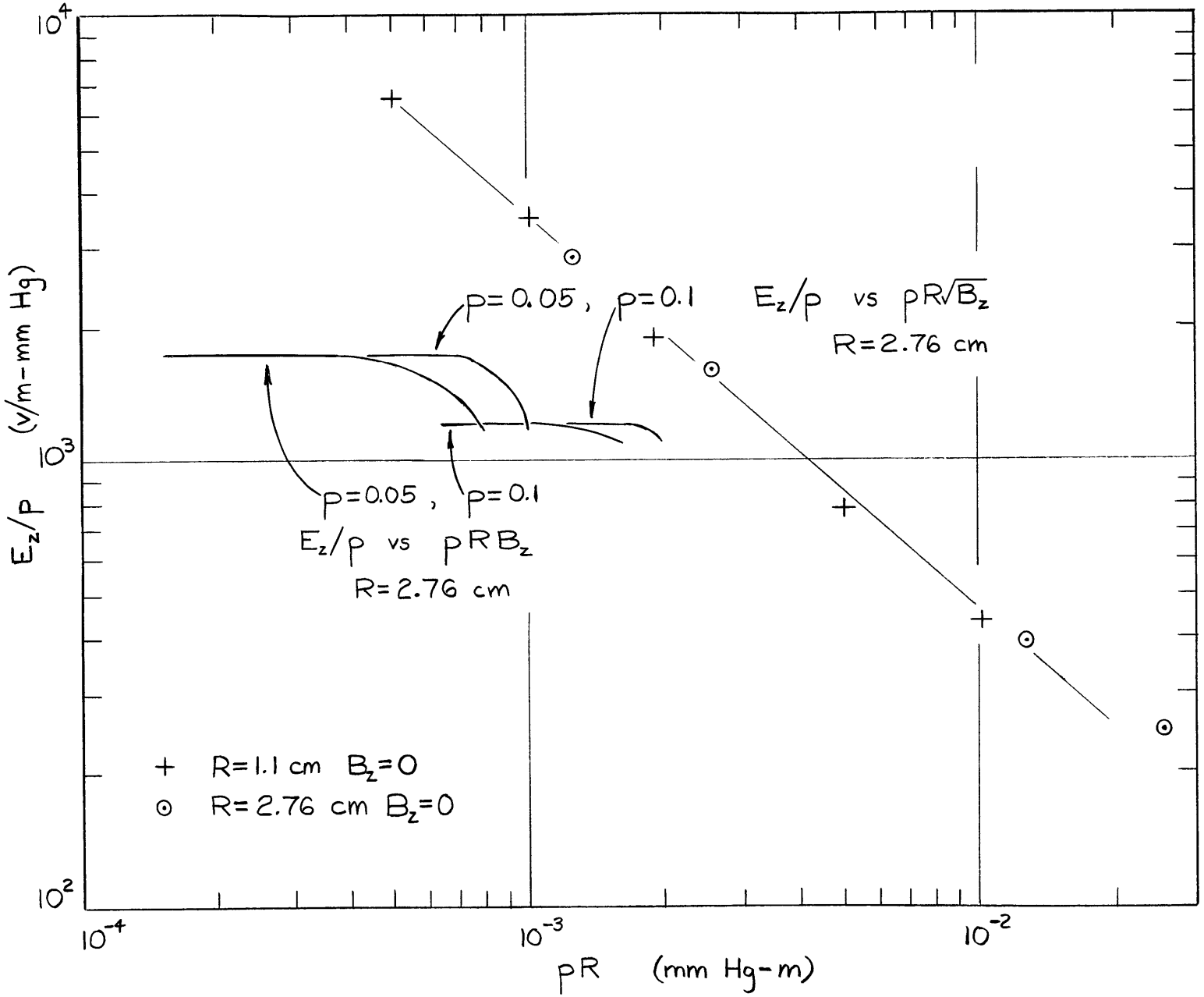

Fig. 4.10 Scaled He results at $B_z = 0$ and in turbulent discharges.

although, since $(\mu_+ B_z)^2 < 1$ (Table 4.1) for most of the $E_z(B_z)$ curves, Kadomtsev's theory would not predict a saturation field. Instead, Eq. (2.48) would predict B_z^{-1} diffusion.

$E_z(B_z)/p$ is plotted against $pR\sqrt{B_z}$ and pRB_z in Fig. 4.11 for the turbulent mode Ar discharge at p = 0.1 mm Hg and I_z = 0.3 amps. On the same graph is the zero magnetic field $E_z(0)/p$ versus pR. The curve plotted against pRB_z(B_z^{-2} diffusion) approaches a slope more nearly that of the zero field results, but more data would be necessary to decide the issue.

The two mode operation of the Ar discharges may be related to a somewhat similar phenomenon in cesium discharges in a longitudinal magnetic field (Robertson, 1964).

4.3.3 Helium-Mercury

Turbulent diffusion in the He-Hg discharges of this experiment is difficult to study since both the Hg and He pressures were varied. There is qualitative similarity between the He-Hg results in the R = 2.76 cm lamp at p_{He} = 0.1 and 0.05 mm Hg and the pure He results at high B_z. The axial electric field comes to a saturation value when $(\mu_+ B_z)^2 \gg 1$ and then decreases slowly after this point. Lack of data precludes further comparisons.

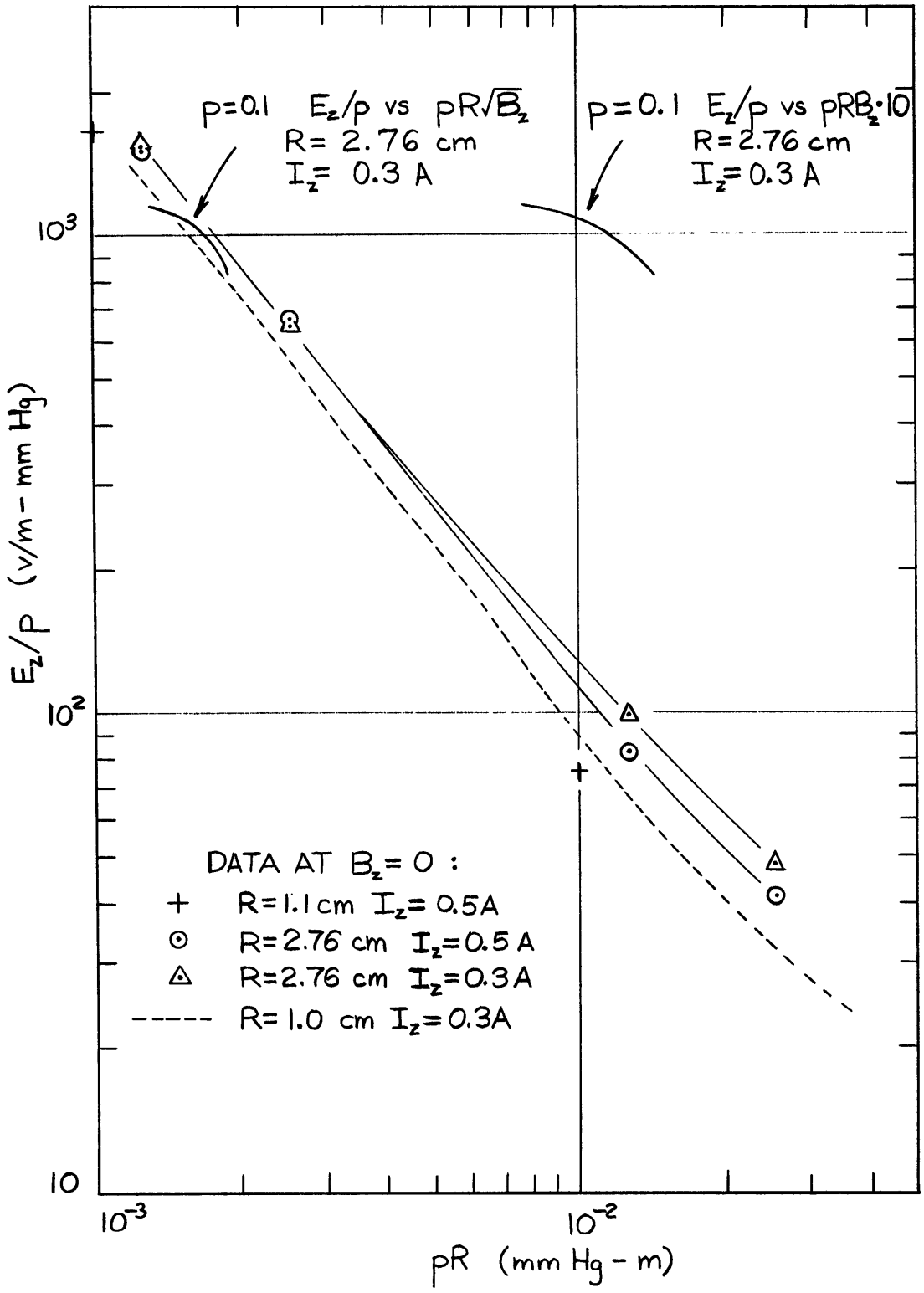

Fig. 4.11 Scaled Ar results at $B_z = 0$ and in turbulent mode. Broken curve from Francis (1956; p. 116).

V. CONCLUSIONS

Classical Diffusion

Transverse plasma diffusion in He and Ar discharges, before the onset of instabilities, is similar to that found by other authors, who show that it is consistent with classical theory. Transverse diffusion in the He-Hg discharges, studied by the variation of the axial electric field and radial potential drop as a function of axial magnetic field, agrees fairly well with theory for the R = 2.76 cm discharge, but shows greater than predicted diffusion for the R = 1.1 cm case. Decreasing the electron mobility in He in the theoretical calculations would give somewhat better agreement with experiment.

Kadomtsev and Nedospasov (KN) Instability

The critical magnetic field data for He discharges agrees well with the theory of Kadomtsev and Nedospasov (1960) as found by others. For Ar discharges at pressures below 0.5 mm Hg the KN theory apparently does not apply. A two mode, i.e., low E_z and "turbulent", type of operation is found at low pressures and fairly high magnetic fields; the onset of the turbulent mode is not predicted by KN theory. In He-Hg discharges the KN instability theory predicts the onset of electrical noise, which does not correspond to the minimum E_z for helium pressures below 0.5 mm Hg. A discrepancy between predicted B_c and experiment for the R = 2.76 cm lamp at p_{He} 0.5 mm Hg may be explainable by "channeling" of the discharge to the center of the tube.

Turbulent Diffusion

The Kadomtsev (1962b) theory of turbulent plasma diffusion works well over a limited range of magnetic field for He discharges in the R = 1.1 cm tube, but fails for the R = 2.76 cm tube at He pressures greater than 0.1 mm Hg.

Larger than expected transverse diffusion occurs in this case. The turbulence theory apparently does not apply to Ar discharges in the turbulent mode; the turbulent diffusion rate may have a B_z^{-2} dependence rather than B_z^{-1} as predicted by Kadomtsev. Turbulent diffusion in the He and He-Hg discharges show a return to dependence on the magnetic field after passing through Kadomtsev's turbulent saturation. The diffusion rate is not proportional to B_z^{-1}, but may be closer to B_z^{-2}.

BIBLIOGRAPHY

Akhmedov, A. R., and A. A. Zaitsev, Noise in a Gas Discharge and Instabilities of the Column in a Longitudinal Magnetic Field, Sov. Phys. - Tech. Phys., 8, 126-130, 1963.

Akhmedov, A. R., and A. A. Zaitsev, Instability of a Plasma in a Magnetic Field upon Transition from Low to High Pressures, Sov. Phys. JETP, 18, 977-978, 1964.

Allen, T. K., G. A. Paulikas, and R. V. Pyle, Instability of the Positive Column in a Magnetic Field, Phys. Rev. Letters, 5, 409-411, 1960.

Allis, W. P., Motions of Ions and Electrons, in Handbuch der Physik v. 21, ed. S. Flügge, Springer-Verlag, Berlin, 1956, pp. 383-444.

Artsimovich, L. L., and A. V. Nedospasov, The Radial Distribution of Plasma of a Positive Column in a Magnetic Field, Sov. Phys. Doklady, 7, 717-718, 1963.

Barnes, B. T., Disturbance of a Low-Pressure Discharge by a Probe, J. Appl. Phys., 33, 3319-3322, 1962.

Biondi, M. A., Processes Involving Ions and Metastable Atoms in Mercury Afterglows, Phys. Rev. 90, 730-737, 1953.

Boeschoten, F., Review of Experiments on the Diffusion of Plasma Across a Magnetic Field, J. Nucl. Energy Part C, 6, 339-388, 1964.

Bohm, D., in Characteristics of Electrical Discharges in Magnetic Fields, eds. A. Guthrie and R. K. Wakerling, McGraw-Hill, New York, 1949, ch. 2.

Brown, S. C., Basic Data of Plasma Physics, M. I. T. Press, Cambridge, Mass., 1959.

Cayless, M. A., Theory of the Positive Column in Mercury Rare-Gas Discharges, British J. Appl. Phys., 14, 863-869, 1963.

Chanin, L. M., and M. A. Biondi, Mobilities of Mercury Ions in Helium, Neon and Argon, Phys. Rev., 107, 1219-1221, 1957.

Cravath, A. M., The Rate at Which Ions Lose Energy in Elastic Collisions, Phys. Rev., 36, 248-250, 1930.

Ecker, G., Enhanced Interaction in the Positive Column, Phys. Fluids, 4, 127-138, 1961.

von Engel, A., and M. Steenbeck, Elektrische Gasentladungen, v. II, J. Springer, Berlin, 1932.

Francis, G., The Glow Discharge at Low Pressure, in Handbuch der Physik, v. 22, ed. S. Flügge, Springer-Verlag, Berlin, 1956, pp. 53-208.

von Gierke, G., and Wöhler, K. H., On the Diffusion in the Positive Column in a Longitudinal Magnetic Field, Nuclear Fusion: 1962 Suppl., Part I, 47-53.

Glicksman, M., Instabilities of a Cylindrical Electron-Hole Plasma in a Magnetic Field, Phys. Rev., 124, 1655-1664, 1961.

Golant, V. E., Diffusion of Charged Particles in a Plasma in a Magnetic Field, Sov. Phys. Uspekhi, 6, 161-197, 1963.

Hoh, F. C., Low-Temperature Plasma Diffusion in a Magnetic Field, Rev. Mod. Phys., 34, 267-286, 1962.

Hoh, F. C., and B. Lehnert, Diffusion Processes in a Plasma Column in a Longitudinal Magnetic Field, Phys. Fluids, 3, 600-607, 1960.

Hoh, F. C., and B. Lehnert, Screw Instability of a Plasma Column, Phys. Rev. Letters, 7, 75-76, 1961.

Johnson, R. R., and D. A. Jerde, Instability of a Plasma Column in a Longitudinal Magnetic Field, Phys. Fluids, 5, 988-993, 1962.

Johnson, R. R. and D. A. Jerde, Stability of the Positive-Column in a Time-Dependent Magnetic Field, Phys. Fluids, 7, 103-109, 1964.

Kadomtsev, B. B., Turbulent Loss of Particles from a Discharge in a Strong Magnetic Field, Sov. Phys.-Tech. Phys., 6, 882-888, 1962a.

Kadomtsev, B. B., Convection of the Plasma of a Positive Column in a Magnetic Field, Sov. Phys.-Tech. Phys., 6, 927-933, 1962b.

Kadomtsev, B. B., Turbulent Plasma in a Strong Magnetic Field, J. Nucl. Energy Part C, 5, 31-36, 1963.

Kadomtsev, B. B., and A. V. Nedospasov, Instability of the Positive Column in a Magnetic Field and the 'Anomalous' Diffusion Effect, J. Nucl. Energy Part C, 1, 230-235, 1960.

Kenty, C., Production of 2537 Radiation and the Role of Metastable Atoms in an Argon-Mercury Discharge, J. Appl. Phys., 21, 1309-1318, 1950.

Kovar, F. R., Mobility of Mercury Ions in Mercury Vapor, Phys. Rev., 133A, 681-685, 1964.

Kretschmer, C. B., and H. L. Petersen, Use of Langmuir Probes to Study Ion-Electron Recombination, J. Appl. Phys., 34, 3209-3217, 1963.

Lehnert, B., Diffusion Processes in the Positive Column in a Longitudinal Magnetic Field, Proc. Second Int'l. Conf. on Peaceful Uses of Atomic Energy, v. 32, United Nations, Geneva, 1958, pp. 349-357.

Little, R. G., Experimental Determination of the Perturbation of a Plasma by a Probe, M. S. Thesis, Mass. Inst. of Tech., Cambridge, Mass., 1964.

Loeb, L. B., Basic Processes of Gaseous Electronics, U. of Calif. Press, Berkeley, 1955, pp. 336-351.

Myers, H., Ionization Processes in Decaying Plasmas. I. Helium, Phys. Rev., 130, 1639-1643, 1963.

Nedospasov, A. V., Concerning Ambipolar Diffusion in a Magnetic Field, Sov. Phys. JETP, 7, 923-924, 1958.

Oskam, H. J., and V. R. Mittelstadt, Ion Mobilities in Helium, Neon, and Argon, Phys. Rev., 132, 1435-1444, 1963.

Paulikas, G. A., The Positive Column in a Longitudinal Magnetic Field, Ph.D. Thesis, U. of Calif., Berkeley, UCRL-9588, 1961. (Also Phys. Fluids, 5, 348-360, 1962.)

Phelps, A. V., and S. C. Brown, Positive Ions in the Afterglow of a Low Pressure Helium Discharge, Phys. Rev., 86, 102-105, 1951.

Phelps, A. V., J. L. Pack, and L. S. Frost, Drift Velocities of Electrons in Helium, Phys. Rev., 117, 470-474, 1960.

Prandtl, L., Essentials of Fluid Dynamics, Hafner Publ. Co., New York, 1952, p. 117.

Robertson, H. S., Suppression of Helical Instabilities in Plasma by High Magnetic Fields. Phys. Fluids, 7, 1093-1094, 1964.

Rudakov, L. I. and R. Z. Sagdeev, On the Instability of a Nonuniform Rarified Plasma in a Strong Magnetic Field, Sov. Phys. Doklady, 6, 415-417, 1961.

Rugge, H. F., and Pyle, R. V., Instability of an Alternating-Current Positive Column, Phys. Fluids, 7, 754-759, 1964.

Sato, M., and Hatta, Y., Collision Diffusion of Plasma in Magnetic Field, J. Phys. Soc. Japan, 18, 1507-1514, 1963.

Schottky, W., Diffusionstheorie der Positiven Säule, Phys. Z. 25, 635-640, 1924.

Simon, A., Ambipolar Diffusion in a Magnetic Field, Phys. Rev., 98, 317-318, 1955.

Spitzer, L., Particle Diffusion across a Magnetic Field, Phys. Fluids, 3, 659-661, 1960.

Tonks, L., Diffusion through a Finite Plasma in a Uniform Magnetic Field, Phys. Fluids, 3, 758-764, 1960.

Vdovin, V. L., and Nedospasov, A. V., Instability of Positive Columns in Magnetic Fields, Sov. Phys.-Tech. Phys., 7, 598-601, 1963.

Verweij, W., Probe Measurements and Determination of Electron Mobility in the Positive Column of Low-Pressure Mercury-Argon Discharge, Ph.D. Thesis, U. of Utrecht, 1960.

Walsh, P. J., Imprisonment of Resonance Radiation in a Gaseous Discharge, Phys. Rev., 107, 338-344, 1957.

Walsh, P. J., G. W. Manning, and D. A. Larson, Gradients in Mercury-Rare-Gas Discharges, J. Appl. Phys., 34, 2273-2277, 1963.

Waymouth, J. F., and Bitter F., Analysis of the Plasma of Fluorescent Lamps, J. Appl. Phys., 27, 122-131, 1956. For more detail see the authors' Engineering Report #E-671, Sylvania Electric Products, Inc., Salem, Mass., 1956.

Woehler, K. E., On the Turbulence of the Positive Column in a Large Longitudinal Magnetic Field, Abstracts, Int'l. Symp. on Diffusion of Plasma Across a Magnetic Field, Munich, 1964.

Yoshikawa, S., and D. J. Rose, Anomalous Diffusion of a Plasma across a Magnetic Field, Phys. Fluids, 5, 334-340, 1962.

Zaitsev, A. A., and M. Ya. Vasil'eva, Connection between Oscillation and Rate of Loss of Charged Particles in a Cylindrical Plasma of Low Pressure in a Longitudinal Magnetic Field, Sov. Phys. JETP, 11, 1180-1181, 1960.

Zharinov, A. V., The Diffusion of Electrons in a Magnetic Field, J. Nucl. Energy Part C, 1, 271-274, 1960.

APPENDIX I

CALCULATION OF ELECTRIC FIELDS IN He-Hg DISCHARGES.

The axial field E_z in the He-Hg was computed using the theory of Waymouth and Bitter (1956) with the one modification that the rate of loss of ions to the tube walls is governed by the coefficient of magneto-ambipolar diffusion, Eq. (2.15). Electron mobility and elastic collision losses in helium were calculated from collision probability data of Phelps et al. (1960) for electron temperatures less than two volts and from Brown (1959, p. 5) at higher energies. The computed variation of electron mobility in helium with electron temperature is shown in Fig. A1.1. At the lower He pressures encountered in this experiment, the effect of collisions with Hg atoms must also be included in the calculations. Electron mobility in Hg vapor at 1 mm Hg is taken from Verweij (1960) to be a constant 14 $m^2/v\text{-}s$. The Hg^+ ion mobility in He given by Chanin and Biondi (1957), when reduced to p_{He}= 1 mm, is 1.49 $m^2/v\text{-}s$. The mobility of Hg^+ ions in mercury vapor has been directly measured by Kovar (1964), who finds a value of 0.018 $m^2/v\text{-}s$ for reduced Hg pressure of 1 mm Hg. This mobility agrees well with an indirect measurement by Biondi (1953).

Table AI shows values of important parameters used in the electric field calculations at zero magnetic field and at a typical value of B_z. The correction factor f is applied to make the calculated electric field agree with experiment at B_z= 0. The value of f is assumed to be independent of B_z.

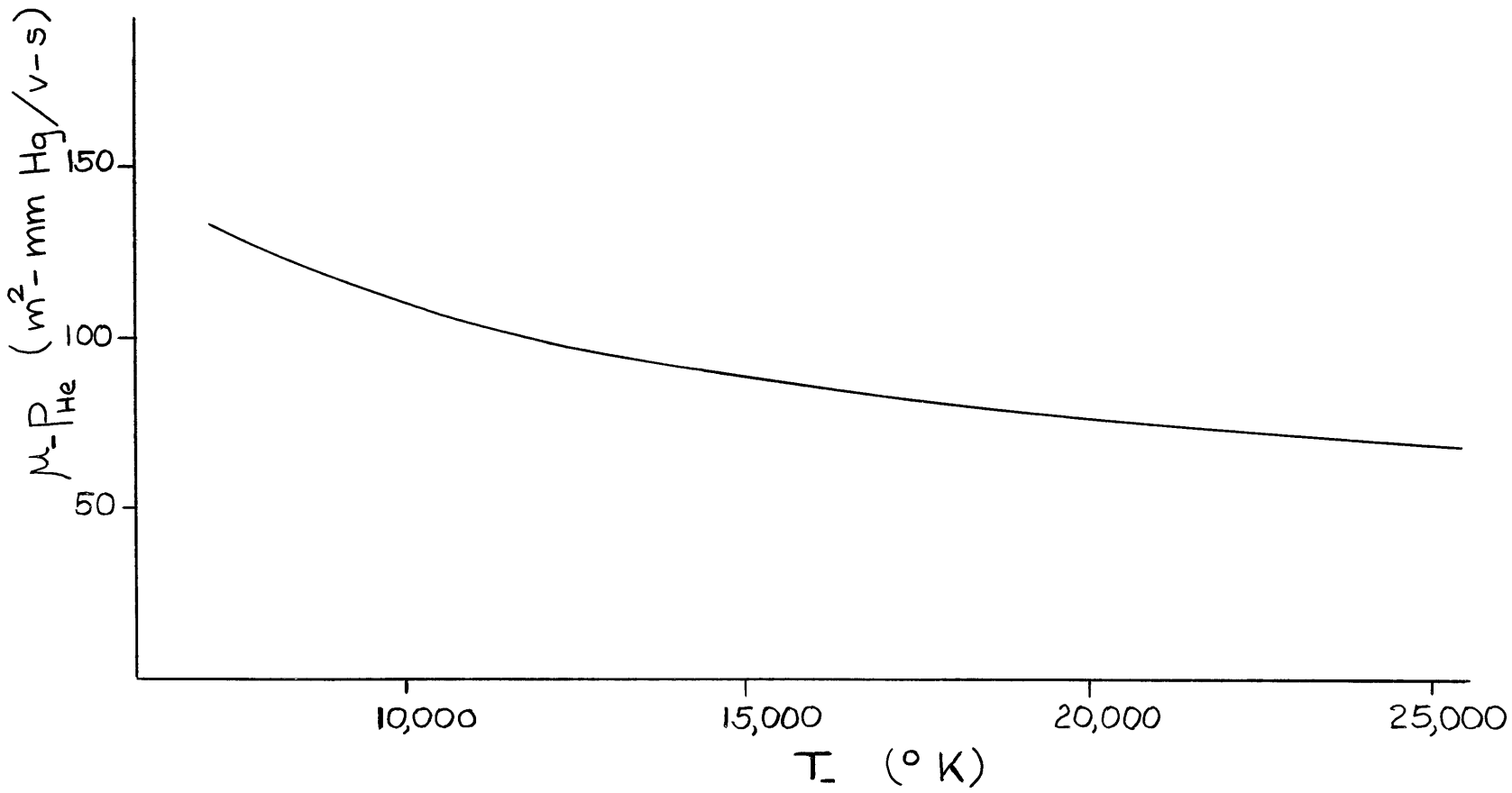

Fig. A1.1 Electron mobility in helium vs. electron temperature. Based on data by Phelps et al. (1960).

TABLE A I

IMPORTANT PARAMETERS IN He-Hg DISCHARGE ELECTRIC FIELD CALCULATIONS

B_z (w/m^2)	R (cm)	p_{He} (mm Hg)	p_{Hg} (mm Hg)	μ_- ($m^2/v\text{-}s$)	μ_+ ($m^2/v\text{-}s$)	T_- (^oK)	E_z (v/m)	Correction factor f	Corrected E_z (v/m)	Average n_- (m^{-3})
0	2.76	0.92	4.6×10^{-3}	94.0	1.20	15,000	170	1.23	209	3.9×10^{16}
0.07	"	"	"	97.2	"	14,300	153	"	188	4.4×10^{16}
0	1.1	0.92	6.6×10^{-3}	86.0	1.02	17,100	277	1.13	312	1.8×10^{17}
0.07	"	"	"	88.5	"	16,200	242	"	272	2×10^{17}
0	2.76	0.46	3.6×10^{-3}	176	1.98	16,400	129	1.13	146	3×10^{16}
0.05	"	"	"	184	"	15,000	106	"	120	3.5×10^{16}
0	1.1	0.46	5×10^{-3}	154	1.70	19,700	222	1.02	227	1.4×10^{17}
0.05	"	"	"	164	"	18,200	187	"	191	1.6×10^{17}
0	2.76	0.092	2.8×10^{-3}	724	4.62	19,700	73.8	1.00	73.8	1.5×10^{16}
0.02	"	"	"	770	"	17,000	58.0	"	58.0	1.8×10^{16}
0	1.1	0.092	3.3×10^{-3}	662	4.08	26,000	135	0.887	120	6.5×10^{16}
0.02	"	"	"	660	"	23,000	104	"	92	8.1×10^{16}
0	2.76	0.046	2.6×10^{-3}	1260	5.72	20,500	57.9	1.00	57.9	1.1×10^{16}
0.02	"	"	"	1370	"	16,600	36.4	"	36.4	1.6×10^{16}
0	1.1	0.046	3.3×10^{-3}	1080	4.66	26,700	113	0.893	91.6	5×10^{16}
0.02	"	"	"	1170	"	21,400	69.0	"	61.6	6.9×10^{16}

APPENDIX II

CALCULATION OF ION TEMPERATURE IN He-Hg DISCHARGES

The ion temperature is found by equating the ion energy gain from the longitudinal electric field to the average energy lost in collisions.

$$e\mu_+ E_z^2 = \nu_{c1}\kappa_1 u_+ + \nu_{c2}\kappa_2 u_+ \qquad \text{(A2.1)}$$

where u_+ is the average ion energy, ν_c is the collision frequency between ions and neutrals, κ is the average energy loss per collision, and the subscripts 1 and 2 refer to the species of particles with which the ions collide.

For ions with a Maxwellian velocity distribution, colliding elastically with gas atoms at a temperature T_g, κ is given (Cravath, 1930) by

$$\kappa = \frac{8}{3}\frac{m_+ m_g}{(m_+ + m_g)^2}\left(1 - \frac{T_g}{T_+}\right) \qquad \text{(A2.2)}$$

Solving for u_+ and assuming that

$$\nu_{c1} = \frac{e}{m_+\mu_1} \quad \text{, etc.,}$$

$$u_+ = \frac{3}{2}eT_+(v) = \frac{\mu_+ m_+ E_z^2}{\kappa_1/\mu_1 + \kappa_2/\mu_2} \qquad \text{(A2.3)}$$

If the ion temperature is much greater than the gas temperature, the Hg^+ ion temperature in a He-Hg mixture is

$$T_+(v) = \frac{3.54\times10^{-6}\mu_+ E_z^2}{0.036p_{He} + 40p_{Hg}} \qquad \text{(A2.4)}$$

where p_{He} and p_{Hg} are in units of mm Hg. The value of κ used in Eq. (A2.4) is taken to be 0.72 instead of 2/3 to allow for some energy loss to charge exchange collisions. Kovar's (1964) data indicates that the mobility of Hg_2^+ in Hg is considerably greater than that of Hg^+; the Hg^+ ion velocity is presumably limited by charge exchange collisions with neutral mercury.

Table AII shows Hg^+ ion temperature and mean free path in Hg vapor calculated for $B_z = 0$ and at a typical value of B_z. The ion temperature is considerably higher than usually found in gas discharges, but such high temperatures have been suspected in He-Hg discharges (Little, 1964) under comparable experimental conditions.

TABLE AII

CALCULATED ION TEMPERATURES FOR He-Hg DISCHARGES

B_z (w/m^2)	R (cm)	p_{He} (mm Hg)	p_{Hg} (mm Hg)	E_z (v/m)	T_+ (volts)	$\lambda_{c+}(Hg^+-Hg)$ (cm)
0	2.76	0.92	4.6×10^{-3}	190	0.81	0.16
0.07	"	"	"	186	0.67	"
0	1.1	0.92	6.6×10^{-3}	306	1.13	0.096
0.07	"	"	"	288	1.00	"
0	2.76	0.46	3.6×10^{-3}	148	0.95	0.18
0.05	"	"	"	134	0.78	"
0	1.1	0.46	5×10^{-3}	229	1.46	0.13
0.05	"	"	"	210	1.23	"
0	2.76	0.092	2.8×10^{-3}	74	0.79	0.23
0.02	"	"	"	64	0.58	"
0	1.1	0.092	3.3×10^{-3}	120	1.54	0.19
0.02	"	"	"	108	1.25	"
0	2.76	0.046	2.6×10^{-3}	58	0.65	0.24
0.02	"	"	"	48	0.45	"
0	1.1	0.046	3.3×10^{-3}	92	1.04	0.19
0.02	"	"	"	81	0.81	"

APPENDIX III

CALCULATION OF RADIAL POTENTIAL DROP IN He-Hg DISCHARGES

The radial potential drop V_r between the lamp wall and center is calculated from Eq. (2.18). The diffusion coefficients $D_{\pm}$ are evaluated using the Einstein relation Eq. (4.1) and the calculated electron and ion temperatures from Appendices I and II. The logarithmic term is found by normalizing the zero magnetic field calculation of V_r to the experimentally observed V_r. The normalizing factor F is then assumed to be independent of magnetic field. Table AIII shows the important parameters used in calculating V_r at magnetic field strengths of zero and a typical value.

TABLE AIII

IMPORTANT PARAMETERS IN He-Hg DISCHARGE Vr CALCULATIONS

B_z (w/m^2)	R (cm)	P_{He} (mm Hg)	P_{Hg} (mm Hg)	$\mu_{\perp+}$ ($m^2/v\text{-}s$)	$\mu_{\perp-}$ ($m^2/v\text{-}s$)	$D_{\perp+}$ (m^2/s)	$D_{\perp-}$ (m^2/s)	F	V_r (volts)
0	2.76	0.92	4.6×10^{-3}	1.20	94.0	1.17	121	-2.42	-3.05
0.07	"	"	"	1.20	2.06	0.94	2.53	"	-1.19
0	1.1	0.92	6.6×10^{-3}	1.02	86	1.19	127	-1.09	-1.57
0.07	"	"	"	1.01	2.22	0.90	3.09	"	-0.74
0	2.76	0.46	3.6×10^{-3}	1.98	176	1.83	249	-2.48	-3.45
0.05	"	"	"	1.96	2.14	1.20	2.77	"	-0.85
0	1.1	0.46	5×10^{-3}	1.70	157	2.44	266	-1.35	-2.24
0.05	"	"	"	1.69	2.41	3.78	3.78	"	-0.51
0	2.76	0.092	2.8×10^{-3}	4.62	724	3.57	1230	-2.08	-3.50
0.02	"	"	"	4.58	3.24	2.16	4.72	"	-0.68
0	1.1	0.092	3.3×10^{-3}	4.08	662	6.29	1438	-1.135	-2.60
0.02	"	"	"	4.06	3.79	5.76	7.52	"	-0.35
0	2.76	0.046	2.6×10^{-3}	5.72	1260	3.71	2220	-1.995	-3.50
0.02	"	"	"	5.65	1.82	1.45	2.59	"	-0.30
0	1.1	0.046	3.3×10^{-3}	4.66	1080	4.83	2480	-1.37	-3.12
0.02	"	"	"	4.62	2.25	3.74	4.81	"	-0.21

APPENDIX IV

SYMBOLS

B	magnetic field (weber/m^2)
b, c, C, d	proportionality factors
D	diffusion coefficient (m^2/s)
e	electron charge (1.6×10^{-19} coulomb)
f	correction factor; function; frequency (s^{-1})
F	correction factor; Eq. (2.33)
g	function
G	Eq. (2.33)
i	$\sqrt{-1}$
I	current (ampere)
k	wave number (m^{-1})
K	Eq. (2.33)
ℓ	mixing length (m), Eq. 2.45
ℓ_c	mean-free-path (m)
m	meter; mass (Kg); mode number
n	ion or electron density (m^{-3})
p	pressure (newton/m^2 or mm Hg)
r	radial distance (m)
R	tube radius (m)
R'	Eq. (2.22 b)
s	second
t	time (s)
T	temperature (v or ^oK)
u	unit vector, energy (joule)

v	volt; velocity (m/s)
V	potential (v)
V_r	radial potential drop (v), Eq. (3.2)
w	weber (v-s)
X	Eq. (2.33)
y	Eq. (2.33)
α	recombination coefficient (m^3/s)
γ	Eq. (2.42)
Γ	particle flux (m^{-2} - s^{-1})
ϵ	Eq. (2.20)
θ	azimuthal angle; Eq. (2.24)
κ	Eq. (A2.2)
λ	characteristic length (m)
Λ	diffusion length (m)
μ	electron or ion mobility (m^2/v-s)
ν	excitation or ionization frequency (s^{-1})
τ	Eq. (2.28)
φ	potential (v)
ω	angular frequency (s^{-1})

SUBSCRIPTS

a	ambipolar
c	collision; critical value
d	dissociative
f	"floating"
g	gas quantity
i	ionization; imaginary part

m	"mercury"
r	radial component; "rare gas"; radiative
s	saturation value
T	turbulent value
z	longitudinal component
θ	azimuthal component
+	ion quantity
-	electron quantity
$\perp$	transverse component
*	excited
o	undisturbed value; unit pressure
1	perturbed value; first component

BIOGRAPHICAL NOTE

The author was born in Indianapolis, Indiana in 1934. He attended M.I.T. from 1952-1956 and received a degree of Bachelor of Science in Geophysics. In 1956-57 he performed a one-year "stage" in geophysics at the Institut Francais du Pétrole in Paris, France. From 1957 to 1961 he worked for the General Motors Corporation on space flight research. Since 1961 he has been a graduate student at M.I.T. and has contributed to a graduate course on the Van Allen radiation belts of the earth.